

https://dspace.org/

The optimal milling and mainstream flotation circuit configuration for Mogalakwena Platreef ore

Khumalo, Mgciniwethu

2021

https://hdl.handle.net/10539/31905

Downloaded from a DSpace repository. https://dspace.org/

MSC RESEARCH REPORT

CHMT 7008A

THE OPTIMAL MILLING AND MAINSTREAM FLOTATION CIRCUIT CONFIGURATION FOR MOGALAKWENA PLATREEF ORE

Prepared by

Mgciniwethu Khumalo

Student number

326668

Submitted to

PROF VUSUMUZI SIBANDA

School of Chemical and Metallurgical Engineering, Faculty of Engineering and the Built Environment, University of the Witwatersrand, Johannesburg, South Africa

ABSTRACT

Mogalakwena Complex is located approximately 35 km to the north of the town of Mokopane in the northern limb of the Bushveld complex. The ore mined is of Platreef type mineralization. The material of value at the concentrator plant is recovered using the froth flotation process. The current circuit configuration at Mogalakwena North Concentrator is a mill-float-mill-mill-float (MF2) configuration. This circuit configuration results in overgrinding of the secondary milling circuit product resulting in generation of ultrafines which ultimately results in poor recovery of valuable material. Overgrinding reduces the probability of collision between the mineral particle and the bubble which has a negative effect on the efficiency of the flotation process**.** Fine particles also exhibit a high surface area which increases the rate of oxidation. Oxidation results in formation of a hydrophilic layer on the metal sulphide surface thereby negatively impacting recovery**.** In addition overgrinding increases the rate of entrainment of non-value particles thus negatively impact the product quality. The testwork conducted explored the feasibility of using an alternative circuit configuration in a bid to improve metallurgical performance.

Two circuit configurations were tested, the base case scenario which is the mill-float-mill-mill-float (MF2) and the mill-float-mill-float-mill float (MF3) circuit configuration in which the tertiary milling circuit was decoupled from the secondary milling circuit. Three back-to-back campaigns were conducted of the flexi-float pilot plant for the two circuit configurations.

The MF3 circuit yielded a superior metallurgical performance compared to the MF2 circuit for all the runs that were conducted. An average improvement in recovery of 3.20% for nickel and 1.78% for copper was observed when running the MF3 circuit configuration. The MF3 circuit configuration also yielded a better product quality due to the circuit configuration not exposing ultrafines to extended residence time conditions which promotes entrainment. A feasibility study on converting the current circuit configuration at Mogalakwena North Concentrator to MF3 was conducted looking at the production profile for the next 5 years. The conversion process has a payback period of 2 years 3 months and internal rate of return of 80%. The infrastructure assessment conducted indicated that the conversion process is feasible as the proposed changes to the circuit are of relatively low complexity and risk. Mogalakwena North Concentrator will be converting its MF2 circuit to MF3 configuration in the year 2020 and the initial benefit will be achieved in the year 2021. New knowledge on the processing of Platreef was generated and Mogalakwena Concentrator has embraced it. The knowledge generated will be considered for future plant design.

DECLARATION

I hereby certify that the work embodied in this dissertation is my own unaided work. It is being submitted to the University of the Witwatersrand for the Master of Science in Engineering degree. This dissertation has not been submitted before for any other degree or examination at any other University.

.

_____

Mgciniwethu Khumalo

Date

ACKNOWLEDGEMENTS

First, I would like to thank Professor Vusumuzi Sibanda who was my supervisor for his support and guidance and making this project a success. I would also like to extend my vote of thanks to Anglo American Mogalakwena Management for entrusting me with this project and funding it. Special mention to Ashina Buddu and Albert Blom for their input and support. My earnest thanks also go the team at Anglo Research for availing the flexi-float test rig for these campaigns and assisting with sampling, sample preparation, assay analysis and mineralogical analysis. Special mention to Kaja Tshimanga my industry supervisor for this project for his guidance and invaluable support throughout the project. Last but not least, this project was not going to be a success without the support from my wife Lorain Samukelisiwe Khumalo, for that I am grateful.

TABLE OF CONTENT

1. ABSTRACT i
2. DECLARATION ii
3. ACKNOWLEDGEMENTS iii
1. INTRODUCTION xiii
1.1 Introduction 1
1.2 Project Background 3
1.3 Problem Statement 4
1.4 Project Justification 4
1.5 Research Objectives 5
1.6 Dissertation layout 6
2. LITERATURE REVIEW 7
2.1 Introduction 8
2.2 Mineralogy Analysis 9
2.3 Flotation as we know it 14
2.3.1 Flotation separation process 14
2.3.2 Flotation reagents 15
2.3.3 Equipment components 16
2.3.4 Flotation models 17
2.4 Effect of Particle size on flotation 19
2.5 Effect of Particle size on product quality 23
2.6 Introduction of inert fine grinding at Anglo American Platinum 25
2.7 Effect of particle size on oxidation rate 26
2.8 Alternative circuit configuration 28
2.9 Summary of the literature review 30
3. EXPERIMENTAL MATERIALS AND METHODOLOGY 31
3.1 Introduction 32
3.2 Ore sampling and characterization 32
3.2.1 Ore sampling and crushing 32
3.2.2 Density determination using a pycnometer 32
3.2.3 Bond Ball Mill Grindability Index 32
3.3 Equipment and Materials 34
3.3.1 List of main equipment 34
3.2.2 Reagents 35
3.3 Experimental design 35
3.4 Survey Process 35

3.5 Analytical techniques 39
3.6 Data Analysis 40
3.7 Comparison Techniques 42
3.6 Data validation 44
3.7 Assumptions 44
4. RESULTS AND DISCUSSION 45
4.1 Ore characterization 46
4.2 Campaign number 1 51
4.3 Campaign number 2 60
4.4 Campaign number 3 66
4.5 Mogalakwena North Concentrator circuit retrofit 72
4.6 Economic evaluation 74
4.7 Implementation schedule 79
5. CONCLUSION AND RECOMMENDATIONS 80
6. REFERENCES 83
7. APPENDICES 88

LIST OF FIGURES

Figure 1.1: Pt Basket price trend (Blom, 2018) 2
Figure 1.2: Cost of production for different Platinum producers for the first half of 2017 (Blom, 2018) 2
Figure 2.1: Mogalakwena North Concentrator current wet circuit configuration 8
Figure 2.2: PGM grain size for different reefs (Rixom, 2015) 10
Figure 2.3: PGM fraction per size class for the feed and product streams 11
Figure 2.4: BMS fraction per size class in the feed and combined product stream 11
Figure 2.5: Benchmark Mineralogical Investigation of Mogalakwena North Concentrator –February 2017 12
Figure 2.6: Benchmark Mineralogical Investigation of Mogalakwena North Concentrator –November 2017 12
Figure 2.7: Benchmark Mineralogical Investigation of Mogalakwena North Concentrator –March 2018 13
Figure 2.8: Categories of critical flotation parameters (Klimpel, 1984) 14
Figure 2.9: Interaction between zones in a flotation cell (Dobby et al, 1982) 19
Figure 2.10: The conventional view (Pease et al 2006) 20
Figure 2.11: Recovery by size based on March 2018 performance 21
Figure 2.12: Fine particles and their behavior in flotation (Mugadza, 2015) 23
Figure 2.13: Size by size recovery in relation to water recovery (Engelbrecht and Woodburn, 1975) 24
Figure 2.14: The relationship between degree of entrainment and the particle size for hydrophilic silica in a laboratory flotation cell (Bisshop, 1974) 25
Figure 2.15: Rougher Recovery vs time (Anyimadu et al, 2006) 26
Figure 2.16: Galvanic interactions model (Greet, 2019) 27
Figure 2.17: Flotation behavior of the three different size fractions of galena (Lu et al, 2018) 28
Figure 2.18: Mill-Float-Mill-Float-Mill-Float (MF3) wet circuit configuration 29
Figure 3.1: Grinding disk and shaft of M4 IsaMill and flexi-float flotation cells 34
Figure 3.2: Flexi-float MF2 circuit sampling points and analysis conducted 38
Figure 3.3: Flexi-float MF3 circuit sampling points and analysis conducted 38
Figure 3.4: Approach to data set comparison 43
Figure 3.5: Mass pull vs. upgrade ratio graphical relationship 43
Figure 4.1: Feed and product size distribution profile 47
Figure 4.2: Particle size distribution of flexi-float feed 48
Figure 4.3: Primary mill grind cumulative passing 75 microns 52
Figure 4.4: Final grind cumulative passing 75 microns 52
Figure 4.5: Campaign 1 mass balance data integrity 54
Figure 4.6: Nickel kinetic curve for the different configurations 55
Figure 4.7: Copper kinetic curve for the different configurations 55
Figure 4.8: Enrichment ratio vs mass pull relationship 57
Figure 4.9: Enrichment ratio vs mass pull relationship 58
Figure 4.10: PGM association for sized tailings from different circuit configurations 59
Figure 4.11: Campaign 2 mass balance data integrity 62
Figure 4.12: Campaign 2 Nickel kinetic curve for the different configurations 63
Figure 4.13: Campaign 2 Copper kinetic curve for the different configurations 63
Figure 4.14: Nickel Enrichment ratio vs mass pull relationship 64
Figure 4.15: Copper Enrichment ratio vs mass pull relationship 64
Figure 4.16: Particle size distribution comparison of the tailings streams 65
Figure 4.17: Nickel Enrichment ratio vs mass pull relationship 67
Figure 4.18: Copper Enrichment ratio vs mass pull relationship 67
Figure 4.19: Comparison of copper and nickel kinetics 69
Figure 4.20: Copper flotation rate constants 69
Figure 4.21: Nickel flotation rate constants 70
Figure 4.22: Oxygen demand of the different process streams 71
Figure 4.23: MF3 Secondary rougher setup at Mogalakwena North Concentrator 74
Figure 4.24: Project implementation schedule 79
Figure 7.1: Flexi-float pump calibration 93
Figure 7.2: Campaign 3 data integrity 122

Figure 7.3: Current wet section plant setup 132
Figure 7.4: Proposed MF3 Circuit plant setup 132
Figure 7.5: Plant retrofit conceptual design..... 133
Figure 7.6: Proposed plant layout for secondary roughers and tertiary roughers..... 134

LIST OF TABLES

Table 2.1: Bulk mineralogy and PGM distribution for Merensky,UG2 and Platreef ore (Shamaila & O'Connor, 2008) 9
Table 2.2: PGM grain sizes (Anglo Mineralogy Reports) 10
Table 3.1: Flexi-float test rig main equipment 34
Table 3.2: Flotation reagents and dosages 35
Table 3.3: Testwork schedule 35
Table 3.4: Flexi-float throughput and running time 39
Table 4.1: Flexi-float feed ore SG 46
Table 4.2: Bond Work Index determination 46
Table 4.3: Bond Work Index 47
Table 4.4: Flexi-float feed bulk mineralogy 48
Table 4.5: Flexi-float feed base metal distribution 49
Table 4.6: Flexi-float feed base metal grain size distribution 49
Table 4.7: Flexi-float feed PGM grain size distribution 50
Table 4.8: Campaign 1 Power Intensity comparison 51
Table 4.9: Campaign 1 Grind comparison 51
Table 4.10: Campaign 1 Grind Statistical Analysis 53
Table 4.11: Run 1 bank recoveries 56
Table 4.12: Campaign 1 recovery comparison 58
Table 4.13: Percentage liberated PGMs per size fraction in the tailings 60
Table 4.14: Campaign 2 Power intensity comparison 60
Table 4.15: Campaign 2 Grind comparison 61
Table 4.16: Campaign 2 Grind statistical analysis 61
Table 4.17: Campaign 2 recovery comparison 65
Table 4.18: Percentage liberated PGMs per size fraction in the tailings 66
Table 4.19: Campaign 3 recovery comparison 68
Table 4.20: Proportions and flotation constants in the rougher feed 70
Table 4.21: Recovery comparison summarized 72
Table 4.22: Additional pumps operating cost 75
Table 4.23: Bill of quantities for circuit conversion (Smith, 2019) 76
Table 4.24: Assumptions for Net Revenue Calculation 78
Table 4.25: Economic Evaluation 79
Table 7.1: Sample Splitting efficiency 90
Table 7.2: Typical BWI from drill core samples 91
Table 7.3: Air rate calibration at different supply pressure 94
Table 7.4: Primary mill energy intensity 96
Table 7.5: Primary mill energy intensity normality test 96
Table 7.6: Primary mill energy intensity variance test 97
Table 7.7: Primary mill energy intensity Mann-Whitney test 97
Table 7.8: Primary rougher float feed particle size distribution normality test 98
Table 7.9: Primary rougher float feed particle size distribution variance test 98
Table 7.10: Primary rougher float feed particle size distribution 2 sample t-test 99
Table 7.11: Secondary mill energy intensity 99
Table 7.12: Secondary mill energy intensity normality test 100
Table 7.13: Secondary mill energy intensity variance test 100
Table 7.14: Secondary mill energy intensity 2 sample t-test 101
Table 7.15: IsaMill energy intensity normality test 101
Table 7.16: IsaMill energy intensity variance test 102
Table 7.17: IsaMill energy intensity Mann-Whitney test 102
Table 7.18: Final grind normality test 103
Table 7.19: Final grind variance test 103
Table 7.20: Final grind 2 sample t-test 104
Table 7.21: Run 1 MF2 Mass balance summary PGMs 105

Table 7.22: Run 1 MF2 Mass balance summary copper and nickel 105
Table 7.23: Run 1 MF3 Mass balance summary PGMs 106
Table 7.24: Run 1 MF3 Mass balance summary copper and nickel 106
Table 7.25: Primary mill power intensity 108
Table 7.26: Primary mill power intensity normality test 108
Table 7.27: Primary mill power intensity variance test 109
Table 7.28: Primary mill power intensity 2 sample t-test 109
Table 7.29: Primary float feed particle size distribution normality test 110
Table 7.30: Primary float feed particle size distribution variance test 111
Table 7.31: Primary float feed particle size distribution 2 sample t-test 112
Table 7.32: Secondary mill power intensity 113
Table 7.33: Secondary mill power intensity normality test 113
Table 7.34: Secondary mill power intensity variance test 114
Table 7.35: Secondary mill power intensity 2 sample t-test 114
Table 7.36: IsaMill power intensity normality test 115
Table 7.37: IsaMill power intensity variance test 115
Table 7.38: IsaMill power intensity 2 sample t-test 116
Table 7.39: Final grind normality test 117
Table 7.40: Final grind variance test 118
Table 7.41: Final grind 2 sample t-test 118
Table 7.42: Run 2 MF2 Mass balance PGMs 119
Table 7.43: Run 2 MF2 Mass balance base metals 119
Table 7.44: Run 2 MF3 Mass balance PGMs 120
Table 7.45: Run 2 MF3 Mass balance base metals 120
Table 7.46: Run 3 MF3 Mass balance summary PGMs 123
Table 7.47: Run 3 MF3 Mass balance summary base metals 123
Table 7.48: Run 3 MF2 Mass balance summary PGMs 124
Table 7.49: Run 3 MF2 Mass balance summary base metals 124
Table 7.50: Feed PGM speciation 126
Table 7.51: Campaign 1 detailed tailings mineralogy MF3 127
Table 7.52: Campaign 1 detailed tailings mineralogy MF2 128
Table 7.53: Campaign 2 detailed tailings mineralogy MF3 129
Table 7.54: Campaign 2 detailed tailings mineralogy MF2 130
Table 7.55: Additional pump operating costs 136
Table 7.56: Cost benefit analysis optimistic approach 137
Table 7.57: Pessimistic approach 150% cost of implementation 138

NOMENCLATURE

Abbreviations

BMS	Base Metal Sulphides
H1	Half year
IRR	Internal rate of return
HPGR	High Pressure Grinding Rolls
MF1	One milling stage followed by a flotation stage
MF2	Two milling stages with each followed by a flotation stage
MF3	Three milling stages with each followed by a flotation stage
NPV	Net present value
PGM	Precious Group Metals

Symbols

4T	Precious metal grade (Platinum, Palladium, Rhodium and Gold)
C	Concentration of valuable mineral (g/t)
c_g	Concentrate grade (g/t or %)
c_{gij}	Grade of component i in the concentrate of flotation unit j (g/t or %)
C_j	Mass flow of component i in the concentrate from unit j (kg/h)
C_j	Mass flow of concentrate for flotation unit j (kg/h)
Cm	Concentrate mass produced (g)
d_{50}	Average particle size (microns)
d_{b32}	Sauter mean diameter (mm)
f	Feed grade (g/t or %)
F	Feed mass treated (kg)
$g_{i,j}$	Split ratio of component i in unit j
j_j	Fraction of mass flow rate of component i in the feed to unit j
k	Flotation rate constant (min^{-1})
k_f	Flotation rate constant for the fast floating component (min^{-1})
k_s	Flotation rate constant for the slow floating components (min^{-1})
M	Mass flow of component i in the circuit feed (kg/h)
p50	Diameter at which 50% by mass of particles will have a diameter less than this value (microns)
P_a	Probability of attachment
P	Particle floatability
P_c	Probability of collision
P_{ca}	Probability of capture
P_d	Stability efficiency given by the probability of staying attached without being detached
P_f	Fraction of fast floating particles
P_n	Fraction of non-floating particles
P_s	Fraction of slow floating particles
Rc	Cumulative recovery (%)

R_i Recovery of component i (%)

S_b Bubble surface area flux (s^{-1})

$T_{i,j}$ Mass flow of component i in the tailings of unit j (kg/h)

X^{-1} Inverse of matrix X

CHAPTER ONE

INTRODUCTION

“The most beautiful thing we can experience is the mysterious. It is the source of all true art and science. He to whom this emotion is a stranger, who can no longer pause to wonder and stand rapt in awe, is as good as dead: his eyes are closed.”~ Albert Einstein

1.1 Introduction

Mogalakwena Complex is located approximately 35 3km to the north of the town of Mokopane in the northern limb of the Bushveld complex. The ore mined is of Platreef type mineralization. The Platreef ore is an orthomagmatic PGE-Cu-Ni sulfide deposit (Howell and McDonald, 2007). Mogalakwena Complex is Anglo American Platinum's flagship platinum mining and concentrating operation. This is driven by the lower mining cost due to open cast mining and the presence of large amounts of copper and nickel which increase the basket price per platinum ounce produced. Mogalakwena concentrators consists of the North, South and Baobab concentrating operations situated in the Limpopo province. The froth flotation process is used to concentrate the material of value and the product from the concentrator plant is taken to the smelter for further upgrading. It is of vital importance to ensure the process is efficient as measured by the recovery and the concentrate grade. The prolonged suppressed PGM price due to the slowing down of global demand has caused a strain for the PGM producers. This has been exacerbated by the increase in operating costs, decline in head grade and to a less extent the recycling of these metals. Despite South Africa holding the largest share of the world's PGM resources and reserves, the South African PGM industry finds itself competing with low cost producers (Russia and Zimbabwe) for capital and market share (IDC Department of Research and Information Report, 2013). The electricity supply is and will remain a challenge for the South African Mining and Metal Processing Industries. These two challenges among others have elevated the need to improve efficiencies. Anglo American's strategy to reduce its carbon footprint also necessitates the need to optimize the entire value chain. Mogalakwena Concentrator like all the other PGM producers based in South Africa needs to improve on its efficiencies in terms of both base metal recovery, PGM recovery and the product quality.

The figures below show the trend of the PGM prices and the operating costs of the key players in the PGM industry in South Africa. In Figure 1.1, the change in basket prices is illustrated in percentage form with reference to the basket price in 2011 (100%) . Figure 1.1 illustrates a decrease in platinum US dollar price by 46% from 2011 to 2014.

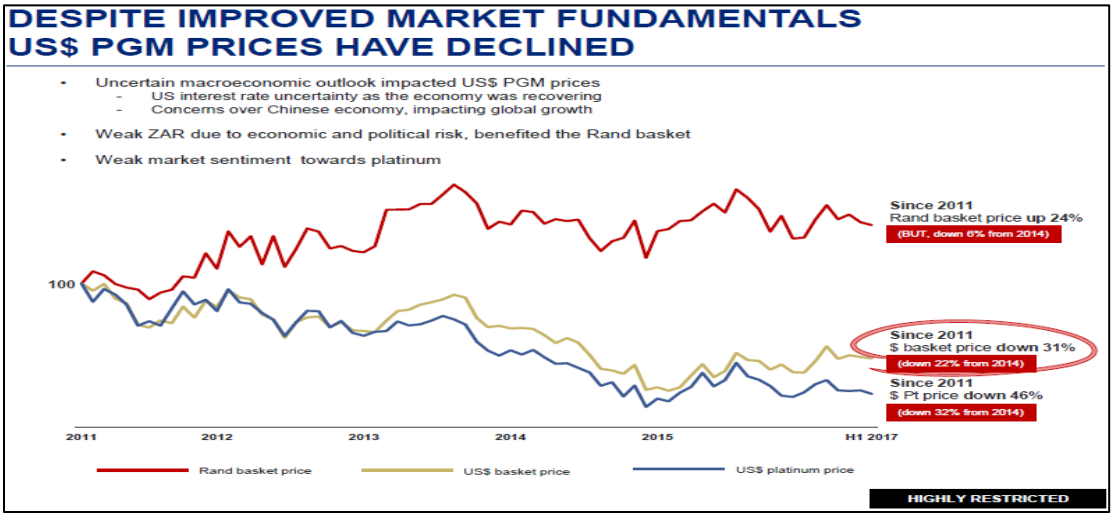

Figure 1.1: Pt Basket price trend (Blom, 2018)

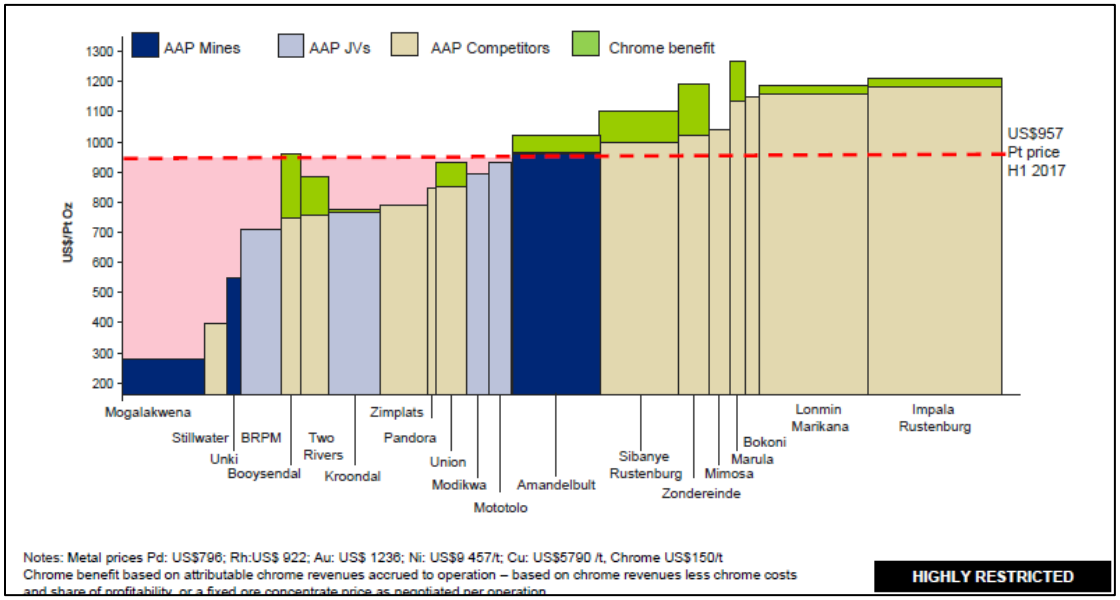

Figure 1.2: Cost of production for different Platinum producers for the first half of 2017 (Blom, 2018)

Figure 1.2 depicts the cost of production per platinum ounce. The red line indicates the breakeven point. It can be observed that approximately 50% of PGM producers are loss making which is not only a serious business risk but also a risk to the socio economic health of the country as mining is one of the top GDP earners.

1.2 Project Background

Multiple mineralogy results of the tailings stream from both Mogalakwena North and Mogalakwena South concentrator plant have revealed that the bulk of the material of value lost in the tailings stream is in the -10 micron size class and these particles are well liberated. The -10 micron size class is known to be difficult to recover through conventional flotation mechanisms due to their low probability of collision with the bubbles and low momentum. This results in poor process efficiency. The question one would raise though is that if fines are difficult to recover by conventional flotation methods why then create them in the first place. It is vital that the ore is ground to the optimal size in order to liberate the minerals of value so that they can be recovered by the flotation process and separated from the gangue to yield a good product quality. An optimum point thus exists between liberation, recovery and product quality.

Energy is applied to the ore to break it but breaking the ore below a certain size class results in losses of material of value and waste of energy. Breaking the rock also liberates floatable gangue material, which affects the product quality. The argument brought forth is that as much as it is necessary to put energy into the rock in order to maximize liberation, the stage of the circuit where the energy is added may influence the recovery process and the product quality. The work conducted was a bid to understand the potential benefit of redistributing the comminution energy requirements of the grinding circuit while optimizing the recovery of material of value. The challenge presented was to minimize overgrinding of material of value that has been ground to the optimal size without compromising liberation. Circuit configuration was explored as an optimization tool.

1.3 Problem Statement

It is postulated that the current circuit configuration at Mogalakwena North Concentrator leads to overgrinding of the secondary mill product which results in losses in the downstream flotation process. This hypothesis is underpinned by the tailings mineralogy reports which indicate that the bulk of the losses in the tailings stream are in the -10micron size fraction and the material of value is in this size class is liberated. Fines are difficult to recover using conventional flotation mechanisms thus to avoid dealing with fines in the flotation circuit rather not generate them in the first place. Particle size reduction in mills is not only selective to material of value, size reduction will also apply to the floatable gangue which has a negative impact on the product quality. Overgrinding also has a detrimental effect on the product quality because of the inverse relationship between entrainment and particle size. Poor product quality in terms of the concentrate grade leads to an increase in the smelting cost which leads to an increase in the entire value chain unit production cost. Therefore an ideal PGM concentrator plant should have a circuit for size reduction and flotation that minimizes overgrinding but still recovers the valuable minerals optimally. To make the necessary adjustments to the existing circuit configuration at Mogalakwena North concentrator will however require significant capital investment and higher operational costs. This project was conducted to explore whether the impact of reconfiguring the circuit was worth the capital investment and the associated higher operational costs.

1.4 Project Justification

This project evaluated the potential to improve metal recovery and product quality in a cost effective manner thus the potential to increase the revenue of the operation and ensure sustainable mining and job preservation. The project also has the potential to generate new knowledge in terms of the design of circuits for processing of Platreef ore. The knowledge generated from this project also has the potential to increase the value of the ore reserves as more metal will be produced per ton mined due to higher efficiencies. The higher efficiencies also present a tremendous potential to reduce the environmental footprint and carbon footprint of the mining activities. Value addition in terms of responsible mining and processing will ensure that future generations still benefit from the South African Platinum reserves in line with the company's strategy to reimagine mining for the benefit of all stakeholders. This project has the potential to assist South African producers to compete in the global market by reducing the unit cost of production thereby attracting investors and securing long term beneficiation of the mineral

reserves. The commodity prices have been exhibiting a downward trend since 2010 yet the labor costs increase year on year resulting in lower profit margins. This is a business risk that can be alleviated by improving process efficiency. An improvement in efficiencies can protect profit margins and may mean that jobs are not lost and ensure a healthy socioeconomic status of the country. The platinum sector employs 197 847 people who receive an income of R34.4 billion in salaries and wages annually (Baxter, 2014). In addition, many indirect jobs in supply and service industries in South Africa are supported by PGM mining and refining industries therefore, the South African mining industry bears responsibility not only for its own workforce but also for sustaining families and the clusters of other industries that provide support and service.

Application benefits of PGMs should also be considered when looking at the impact of improving efficiencies. The application of PGMs in autocatalytic convertors plays a crucial role in environmental protection. PGMs are also utilized in the manufacture of chemicals and medical treatments just to mention a few applications. An improvement in efficiencies has the potential to ascertain sufficient supply to the market despite the low commodity prices thereby ensuring a wide range of benefits to the world at large (Baxter, 2014).

1.5 Research Objectives

The main objectives of this research were as follows:

(I) To evaluate the feasibility of adopting an alternative circuit configuration for processing the Platreef Ore to the one currently being used using a pilot scale trial.

(II) To minimize overgrinding at Mogalakwena North Concentrator to increase the recovery of material of value and reduce losses to the tailings.

(III) To understand the metallurgical impact of decoupling the secondary milling circuit and the tertiary milling circuit

(IV) To investigate the feasibility of flash floating the secondary mill product before the tertiary grinding circuit for the Platreef Ore, this will help to understand the metallurgical flotation response of the secondary milling stage product.

(V) To determine the circuit configuration which yields the best recovery at an acceptable product quality.

(VI) To understand the capital and operational cost associated with retrofitting the Mogalakwena North Circuit configuration to float the product from the secondary milling stage and conduct a cost benefit analysis.

1.6 Dissertation layout

The dissertation is made up of five chapters. The summary of the chapters is given below:

Chapter One: Introduction

This section covers an overview of the performance of the PGM industry including the challenges faced by the South African PGM Industry. It further links the challenges faced by South African PGM industry to the need for optimizing plant efficiencies. This section then highlights the project statement, project background, the research objectives and the project justification.

Chapter Two: Literature review

This section details the current circuit setup at Mogalakwena North. The circuit setup is then linked to the mineralogy reports analyses with particular emphasis on liberation. The fundamentals of flotation as a separation process are also discussed in this chapter. Furthermore, the effect of particle size on flotation and product quality is discussed in this chapter. This chapter also covers the introduction of ultra-fine grinding at Anglo American Platinum. In addition, the concept of the flexi-float test rig is introduced in this section.

Chapter Three: Experimental Materials and Methodology

This chapter presents the experimental materials and the experimental procedures employed in this study. It details how the experimental work was conducted in order to be able to answer the experimental objectives of this research.

Chapter Four: Results and Discussion

This chapter details the results obtained from the experimental work conducted on the flexi-float test rig. Deductions are made in this section whether the alternative circuit configuration indeed yields better metallurgical performance. The cost benefit analysis is also considered as the alternative circuit configuration may result is significant changes in operational costs in addition to the capital requirement associated with retrofitting the plant.

Chapter Five: Conclusions and Recommendation

Conclusions and recommendations that are underpinned by the results obtained from the experimental work are summarized in this chapter. The conclusions drawn also were also translated to form the basis for future work that needs to be carried out.

CHAPTER TWO

LITERATURE REVIEW

“*If you wish to make an apple pie from scratch, you must first invent the universe”.~ Carl Sagan*

2.1 Introduction

Mogalakwena Complex comprises an open cast mine and two concentrator plants (Mogalakwena North Concentrator and Mogalakwena South Concentrator). Flotation is used to concentrate the material of value for downstream processing at the smelting operation. The study conducted focuses on the circuit setup at Mogalakwena North Concentrator. The dry section circuit at Mogalakwena North Concentrator produces a product with a top size of 10mm, which is the feed to the wet section. The wet section circuit configuration is depicted in Figure 2.1 below:

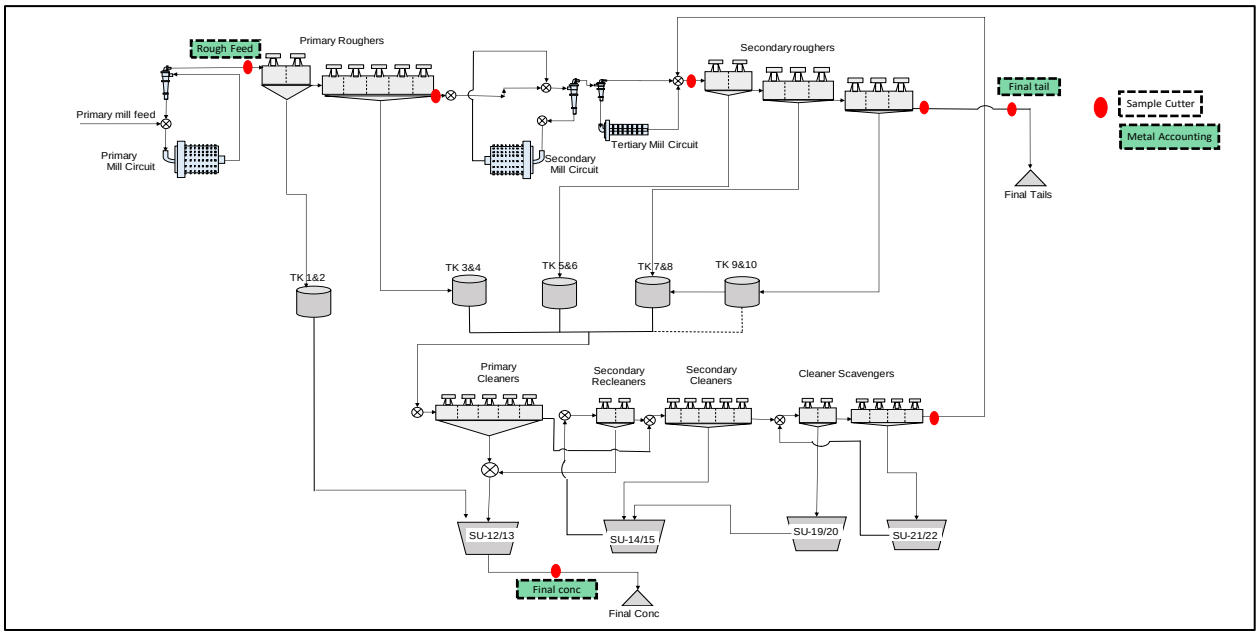

Figure 2.1: Mogalakwena North Concentrator current wet circuit configuration

The primary milling circuit product reports to the primary rougher flotation circuit and the tailings from the primary rougher flotation circuit reports to the secondary milling circuit. The primary milling circuit product has a particle size distribution of approximately 48% passing 75 microns. The product from the secondary milling circuit reports to the tertiary milling circuit. The secondary milling circuit product particle size distribution is approximately 75% passing 75 microns. The product from the tertiary milling circuit has a particle size distribution of approximately 84% passing 75 microns and is the feed to the secondary rougher bank. This process configuration has the potential to result in overgrinding of secondary milling circuit product in the tertiary grinding circuit ultimately resulting in inefficiencies in the downstream flotation circuit.

2.2 Mineralogy Analysis

According to work conducted by Henley (1983), there is a relationship between ore mineralogy and metallurgical performance. The ore mineralogy plays a vital role on the recovery method chosen and thus dictates the process flowsheet for different PGM bearing ore types.

Shamaila and O'Connor (2008) compiled bulk mineralogy data and PGM distribution for Merensky, UG2 and Platreef.

Table 2.1: Bulk mineralogy and PGM distribution for Merensky,UG2 and Platreef ore (Shamaila & O'Connor, 2008)

	Merensky	**UG2**	**Platreef**
Bulk mineralogy	Pyroxene Feldspar Base metal	Chromite Pyroxene Feldspar Base metal	Pyroxene Serpentine Calc silicates Base metal
PGM distribution	Tellurides~30% Arsenides~7% Sulphides~36% Alloys~7% Rest~20%	Tellurides <5% Arsenides <5% Sulphides~70% Alloys~20%	Tellurides~30% Arsenides~21% Sulphides~3% Alloys~26% Rest~20%

The average PGM grain sizes for the different reefs are depicted in Figure 2.2 as published in the work presented by Rixom (2015). This indicates that to maximize the recovery for each ore type, it is important to understand the mineralogy of the reef as it might influence the process design and selection. The variation in grain size for the different reefs indicates that the energy requirements for the desired liberation may be unique to a particular mineralization underlying the importance of mineralogy in circuit design.

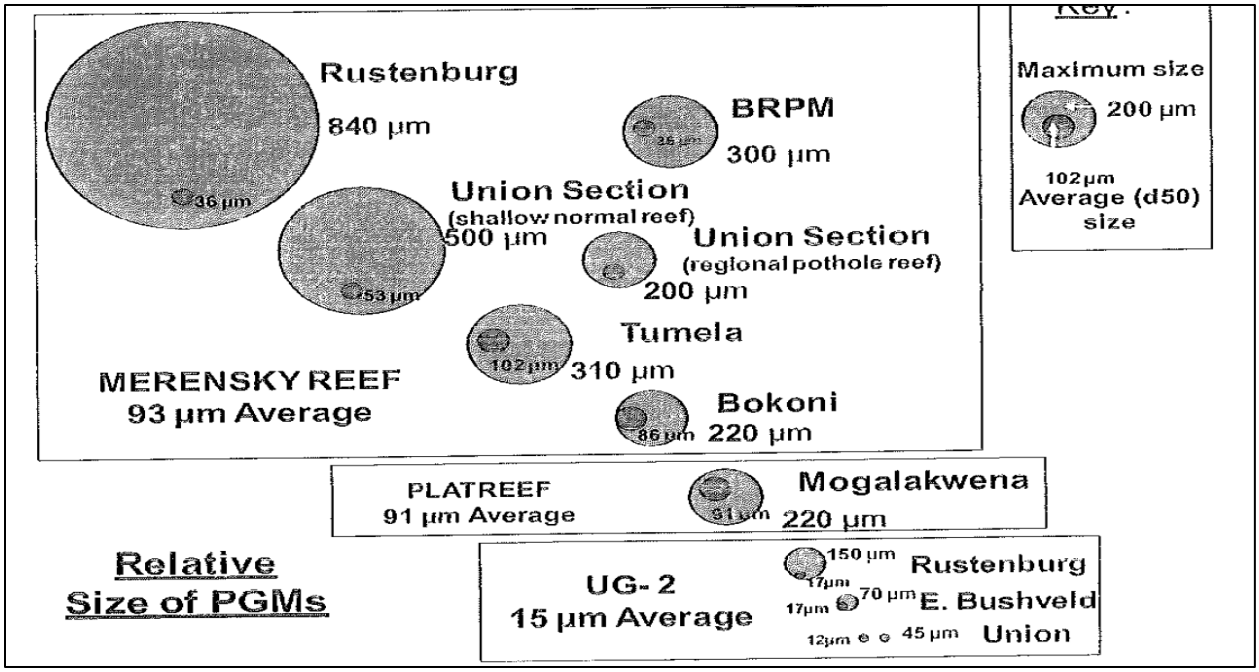

Figure 2.2: PGM grain size for different reefs (Rixom, 2015)

The average PGM grain size in the feed and tail as obtained from the mineralogy reports from Mogalakwena North Concentrator are tabulated below.

Table 2.2: PGM grain sizes (Anglo Mineralogy Reports)

	Mar-16	Jul-16	Feb-17	Nov-17	Mar-18
BMS average grain size in feed d_{50} (microns)	24	*20.8*	29	21	20
PGM Grain size p_{50} (microns) in feed	10.3	*9.5*	12.7	15.0	6.7
PGM Grain size p_{50} (microns) in tail	5.5	*5.7*	6	4.7	6.5

Table 2.2 indicates that the grain size of the PGMs in the feed is on the fine end. The PGM particles lost in the tailings are even finer indicating the breakage of PGM grains in the circuit due to the unselective nature of the particle breakage process in the mills coupled with the poor flotation response of the fine particles To justify the hypothesis of grain breakage due to the unselective nature of the grinding process a 'built up' size distribution (concentrate + tailings) was compared with the feed size distribution for the month of March 2018. Recent data could not be found in the archives as the mineralogy reports of the concentrate were not available. The distribution of the PGMs in each size class for the feed and the concentrator plant combined (concentrate +tailings) product is shown in Figure 2.3.

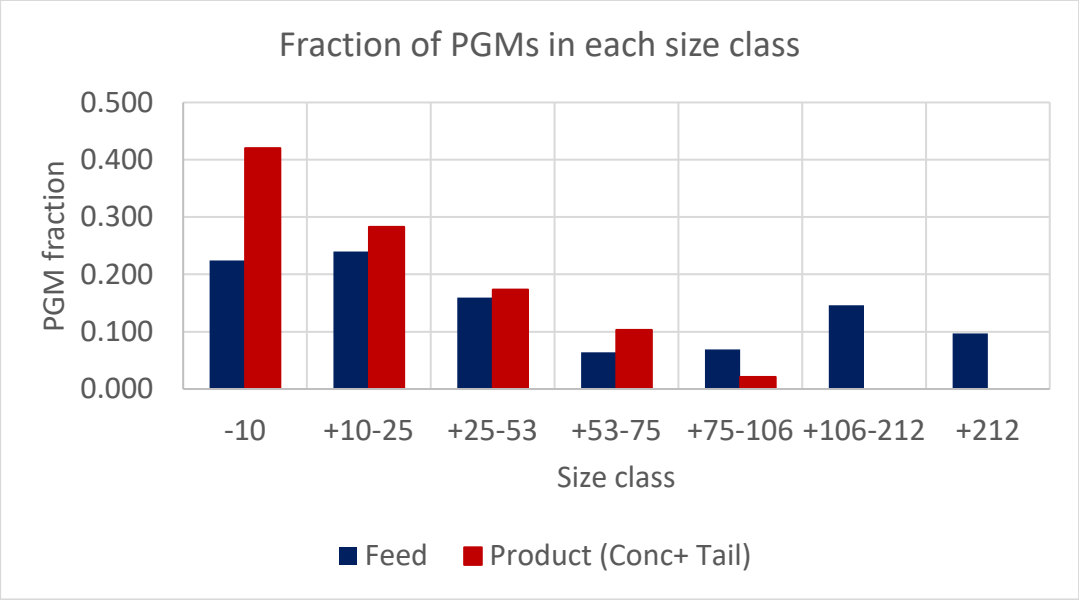

Figure 2.3: PGM fraction per size class for the feed and product streams

A similar comparison as in Figure 2.3 was conducted for the base metal sulphides. The results are shown in Figure 2.4 below.

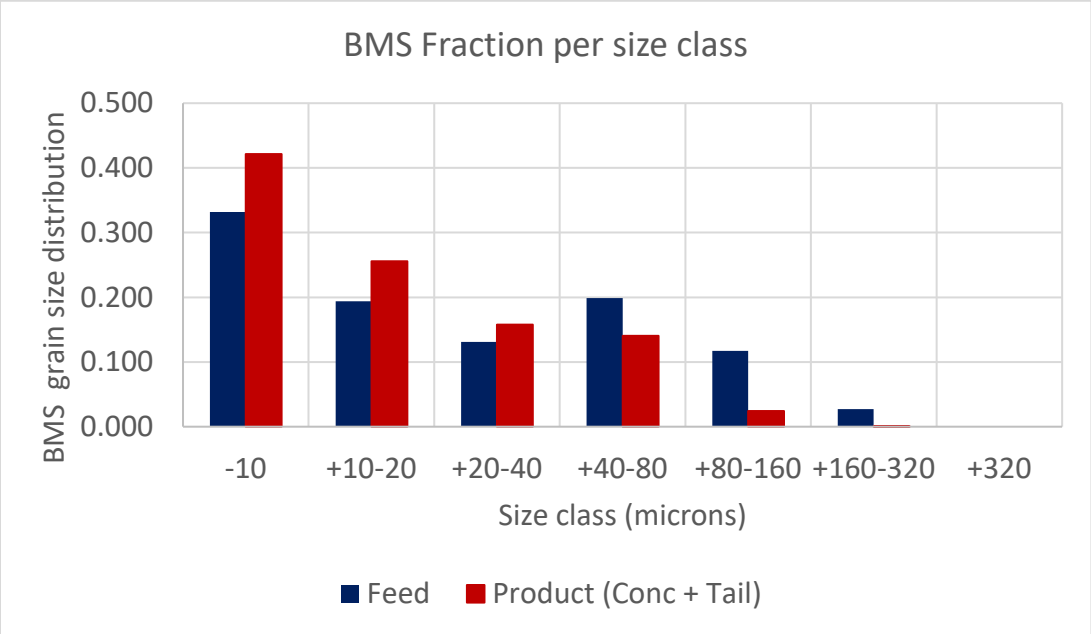

Figure 2.4: BMS fraction per size class in the feed and combined product stream

The graphs shown in Figure 2.3 and Figure 2.4 indicate that there is indeed grain breakage during the process of milling thus having a series of milling stages has the potential to result in overgrinding of the material liberated in one mill in the next milling stage.

Also key to note from Table 2.2 is the base metal grain size compared to the PGM grain size. The BMS grain size is relatively larger than the PGM grain size which means to maximize the recovery of both base metals and PGMs in the same process, there is thus a need to avoid overgrinding of the base metals while for sufficient liberation of fine grained PGMs. This work is of key importance as it forms the basis for assessing the viability of improving the process performance by configuring a circuit that minimizes BMS overgrind while maximizing PGM liberation.

A summary of the mineralogical liberation investigation for the February 2017 composite sample is shown in Figure 2.5. The feed grade for the month was 3.70 g/t and the tailings grade was 1.03 g/t.

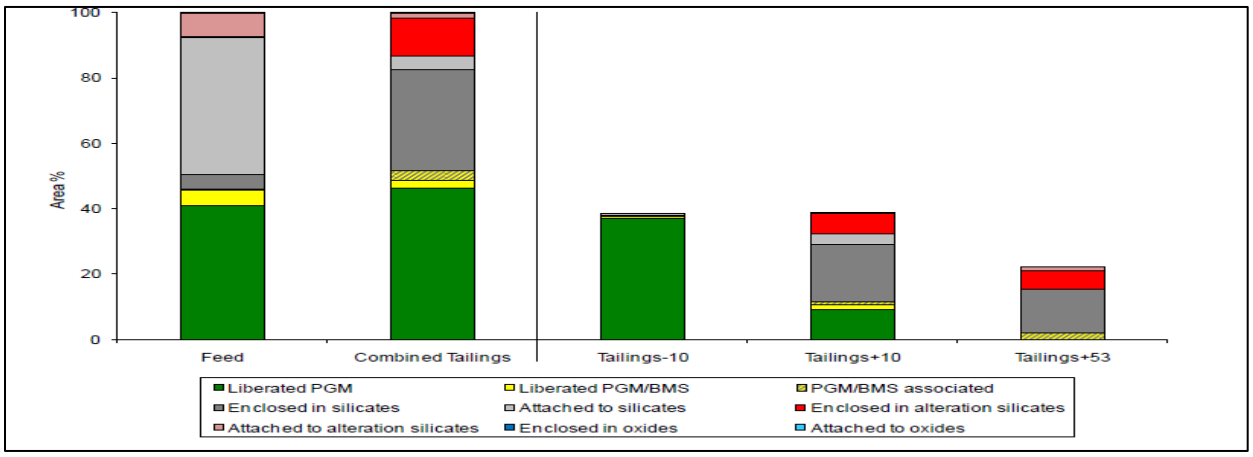

Figure 2.5: Benchmark Mineralogical Investigation of Mogalakwena North Concentrator –February 2017

A summary of the mineralogical liberation investigation for the November 2017 composite sample is shown in Figure 2.6. The feed grade for the month was 3.33 g/t and the tailings grade was 0.812 g/t.

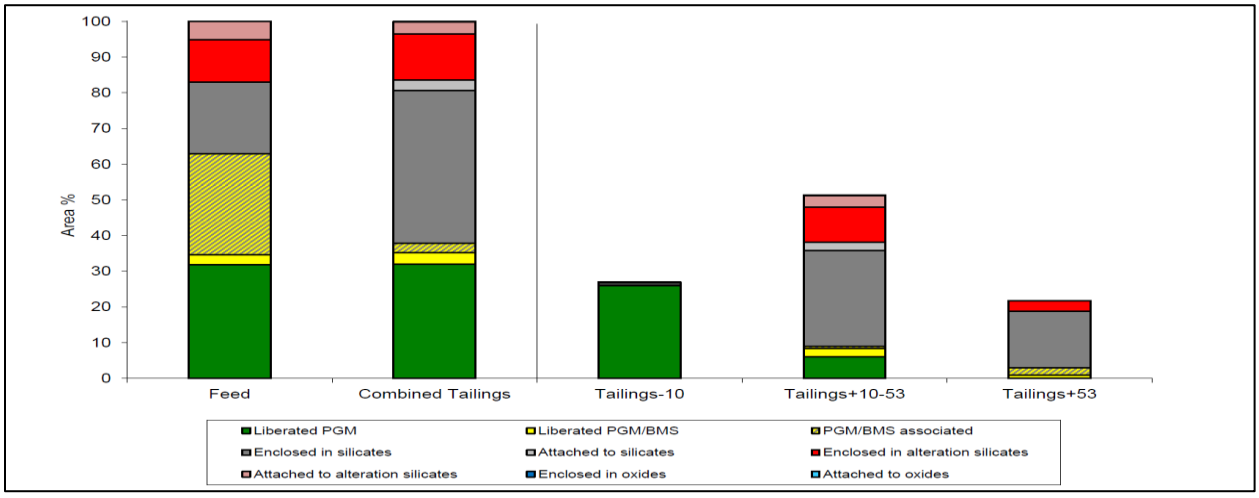

Figure 2.6: Benchmark Mineralogical Investigation of Mogalakwena North Concentrator –November 2017

A summary of the mineralogical liberation investigation for the March 2018 composite sample is shown in Figure 2.7. The feed grade for the month was 2.92 g/t and the tailings grade was 0.61 g/t.

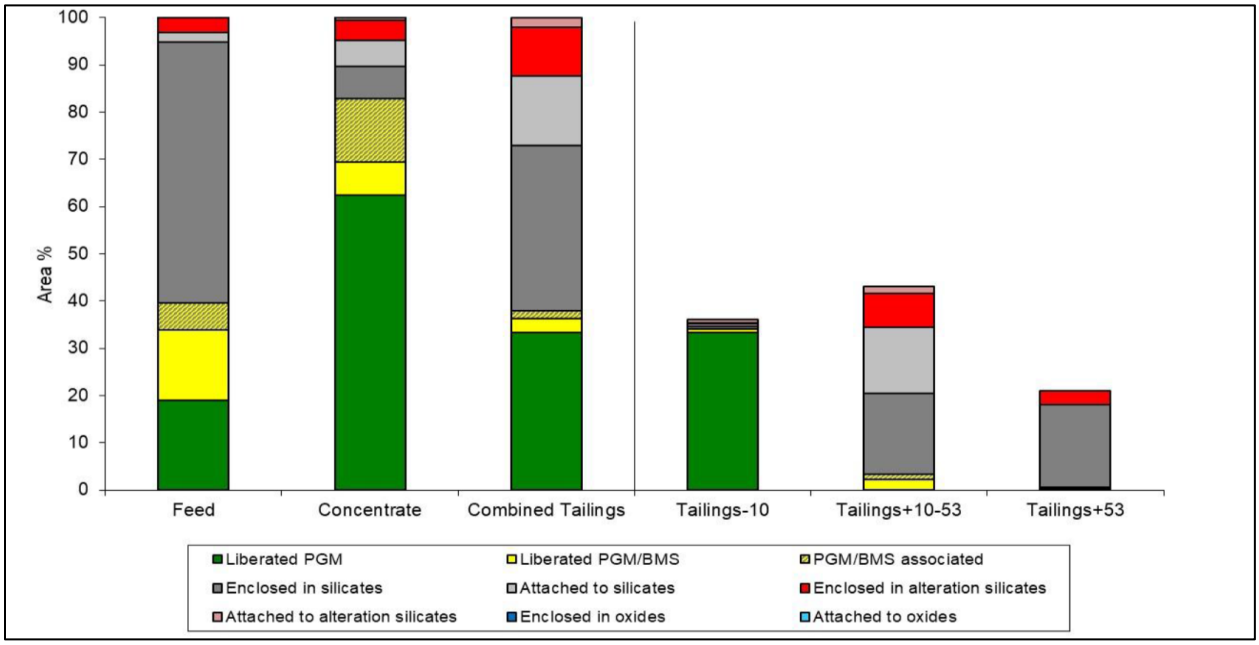

Figure 2.7: Benchmark Mineralogical Investigation of Mogalakwena North Concentrator –March 2018

The common trend observed on these graphs is that there is a significant amount of liberated PGMs in the -10 micron size class that is lost to the tailings. The majority of the PGM particles in this size class are liberated, this is indicative of the poor flotation response of the fine particles. There is also material that is not liberated in the coarser size fractions. The key to optimization is therefore to direct the comminution power to the right particles to liberate the locked material of value without overgrinding the already liberated metals. Floating the product from the secondary mill before tertiary milling thus has the potential to reduce overgrinding of both the PGMs and base metal sulphides which are already liberated in the secondary milling stage, this will improve the overall recovery of the PGMs. This test work conducted provided a platform to test this hypothesis for Platreef ore.

2.3 Flotation as we know it

2.3.1 Flotation separation process

Flotation is a physico-chemical process that utilizes the difference in surface properties of minerals to separate valuable minerals from gangue (Wills, 2005). It is carried out in tanks or columns and the separation is based on the differences in hydrophobicity of the material. Slurry is fed into the cell or column together with air and some reagents that aid the separation based on the surface properties of the particles. (Verrelli et al 2011) documents the attachment process. The attachment process involves the collision of the hydrophobic material with the bubbles resulting in a particle–bubble aggregate. The particle-bubble aggregate rises to the surface of the flotation unit resulting in separation of the hydrophobic material from the hydrophilic material. This attachment process is a function of surface chemistry of the particles, flotation unit hydrodynamics, particle size, contact angle and induction time. In flotation, the material of value is rendered hydrophobic by the collector, attaches to the bubbles and is transported to the froth zone where it is collected as concentrate. The process is driven by the probability of collision of the particle and the bubble, the probability of attachment of the particle on collision and the probability of the particle to remain attached as the bubble rises to the froth phase. There are many parameters which influence the flotation process. Klimpel (1984) divided these parameters into three main categories namely chemistry components, equipment components and operational components.

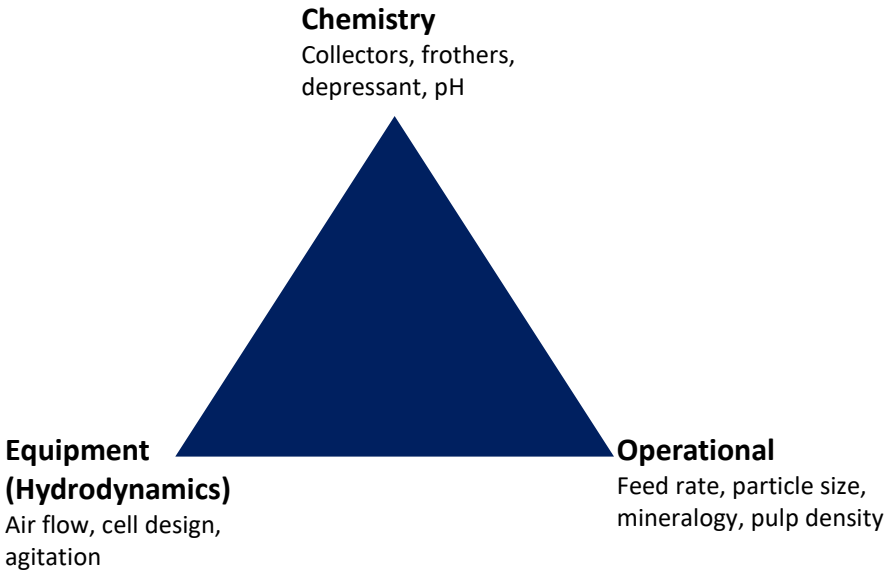

Figure 2.8: Categories of critical flotation parameters (Klimpel, 1984)

2.3.2 Flotation reagents

Reagents are widely used in mineral processing industry to enhance the performance of many processes. Reagents affect the chemistry component of the flotation process. The main reagents used in the flotation of platinum group metals are collectors, depressants and frothers. Despite the different reagents having different roles, there is some interactions and synergistic effects among the reagents. It is therefore important to establish an optimum dosing recipe. Valenta (2007) documented the importance of balancing the reagent regime for optimal circuit performance.

Collectors adsorb on mineral surfaces and modify the surface properties thereby imparting hydrophobicity. This increases the propensity of the particles attaching to the rising air bubbles. The air bubbles collect in the froth phase and report to the concentrate. Ionic collectors are made up of a polar and non-polar group of which the non-polar group is a hydrocarbon chain. During the adsorption process, the polar group is attracted to a charged mineral surface while the non-polar group is oriented towards the water phase which renders the mineral surface hydrophobic.

Depressants are added to the flotation pulp in order to reduce the flotation of unwanted naturally floating gangue minerals. They affect the flotation process by adsorption on gangue minerals and rendering them hydrophilic. The depression of the gangue improves selectivity thereby improving the product quality. Depressants with a high degree of substitution also have the capability to act as dispersants thereby improving flotation hydrodynamics.

Frother is added in a flotation circuit in order to prevent bubble coalescence thereby preserving the bubble size. The attachment of minerals of value occurs on the surface of the bubbles thus a higher surface area (smaller bubbles) is required in order to achieve higher recoveries of material of value. The frother concentration should be maintained above the critical coalescence concentration in order to preserve bubble size. Frother is also added to stabilize the bubbles thereby allowing the froth phase to be able to carry the material of value all the way to the concentrate launder with minimal bursting of the bubbles as bursting of the bubbles leads to detachment of the material of value and hence potential recovery loses. The most commonly used frothers in commercial flotation are those containing a non-polar water-repellent group, as well as a single polar water-avid group (Harris et al, 2000). The frother concentrates at the interface of

water and air bubbles, forming a layer around the bubbles, which prevents the bubbles from colliding. The link between bubble size and metallurgical performance is shown by the flotation rate constant in the pulp phase as proposed by Gorain et al (1998)

$$k = PS_b \qquad \textit{Equation 1}$$

Where:

k is the flotation rate constant

S_b is the bubble surface area flux

P is the particle floatability

The bubble surface area flux is then calculated as follows:

$$S_b = \frac{6J_g}{d_{32}} \qquad \textit{Equation 2}$$

Where

J_g is the superficial gas velocity

d_{b32} is the Saute mean diameter of the bubbles

The bubble surface area flux is a function of superficial gas velocity in the cell, Jg as well as the Saute mean bubble diameter. The Saute mean diameter is a function of the air rate, the cell design and the amount of the concentration of frother in the water hence the link between flotation kinetics and the frother dosage. Frother helps to preserve bubble size at concentrations higher than the critical coalescence concentration

The generation of fines has a potential to increase reagent consumption due to the high specific surface area of the particle, which increases the absorption capacity, this results in an imbalance in the circuit and may ultimately lead to poor metallurgical performance.

2.3.3 Equipment components

The effect of agitation, impellor type and impellor tip speed on flotation kinetics and hence metallurgical performance is documented by Gorain et al (1995). This work indicated that the mean bubble size increases with increase in air flow rate and decreases with increase in impeller

speed. This relationship can be used to predict the impact of these input parameters on the flotation rate constant. Pease et al (2006) documented the considerations to be taken into account when designing flotation cells for coarse particle flotation and for fine particle flotation. According to work conducted by Deglon et al (2000), the larger cells typically operate at lower power density and the efficiency of mixing and solid suspension also decreases with increase in cell size.

Air addition rates play a vital role in flotation. This is because the air addition rate affects both the hydrodynamics and kinetics of the pulp phase as well as the general behaviour of the froth phase. Low air rates, below the peak air recovery (PAR) air rate, produce highly laden, well drained froths but with low mobility resulting in bubbles that largely collapse before overflowing the cell lip. These froths are associated with low air recoveries and low mineral recoveries, but result in high concentrate grades. High air rates beyond the PAR air rate, produce free flowing froths with high water content that are unstable due to low bubble loadings, and so bubbles tend to burst before overflowing, giving low air recoveries. Such froths yield reasonable mineral recoveries but at low concentrate grades. Intermediate air rates yield a balance between the competing effects of bubble loading and froth mobility resulting in a stable froth, a peak in air recovery, and a high mineral recovery, without excessively compromising the concentrate grade (Hadler and Cilliers, 2009). This optimum flotation performance at PAR addition rate is attributed to the increased froth stability and high selectivity at this addition rate

2.3.4 Flotation models

Flotation rate constants can be estimated using fundamental kinetic models. These models have been widely used based on the analogy with homogeneous chemical kinetics, in which the concentration in a batch reactor is modelled by a first-order differential equation (Vinnett, 2015):

$$\frac{dC}{dt} = -kC \qquad \textit{Equation 3}$$

where C = the concentration of valuable mineral

k = the flotation rate constant

Integrating we get:

$$InC = -kt + C'$$

At the initial conditions t = 0, C = C_0 or C' = $\ln C_0$

$C = C_0 e^{-kt}$ *Equation 4*

The first order rate equation can be stated as the rate at which the floatable particles decrease in the batch flotation cell is proportional to the amount of floatable particles in the cell.

Recovery will then be calculated as follows.

$R = \frac{(C_0 - C)}{C_0}$ *Equation 5*

$1 - R = \frac{C}{C_0}$ *Equation 6*

In the flotation process particles can be sub-divided into different classes such as the three component model of fast-floating, slow-floating and non-floating species. Taking this into consideration yields the following equation:

$1 - Ri(t) = P_f e^{-k_f t} + P_s e^{-k_s t} + P_n$ *Equation 7*

Where

k_f is the rate constant for the fast floating component

k_s is the rate constant for the slow floating components

P_f is a fraction of fast floating particles

P_s is a fraction of slow floating particles

P_n is a fraction of non-floating particles

R_i is the recovery of component i

The value of P_n will be estimated from the recovery vs time graph where the graph flattens out.

To estimate the parameters it is assumed that $k_f >> k_s$ at large values of t, $P_f e^{-k_f t}$ is negligible and the equation becomes

$1 - Ri(t) = P_s e^{-k_s t} + P_n$ *Equation 8*

Taking natural logarithms of both sides;

$In(1 - Ri(t) - P_n) = InP_s - k_s t$ *Equation 9*

Plotting ln (1-R_i (t) - P_n) against time (t) gives a straight line where ln P_s is the intercept and k_s is the slope.

To estimate P_f and k_f using the values obtained above, the following approach is followed

$$In\left(1 - Ri(t) - P_n - P_s e^{-k_s t}\right) = InP_f - k_f t \qquad \textit{Equation 10}$$

Plotting ln (1 − $Ri\ (t)$ − $P_s$exp $-k_s t$) against time gives a straight line with P_f as the intercept and gradient equal to k_f.

This approach to modelling the flotation rate constants was applied to model the base metal rate constants.

2.4 Effect of Particle size on flotation

Bubble-particle interactions are a central issue in flotation. They control the selectivity and efficiency of the process (Basaova and Hubicka, 2014). The process can be split into two phases, the pulp phase and the froth phase as indicated in the diagram by (Dobby et al., 1982). This diagram is relevant to this study as it indicates the different zone of the flotation process and the recoveries associated with each zone.

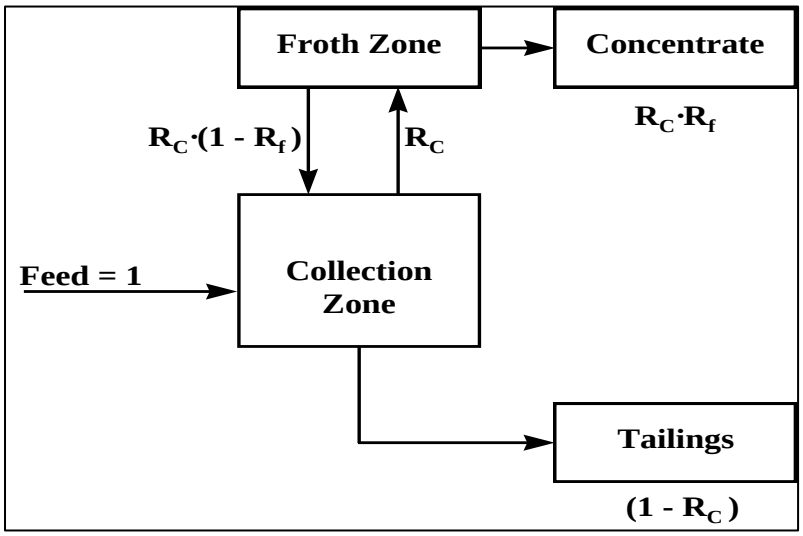

Figure 2.9: Interaction between zones in a flotation cell (Dobby et al, 1982)

The probability of the capture in the flotation process is given by the three steps; collision, attachment and stability, a product formula using the efficiency of each stage of the process is often used (Zongfu et al, 1999) and it states as follows:

$$P_{ca} = P_c P_a P_s \qquad \textit{Equation 11}$$

where Pca is the probability of capture

Pc is the probability of collision

Pa is the probability of attachment

Ps is the stability efficiency given by the probability of staying attached without detaching

The flotation process is particle size dependent and as a result fines and coarse particles in a flotation cell will exhibit different flotation behavior. The general relationship between particle size and flotation response is shown below.

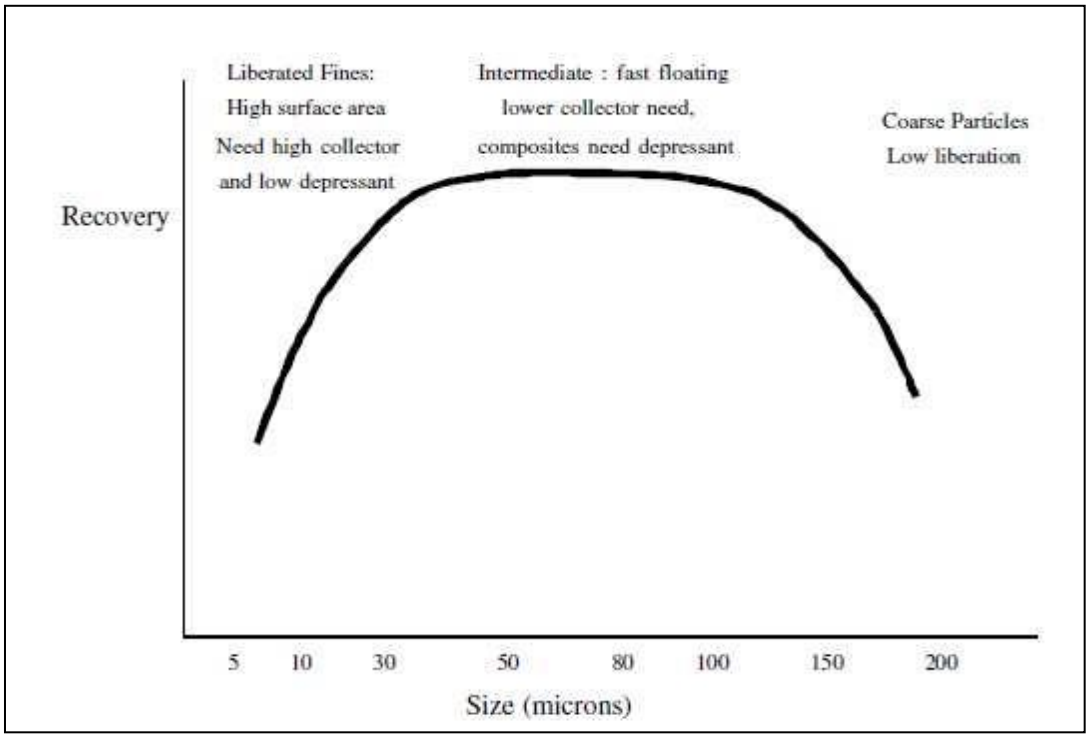

Figure 2.10: The conventional view (Pease et al 2006)

Understanding the parameters that affect the separation process provides a platform for improvement of the process. Bubble-particle interaction is a complex phenomenon as it involves both chemistry aspects and physics aspects. The particle size has an effect on the probability of

particle-bubble collision, attachment of the particle on the bubble and the probability of the particle remaining attached to the bubbles in pulp phase despite the turbulence promotes successful separation (Aldrich and Feng, 1999). Low particle-bubble collision for fine particles is experienced due to the trajectories of the particle around the bubble. The velocity stream lines of the fluid around the bubble reduce the chances for collision as the particles are not able to deviate from the fluid streamlines to collide with the bubbles exhibiting a phenomena of grazing trajectory of colliding particles (Webber and Paddock, 1983; Yoon and Luttrell, 1989). Fine particles do not possess enough kinetic energy to impact the bubble so as to cause deformation of the bubble surface for attachment. They also do not have enough energy to displace the liquid layer between the colliding particle and the bubble (Hewitt et al., 1995), this results in poor probability of attachment. Coarse particles on the other hand result in a particle-bubble aggregate with a low buoyancy hence poor flotation performance. The disruptive forces in the cell due to turbulence result in the detachment of coarse particles in a flotation cell. A comprehensive study on the mechanisms of particle-bubble detachment was conducted by Wang et al (2016). Cheng et al (2017) also studied bubble-particle bubble interaction and deduced that the probability of collision and attachment increased with increase in particle size. This study also highlights the influence of particle size on the probability of detachment and ultimately recovery thereby highlighting the need for an optimal size to maximize recovery. This work underpins the need for investigating the optimum sequence of size reduction and flotation setup for Platreef ore.

A recovery by size graph based on the March 2018 performance at Mogalakwena North Concentrator is shown in Figure 2.11 below.

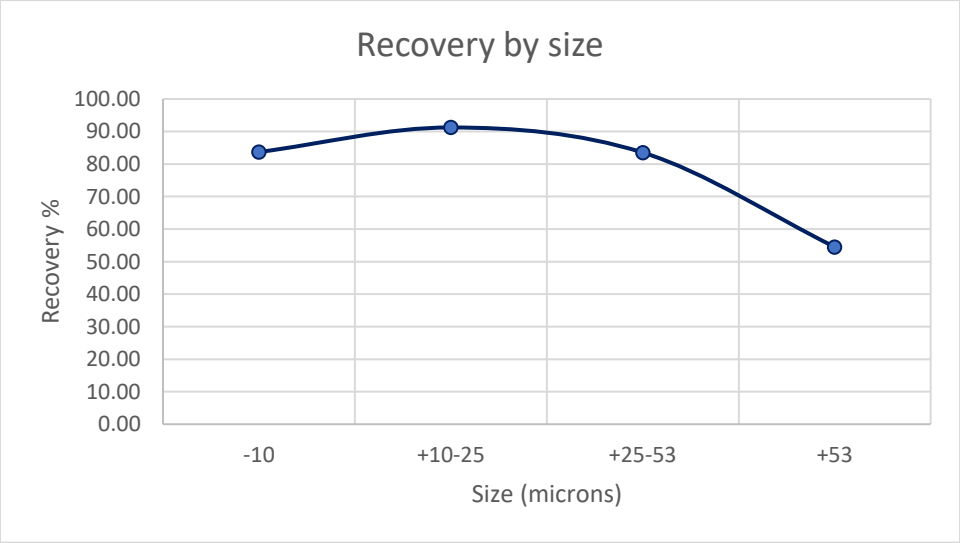

Figure 2.11: Recovery by size based on March 2018 performance

The recovery indicates that the optimum recovery occurs in the +10-25 micron size class, beyond this range the recovery is compromised. An insight that can be drawn from Figure 2.11 is that overgrinding of the metals should be avoided. The recovery can be improved by liberating the material of value in the +25 micron size fraction however this has to be achieved without overgrinding material of value in the +10-25 micron size class. This highlights the need to recover stage wise after each milling stage so that the comminution energy can be directed to the correct size class that needs liberation.

A different approach by Albijanic et al (2015) indicated that bubble-particle attachment depends on the particle surface properties, namely particle composition, this alludes to the issue of liberation. According to work conducted by Pease et al (2006), it was suggested that to optimize the circuit performance there is a need to design the milling in conjunction with the flotation stage to suit the liberation characteristics of the ore. This however results in several stages of grinding and flotation, recovering the mineral as soon as it is liberated and applying further grinding energy only to those particles that still need liberation. This work highlights the importance of circuit configuration and thus justifies the need for this investigation.

Senior et.al. (1994), investigated the selective flotation of a pentlandite from a nickel ore. According to Senior et.al. (1994), nickel recovery can be improved by:

- grinding in stages so that the flotation feed contained a minimum amount of fine (-10 µm) nickel and a maximum amount of nickel in the - 75 + 10 µm range
- It is better to grind coarse upfront than too fine. Coarse particles that fail to float can be recovered and re-ground. Pentlandite that is ground too fine is difficult to float

The studies by Senior et.al. (1994) also highlight the importance of circuit configuration on metallurgical performance and the impact of particle size on flotation in particular of pentlandite. From these studies it is evident that grinding coarser has the potential to improve the recovery of base metals in this case nickel. This is in line with the hypothesis of this study.

Fine particles also exhibit other unwanted behaviors in the flotation process such as rapid oxidation, high reagent consumption due to the higher surface areas and they also easily form slime coatings as indicated in Figure 2.12. All these factors are detrimental to the process efficiency. This study is aimed at reducing the impact that the fines have on the process efficiency.

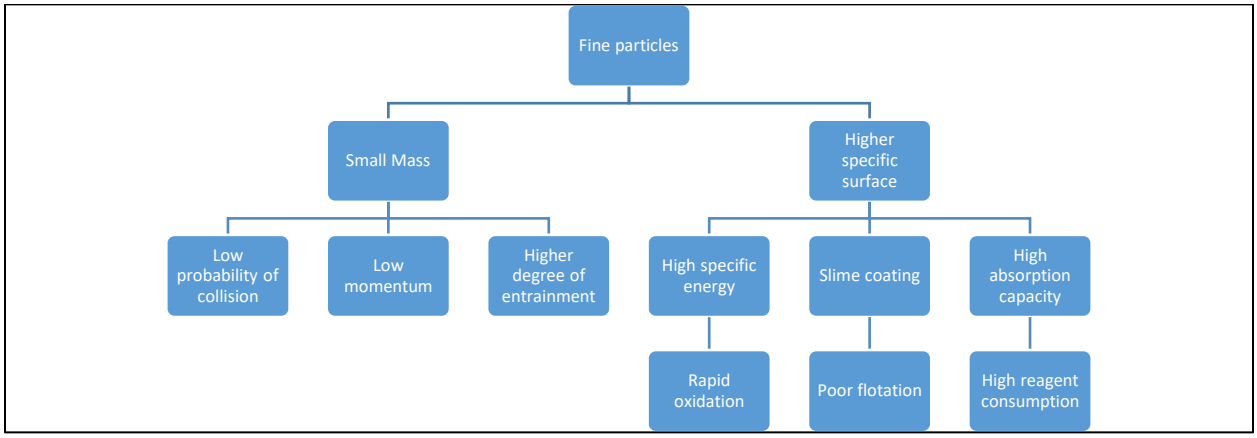

Figure 2.12: Fine particles and their behavior in flotation (Mugadza, 2015)

2.5 Effect of Particle size on product quality

The effect of particle size on product quality can be inferred from the relationship between particle size and entrainment. Entrainment is a process by which none floating material reports to the concentrate stream during the flotation process. It is basically a mechanical transfer process whereby the non-floating material (unattached solids) can be recovered with the water or trapped between the rising bubbles resulting in the particles being transferred to the concentrate zone. This process is not selective. The non-floating material which is not supposed to report to the concentrate zone dilutes the product quality which is detrimental to the downstream processing stages. The relationship between entrainment and particle size is well documented by Engelbrecht and Woodburn (1975). Figure 2.13 depicts this relationship between water recovery and silica recovery for different size silica particles.

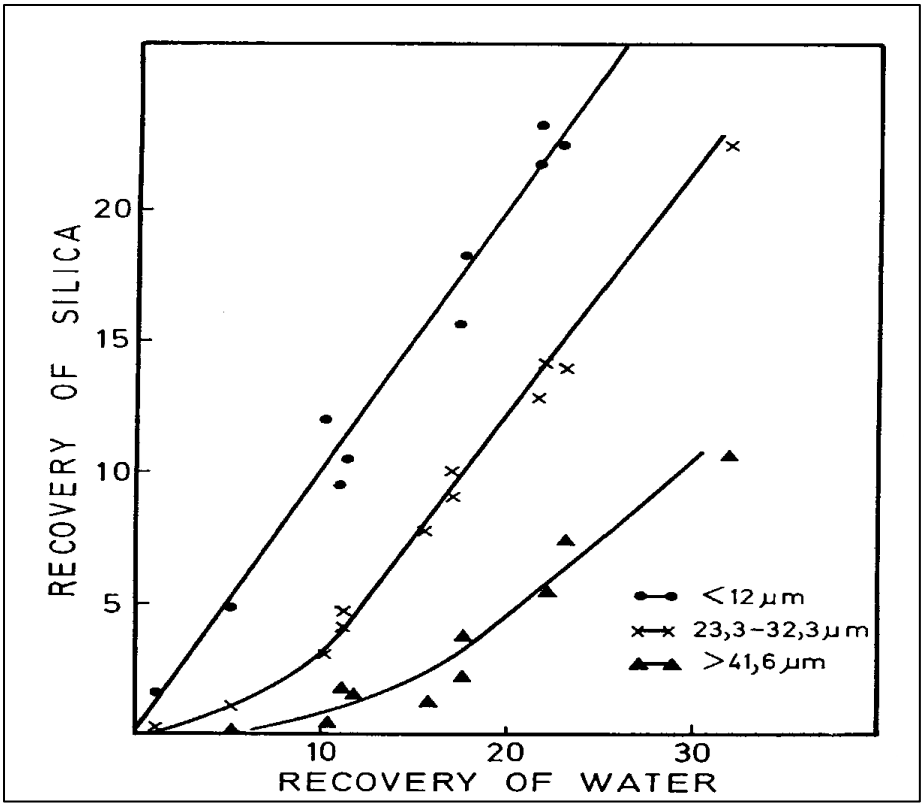

Figure 2.13: Size by size recovery in relation to water recovery (Engelbrecht and Woodburn, 1975)

It can be seen that at the same density, the smaller size particles are lighter and thus stand a higher chance of being recovered with the water in the process reducing the concentrate grade. Rule (2011) on the other hand highlighted the improvement in the grade recovery relationship due to better liberation achieved through ultrafine grinding on the contrary. This can be attributed to the fact that work on the mainstream was conducted based on mineralogy of the tailings stream which indicated that most of the losses were as a result of material of that was not liberated, this is contrary to what is currently observed at Mogalakwena North Concentrator whereby approximately 35% of the material of value lost to tailings is in the -10 micron size fraction and is liberated. Introduction of ultrafine grinding in this case improved the recovery through improved liberation. In addition the ultrafine grinding mills used for this testwork received the flotation tailings as feed whereas in the current circuit configuration at Mogalakwena North Concentrator the ultrafine grinding circuit treats the secondary milling circuit product before the flotation stage. The work conducted by Bisshop (1974) highlighted the same observations made by Engelbrecht and Woodburn (1975). The degree of entrainment decreases with increase in particle size for particles of similar density. This highlights the negative impact of grinding too fine on product quality, as the entrainment process is non-selective. Figure 2.14 below depicts this relationship.

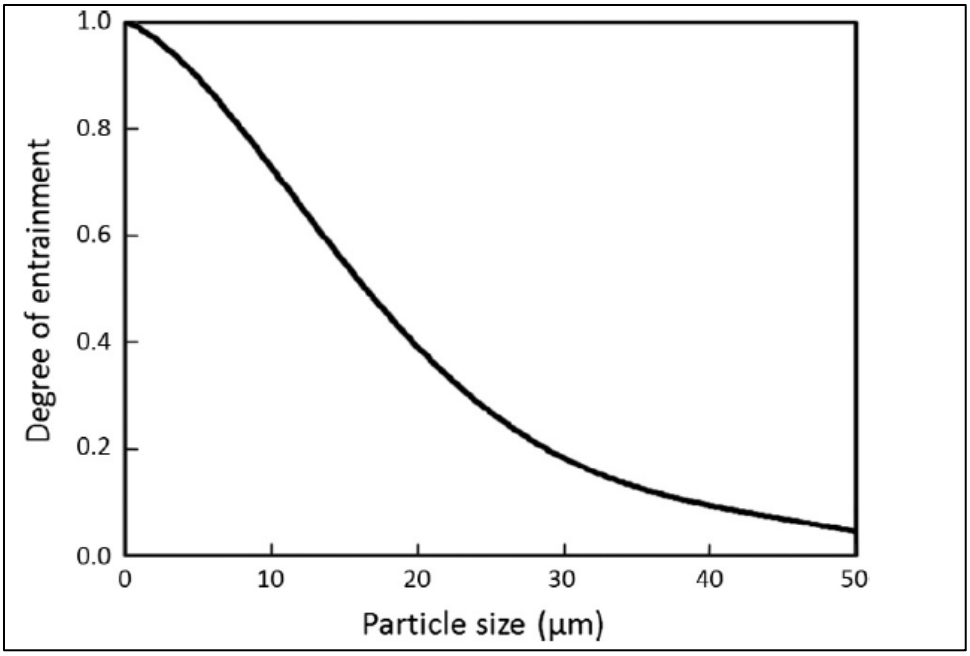

Figure 2.14: The relationship between degree of entrainment and the particle size for hydrophilic silica in a laboratory flotation cell (Bisshop, 1974)

This study also seeks to provide further understanding on the feasibility of getting an optimal product quality through minimizing excessive production of fines by making use of an alternative circuit configuration at Mogalakwena North Concentrator. This is based on the hypothesis that a reduction in overgrinding will translate to a reduction in the entrainment rate.

2.6 Introduction of inert fine grinding at Anglo American Platinum

According to Rule (2011), the need to introduce ultrafine grinding was necessitated by the shift in the mineralogy of the Platinum bearing reef being exploited. The shift was from the beneficiation of the Merensky reef to UG2 and the Platreef ore which are known to have fine grained PGM ores. Rule (2011) highlights that the work on stirred milling at Anglo American began in the year 2000 and it showed a positive shift in the grade-recovery relationship at laboratory scale. According to the work conducted by Anyimadu et al (2006), the introduction of ultrafine grinding using stirred mills and inert grinding media was essential in order to improve the process efficiency in terms of recovery of material of value and obtaining a quality cleaner product in terms of the concentrate grade. The improvement in efficiency was attributed to better liberation with the introduction of ultra-fine grinding. Anyimadu et al (2006) however acknowledged the associated challenges with treating fines.

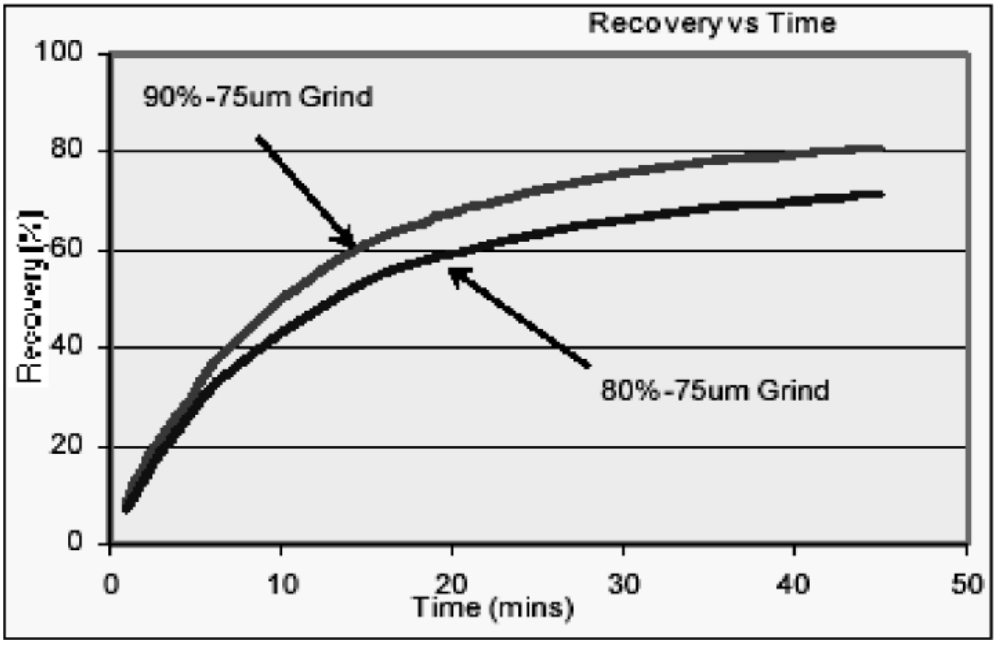

Figure 2.15: Rougher Recovery vs time (Anyimadu et al, 2006)

According to Rule (2009), the Anglo group currently has 22 inert grinding mills typically treating secondary ball mill product and producing a grind of 80% passing 50 microns or finer. The studies by Rule (2011) and Anyimadu et al (2006) are relevant to this work in that there should be a way to incorporate ultrafine grinding at the right stage of the circuit such that the recovery is not compromised due to overgrinding and at the same time good liberation is achieved to yield good recovery and product quality.

The impact of the grinding environment plays a vital role on the flotation performance of sulphide minerals. According to studies by Cullinan et al (1999) and Johnson (2002), the corrosion products of steel grinding media affect flotation performance by precipitating on the mineral surfaces. According to work conducted by Johnson (2002), sulphide minerals are more noble than the grinding media used during comminution as a galvanic couple between the media and sulphide minerals exist, this increases the rate of corrosion of grinding media. The corrosion products of the grinding media precipitate on the surface of the sulphide minerals thereby affecting its flotability. Grano et al (1994) found that this effect is more pronounced on the fine size fractions due to the high surface activity.

2.7 Effect of particle size on oxidation rate

According to Clarke et al (1995), oxidation arises from dissolution of minerals and grinding media. The surface oxidation products consists mainly of metal hydroxides and sulphur-oxy species. The sulphide mineral acts as a cathode for the steel grinding media thereby accelerating the rate of corrosion. The adsorption or precipitation of these oxidation products on mineral surfaces prevents the reagents such as collector to reach the targeted minerals thereby negatively influencing the flotation process. The galvanic interaction model is shown in Figure 2.16. According to Clarke et al (1995), oxidation is more on the fine particles due to the larger surface area.

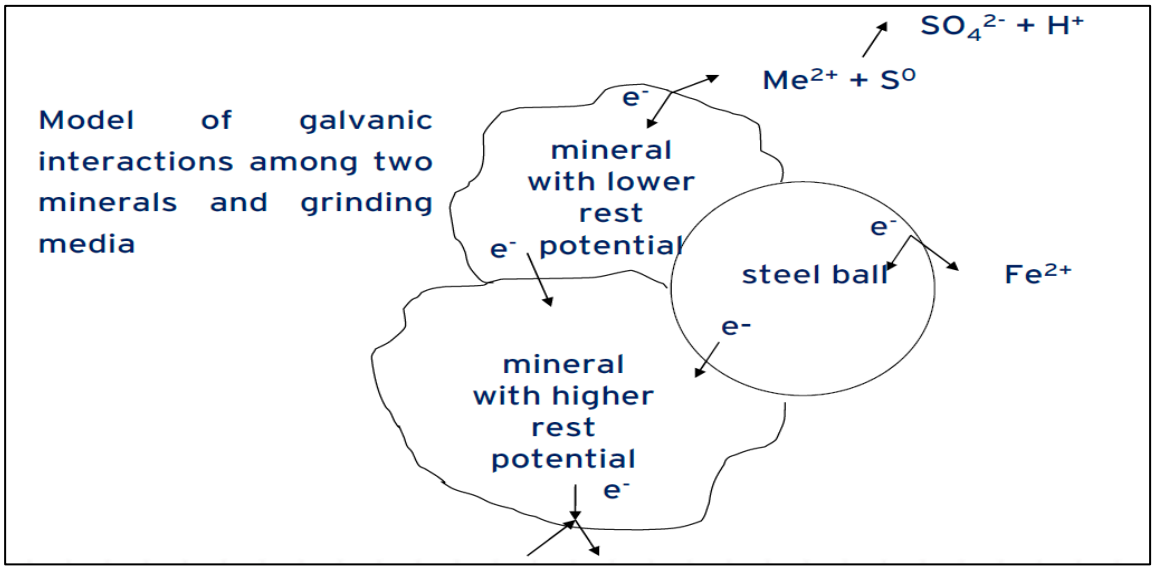

Figure 2.16: Galvanic interactions model (Greet, 2019)

The effect of oxidation on the flotation behavior of Nickel-Copper ores was also explored by Kelebek (1993). Surface oxidation is one of the most important factors that influence the flotation selectivity and recovery in the processing of complex sulphide ores. It is an inherent part of surface chemical reactions that determine whether the surface film formed on a sulphide mineral will be hydrophobic or hydrophilic. Sulphide minerals are subjected to increasing surface oxidation during various milling stages. Kelebek (1993) found that the ease of individual mineral floatability under normal aeration conditions, is:

- Chalcopyrite > pentlandite > pyrrhotite, and it changes to

- Pentlandite > chalcopyrite > pyrrhotite under oxygen-deficient conditions

Lu et al (2018) reported on the effect of particle size on oxidation and flotation behavior of galena particles. Figure 19 shows some of the results by Lu et al (2018). According to the work conducted by Lu et al (2018), the amount of oxidation products extracted using EDTA increased with the decrease of particle sizes. The flotation performance further supported the results obtained from the dissolution tests with the flotation response indicating poor performance for the fine fraction. This was attributed to the high surface area, which increases the rate of oxidation. Despite the increase in the sorption rate of collector with decrease in particle size, the formation of the hydrophilic layer product layer caused by the dissolution of galena is more dominant. This renders the mineral hydrophilic. These results indicate that ultrafine grinding leads to a higher rate of oxidation of sulphides and thus has the potential to result in poor metallurgical performance. Lu et al (2018) also concluded that for fine particles the oxidation was strongest at a pH of 7.3. This work by Lu et al (2018) and Kelebek (1993) indicate the need to recover material after each milling stage to minimize oxidation.

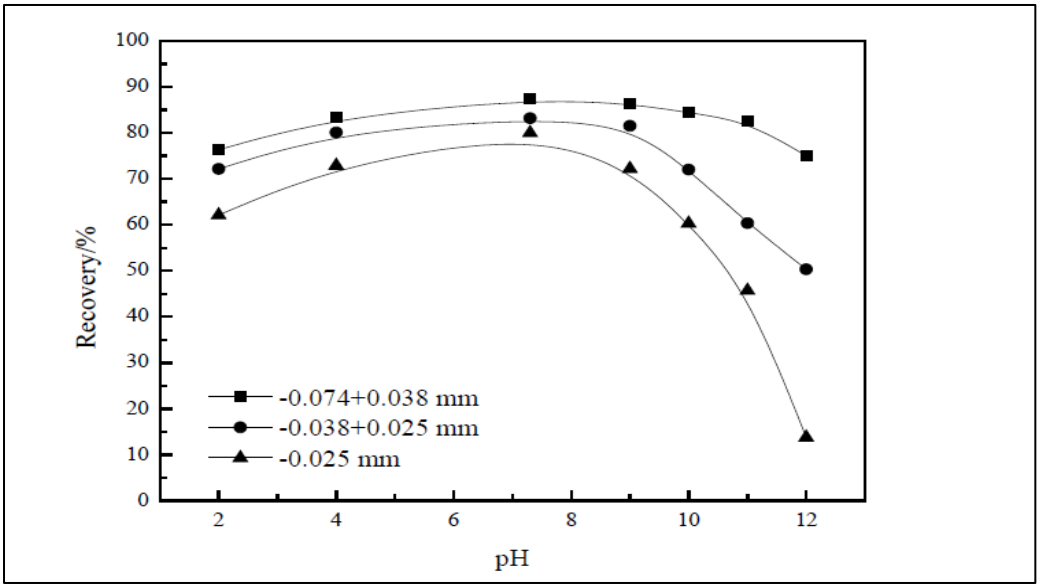

Figure 2.17: Flotation behavior of the three different size fractions of galena (Lu et al, 2018)

2.8 Alternative circuit configuration

According to work conducted by Pease et al (2006), to optimize the circuit performance there is a need to design both the milling in conjunction with the flotation stage to suit the liberation characteristics of the ore. This however results in several stages of grinding and flotation,

recovering the mineral as soon as it is liberated and applying further grinding energy only to those particles that still need liberation. This work highlights the importance of circuit configuration on the process efficiency. This multi milling and flotation stage configuration also assists in controlling the product quality by minimizing liberation of floatable gangue.

Steyn (2012) conducted some work on different circuit configurations using the platinum-bearing UG2 ore. Steyn (2012) deduced that for UG2 ore, the introduction of multiple mill-float stages has the potential to increase recovery in both fine and coarse size fractions. In the fine fractions, multiple mill-float circuits recover liberated particles at incremental intervals and thereby reducing losses due to overgrinding.

The work by Pease et al (2006) also justifies the metallurgical benefit of a stage wise mill-float circuit. The proposed multi mill–float circuit configuration for Mogalakwena North Concentrator is depicted in Figure 2.18 below. This circuit involves decoupling the secondary mill stage and tertiary milling stage by introducing a flotation stage in between the two. The logic behind decoupling the two is to recover the material liberated in the secondary grinding stage before overgrinding it in the tertiary milling circuit.

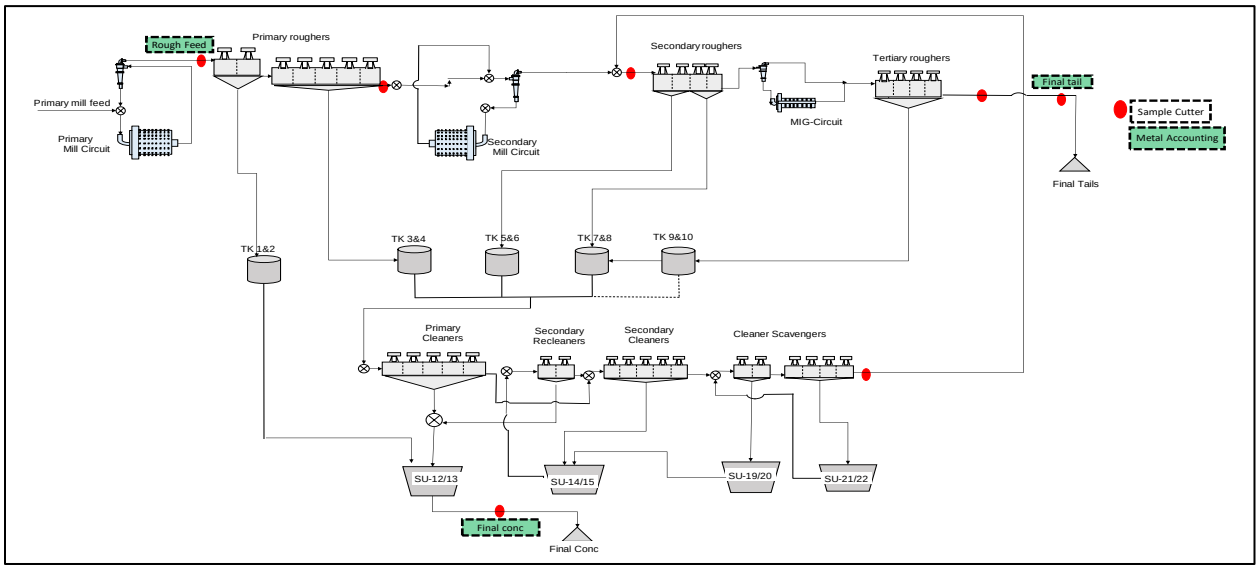

Figure 2.18: Mill-Float-Mill-Float-Mill-Float (MF3) wet circuit configuration

2.9 Summary of the literature review

The following insights can be drawn from the literature review:

(I) The base metal sulphide grain size is relatively coarser than the platinum group metal grain size, to maximize recovery of both base metals and platinum group metals the circuit need to be designed to recover the base metals at a coarser grind before further grinding to maximize the recovery of platinum group metals

(II) Overgrinding reduces the probability of collision between the particle and the bubble which has a negative effect on the efficiency of the flotation process

(III) Multi mill-float stages have the potential to improve process efficiency by incremental recovery of liberated material thereby minimizing overgrinding

(IV) There is an inverse relationship between particle size and entrainment. Entrainment is not selective thus has a negative impact on product quality

(V) Fine particles have a high surface activity for adsorption of reagents thus the generation of fines has the potential to increase reagent consumption

(VI) Fine particles exhibit a high surface activity which increases the rate of oxidation thereby negatively affecting the process efficiency

(VII) There is merit in testing an alternative circuit configuration which will minimize overgrinding thereby contributing to the knowledge of how to unlock full value from the Platreef ore type mineralization

---

CHAPTER THREE

EXPERIMENTAL MATERIALS AND METHODOLOGY

“All truths are easy to understand once they are discovered; the point is to discover them”. ~ Galileo Galilei

3.1 Introduction

In this chapter, the materials, equipment, methodology and analytical techniques that were used are discussed in detail. The process of sampling the ore, ore characterization and reagents preparation is discussed. Also, discussed in this chapter is the experimental design, the sampling techniques and the comparison techniques that were used.

This study focused on evaluating the metallurgical impact of decoupling the secondary mill circuit from the ultra-fine grinding circuit.

3.2 Ore sampling and characterization

3.2.1 Ore sampling and crushing

A sample of the product from the crushing circuit was taken at Mogalakwena North Concentrator. The crushing circuit product stream at Mogalakwena North Concentrator has a top size of 10 mm. The bulk sample was taken to Mintek for further crushing to obtain a product of 100% -3 mm. The top size from the plant had to be reduced from 10 mm to 3 mm because the ball mill at the pilot plant can only treat a top size of 3 mm. A jaw crusher in closed circuit with a 3 mm screen was used. After crushing, the sample was split into 100 kg bags. Sub-samples were taken to check the efficiency of the splitting process by means of a particle size distribution

3.2.2 Density determination using a pycnometer

Gas pycnometry is a common analytical technique that uses a gas displacement method to measure volume accurately. Inert gases such as helium or nitrogen are used as the displacement medium. The sample is sealed in the instrument compartment of known volume, the appropriate inert gas is admitted, and then expanded into another precision internal volume. The pressure before and after expansion is measured and used to compute the sample volume. Dividing this volume into the sample weight gives the gas displacement density.

3.2.3 Bond Ball Mill Grindability Index

A Bond tumbling ball mill measuring 305 x 305 mm inside diameter with no lifters (smooth shell) is used. It is operated at 70 rpm (fraction of critical speed (fCs) = 0. 91) and is equipped with a revolution counter. The ball charge consists of 285 steel balls weighing 20.125 kg representing a ball charge filling of 19.2% by volume. The ball size distribution ranges from a top size of 38.10 mm to 15.87mm. Various limiting screen sizes ranging from 850 µm to 25 µm can be used. For practical purposes, the work index (Wi) of the ore sample is usually determined at the following limiting screens: 300, 212, 150, 106 and 75 µm, although any specified limiting screen can be used depending on the desired product grind. Each limiting screen requires about 5 to 10 kg of representative sample, which is staged-crushed to 100% passing 3.35 mm to minimize fines generation. The crushed material is blended and split into 500 to 600 g-lots to facilitate addition, and minimize particle segregation, of the make-up fresh sample. From these lots a sample was used for size analysis of the feed (to obtain F80) and the rest for the actual test-work. The feed material is classified using the $\sqrt{2}$ ratio sieves of screen sizes. After the first grinding period of 100 revolutions, the mill product is screened on the limiting or closing size screen. The undersize is weighed and a fresh amount of unsegregated feed equivalent to the mass of the undersize is added to bring the mass back to the original mass. The number of revolutions needed is determined from the results of the previous period to produce sieve undersize equal 1/3.5 of the total charge in the mill. The grinding period cycles are continued until the net grams of sieve undersize per mill revolution reach equilibrium. An average value of the last three net grams per revolution (Gbp) of undersized material produced is then obtained. The ball mill work index (kWhr/t) is calculated using the Bond revised equation (Napier-Munn et al, 2005)

3.3 Equipment and Materials

The list of the main equipment used for the survey campaign is shown in the Table 3.1 below.

3.3.1 List of main equipment

Table 3.1: Flexi-float test rig main equipment

Primary Mill	0.920 m×0.636 m
Primary mill discharge screen	600 µm
Primary roughers	8×8.5 L
Secondary mill	0.900 m × 0.610 m
Isa-mill	1×M4
Secondary roughers	8×8.5 L
Tertiary roughers	3×10 L
Primary cleaners	12×1.7 L
Secondary cleaners	12×1.7 L

Figure 3.1 below shows some of the equipment used for the campaign.



Figure 3.1: Grinding disk and shaft of M4 IsaMill and flexi-float flotation cells

3.2.2 Reagents

The same reagents used at Mogalakwena North Concentrator were used for the pilot testwork and these are supplied by Senmin. The overall dosage rate was kept constant for the back to back surveys.

Table 3.2: Flotation reagents and dosages

Reagent	**Reagent group**	**Dosage**
Collector (Sodium isobutyl xanthate)	Xanthate	273 g/t
Promotor (Senkol 3)	Dithiophosphate	46 g/t
Frother (Senfroth 516)	Polygycol	130 g/t
Depressant (Norilose 6064)	Carboxymethyl cellulose	306 g/t

3.3 Experimental design

In order to eliminate the effect of a systematic change throughout the period of the trial, the following sequence shown in Table 3.3 was followed for the test-work schedule:

Table 3.3: Testwork schedule

Run1	Base Case	MF3
Run 2	Base Case	MF3
Run 3	MF3	Base case

3.4 Survey Process

1) A hazard and risk identification exercise was carried out before any of the tasks were conducted. The prescribed PPE for the various tasks was worn when the various tasks are conducted. The equipment were operated as per the standard operating procedure for the pilot plant.

2) All the pumps were calibrated prior to commencing the campaign. The pump calibration curve is shown in Appendix B. The mass of the IsaMill media used for trial was kept at the same mass.

3) Reagents were prepared to the desired active content a day before the actual survey campaign. The active content was validated by making use of a refractometer.

4) A practice run was conducted a day before the actual day of the sampling campaign to make sure all the equipment was running well and to build up residual reagents in the process water. The pre-run time duration was between 3 to 4 hours. Air and level calibration for the flotation cells were conducted and recorded for future reference. During this time the setting of operational parameters were set and maintained constant during the duration of the test campaign. The operating parameters of concern are primary mill feeder speed, inlet water, cell level and air and tertiary grinding mill media loading. This pre-run was also done to generate process water (buildup reagents concentration in the recycled water to mimic plant conditions) for the actual runs. Calibration of the air rates at different air supply pressure is shown in Appendix B. In addition, this also helped to remove some rust from the steel balls in the two ball mills.

5) The ore sample was processed through the specific circuit configuration for a minimum of eight hours with samples taken on an hourly basis. The primary mill discharge density, cyclone underflow and cyclone overflow density and the IsaMill feed density were also measured every hour and recorded on the dashboard to keep track of the operating parameters and make adjustments in the event of process deviations.

6) Concentrate samples were taken from each flotation cell at the same time at as per the set sampling interval using an automated sampling system. The concentrate mass collected was measured every hour to estimate the mass pull. The dashboard strategy used allowed the team to control the densities across all streams, estimate cells concentrate mass pulls, monitor cyclone performance and record all variation of the input data.

7) Pulp chemistry data was measured using the TPS meter. Three readings were taken per run.

8) A sample of the feed and product from each grinding stage was taken to understand the PSD and the liberation. Specific energy data was also calculated

9) Samples were taken as illustrated in Figure 3.2 and Figure 3.3. The pilot plant utilizes an automated sampling system which is programmed to take all the samples at the same time. A minimum of 6 increments were taken per stream during the duration of the survey. Each survey campaign was run for a minimum of 8 hours. A composite sample for the 8 hour period was prepared for each stream.

10) The circuit was then reconfigured to a different trial setup while keeping the air, level and reagent dosage settings constant. The flexi-float runs were conducted until the three runs for each circuit configuration were achieved.

11) The samples collected were prepared as per the Anglo Standard Procedures for sample preparation. The samples were split in order to have a representative sample for particle size distribution, assay analysis and mineralogy. Key for the mass balancing process were the assay results for each concentrate stream and the tailings streams assay results for each bank. This balanced data was required to quantify the recovery of each flotation cell and hence enable one to conduct a down the bank analysis. Each back to back campaign generated a total of 168 samples for assay analysis.

Figure 3.2 and Figure 3.3 depict the flexi-float set-up for the MF2 and MF3 circuit configuration respectively. The cleaner circuit was setup as an open circuit meaning the cleaner tailings stream was combined with the tertiary rougher tailings to make up the final tailings stream.

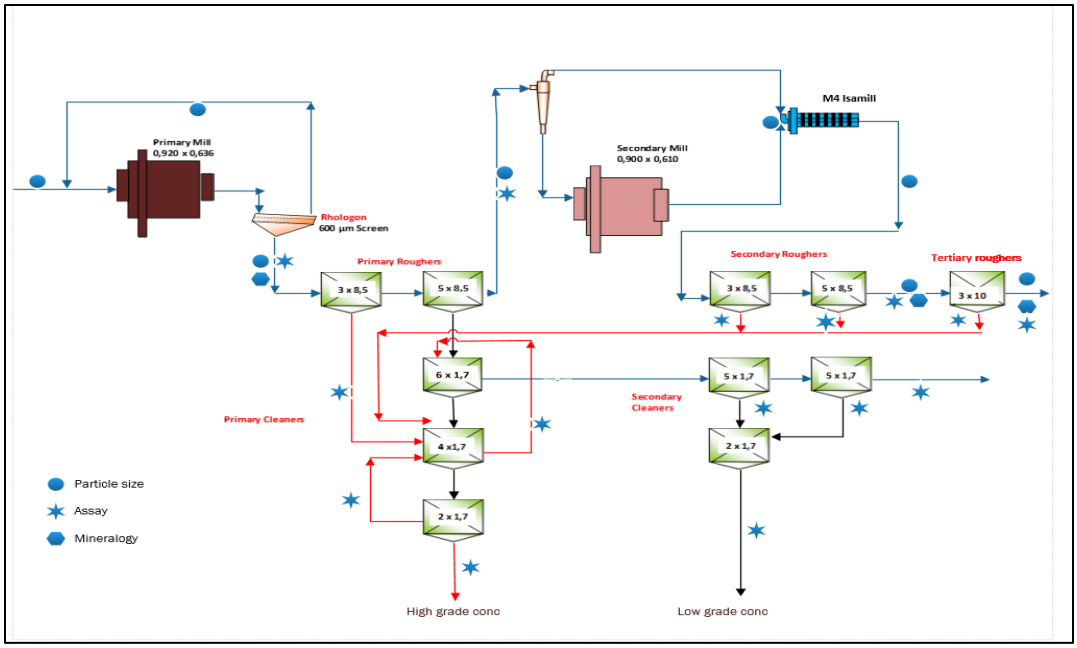

Figure 3.2: Flexi-float MF2 circuit sampling points and analysis conducted

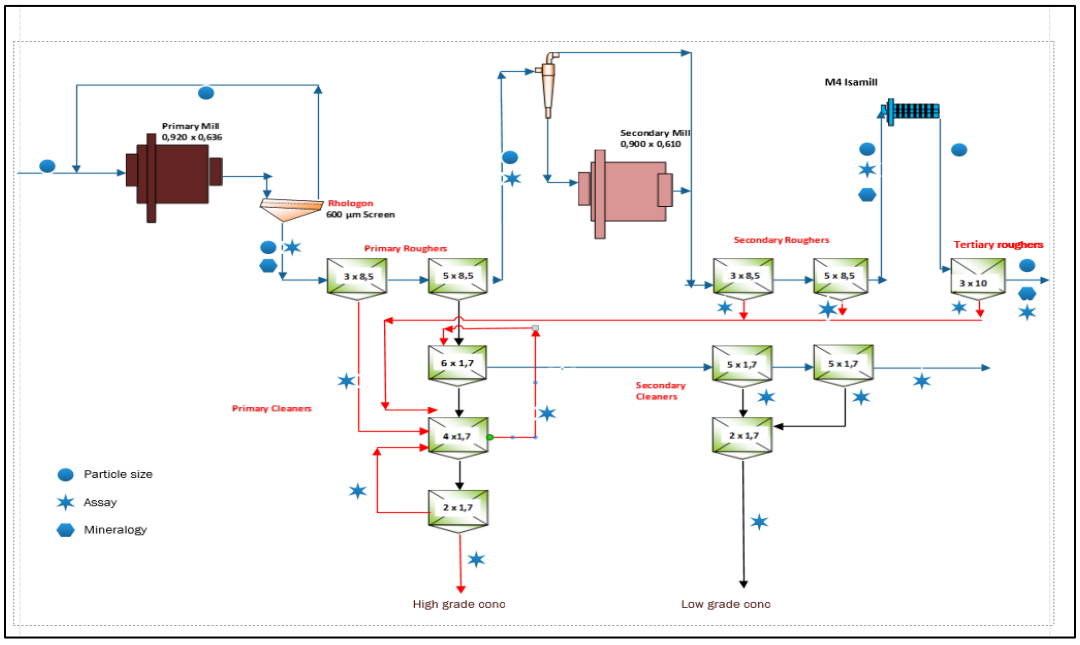

Figure 3.3: Flexi-float MF3 circuit sampling points and analysis conducted

Table 3.4 summarizes the number of campaigns that were conducted. One of the challenges encountered during the pilot plant trial was the failure of the IsaMill during the run that was conducted in May 2019. The parts required to fix the mill were not available in stock and had to be imported resulting in a significant delay in the project. The lesson learnt from this unwanted

event was the need to keep all the parts with a long lead time in stock. The results of the run conducted in May 2019 thus do not form part of this report.

Table 3.4: Flexi-float throughput and running time

Flowsheet	Date Run	Milled	Running Time	Campaign Run No
MF2	14-Mar-19	656	7.00	Run No1
MF3	15-Mar-19	701	7.5	
MF2	09-Apr-19	764	8.50	Run No2
MF3	10-Apr-19	740	8.50	
MF3	28-May-19	M4 ISA Mill Breakdown (MF2 run conducted but MF3 run could not be conducted)		Run No3
MF2	29-May-19			
MF2	26-Sep-19	791	9.00	Run No4
MF3	27-Sep-19	714	8.00	

3.5 Analytical techniques

The use of sieves with different sized mesh is one of the oldest, most reliable, and most commonly used methods for providing an analysis of particle size distribution. The commonly used particle size analysis is determined by passing the sample through a series of sieves of known apertures. The sample goes through sieves of progressively smaller aperture and the mass of the sample retained on each sieve is measured to determine the size distribution. This method was applied to determine particle size distributions for this test-work

Fire assay with gravimetric finish was used for the analysis for quick turnaround to test the proof of concept. For this technique a 5 g sample is mixed with lead flux. It is then fused in a furnace. The resulting lead button is then separated from the slag. Silver is then driven off at 300 degree Celsius. The lead button is then subjected to cupellation, for absorption of lead. The resulting prill is then weighed on a micro-scale. Nickel sulphide collection coupled with an inductively coupled plasma optical emission spectroscopy wet chemistry analysis was used for the final results due to the accuracy of the method. This procedure uses nickel flux, which is a better collector than lead flux, provides more accurate results for individual elements but requires more time. The sample is fused in the furnace using a nickel flux. The nickel button is separated from the slag,

allowed to cool then it is pulverized before leaching in aqua regia. The wet chemistry analysis is conducted in an inductively coupled plasma optical emission spectrometry device (ICP-OES).

The mineral liberation analyzer was used to determine the liberation indices in the rougher feed, secondary rougher tail and tertiary rougher tailings samples. The mineral liberation analyzer is a scanning electron microscope that takes measurements based on a backscattered electron image analysis. These machines are capable of measuring grain size, mineral association, porosity, and bulk modal mineralogy. According to Sylvester (2012), the scanning electron microscope generates a beam of electrons in a vacuum that is focused by a series of electromagnetic lenses separated by apertures in the electron column and scanned in raster pattern over a specific area of the rock or sediment sample. Backscattered electrons reflected off the minerals are collected on a screen to produce an image. Electrons that interact with the minerals generate X-rays with energy levels that are characteristic of the elements present. This technique identifies and maps mineral particles with a high backscattered image intensity using set grey levels. The detected particles are then analysed using dispersive x-ray analysis information on the precious group metals and base metal sulphides of interest is collected. The MLA software for automated mineralogy integrates the images and the X-rays to identify the minerals and map their distribution.

3.6 Data Analysis

The assay data together with the process data measured during the survey proceedings were used for the mass balance. The MS Excel tool was used for the mass balance. The matrix method was used for mass balancing. When using the matrix method for mass balancing the circuit is described in terms of the following:

1) A connection matrix which describes how the streams and units are connected
2) The identifiable constituents of the feed entering the circuit (elements, total mass, water
3) Split ratios of these constituents in units in the circuit
4) Mass flows of these constituents in the tail and concentrate streams exiting units

Flotation cells split the input stream to two products, a concentrate stream and a tailings stream. The split ratio is calculated for every unit where the input streams are split into two product streams. The split ratio is calculated as follows

$$g_{i,j} = \frac{M_{i,j}}{T_{i,j}}$$ *Equation 12*

$M_{i,j}$ is the mass flow of component i in the concentrate of unit j

$T_{i,j}$ is the mass flow of component i in the tailings of unit j

$g_{i,j}$ is the split ratio of component i in unit j

To setup the connection matric, a circuit consisting of n units is described by an n x n array. The connection matrix, X, is then constructed as follows:

1) Each unit in the circuit is numbered from 1 to n
2) Each element in the array indicates a stream received by unit [Row No] from unit [Column No]

    - Row 1 of the array records all the input streams to unit 1
    - Row 2 records all the input streams to unit 2 etc
    - The columns indicate which unit the stream came from

3) If a unit receives no streams from another unit: 0
4) If a unit receives a tails stream from another unit: 1
5) If a unit receives a con stream from another unit: g_{unit}
6) The left to right diagonal of the array is the stream exchange of a unit with itself, ie. -(1+g_j) (j=1 to n)

After setting up the connection matrix, the balanced data is calculated using the feed constituents, guessed spilt values and the connection matrix.

$$T = -M_{ij}X^{-1}$$ *Equation 13*

T_j is the mass flow of component i in the tails from unit j

C_j is the mass flow of component i in the con from unit j

g_j is the split ratio of component i in unit j

M is the mass flow of component i in the circuit feed

j_j is the fraction of mass flow rate of component i in the feed to unit j

X^{-1} is the inverse of matrix X

The sum of squared errors between the balanced data and measured data is then calculated. The solver tool is then used to minimize the sum of squared errors by manipulating the split ratios. A comparison of the balanced data and raw data is conducted to assess the data integrity. The mass balance results were used to compare the metallurgical performance of the two circuit configurations. The key output parameters were mass pull, recovery and concentrate grade.

3.7 Comparison Techniques

The change introduced decouples the secondary milling circuit and the tertiary milling circuit. This influences the performance of the mainstream circuit. In this study, the comparison between the two circuit configurations focused on the performance of the mainstream. A graphical presentation of recovery kinetics for different circuit configurations were plotted on the same axis for comparison. The kinetic curve graph is a plot of cumulative recovery against residence time. The cumulative recovery is calculated as the cumulative recovery down the bank. The residence time was calculated by dividing the cumulative flotation cell volume by the flow rate. Grade recovery plots for the different circuit configurations were plotted on the same axis. A cost benefit analysis incorporating the additional costs associated with operating the MF3 circuit was conducted.

A two sample t-test was used for the comparison of the process input parameters for the two trial conditions. To conduct a two-sample t-test one must first understand whether the variance between the two data sets is equal or not. The test for equal variance can be conducted using either the Levene or the Bartlete test. The Levene test is applicable if the data set is coming from a non-normal distribution whereas the Barlete test is applicable for a data set coming from a normal distribution. The Anderson-Darling normality test was used to determine if the data is coming from a normal distribution or not. For data that is non-normal, the Mann-Whitney Test was used to compare the median. Figure 3.4 below indicates the approach taken for the statistical comparison.

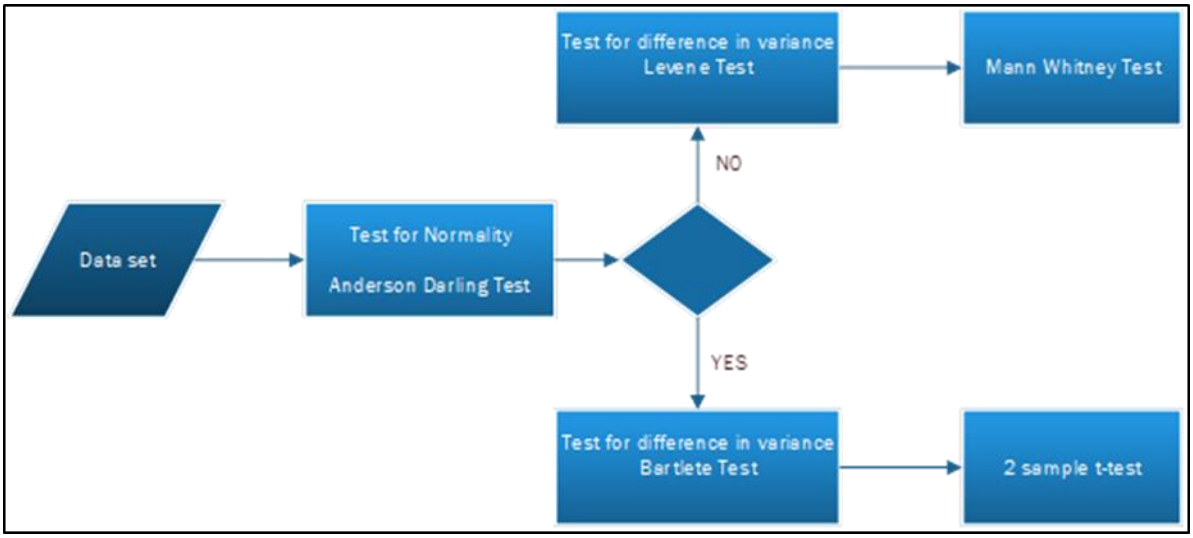

Figure 3.4: Approach to data set comparison

One of the key relationships which is used to define the performance of a concentrator plant is the relationship between concentrate mass pull or mass yield and upgrade ratio (concentrate grade divided by feed grade). This relationship can typically be defined by the following equation and Figure 3.5.

$$Upgrade\ ratio = A\ x\ \ Mass\ pull^{-b} \qquad \textit{Equation 14}$$

Where A, b are coefficients from fitting an exponential equation to the above relationship

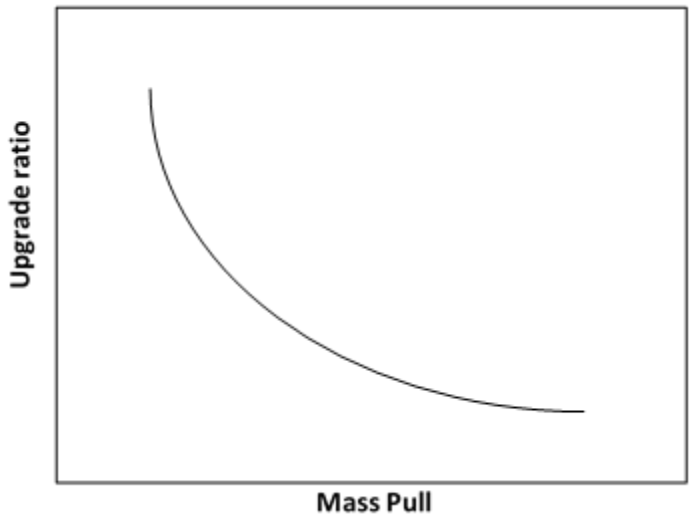

Figure 3.5: Mass pull vs. upgrade ratio graphical relationship

Recovery can be calculated by the product of mass pull and upgrade ratio.

$$Recovery = \frac{C_m c_g}{fF} = Mass\ Pull\ x\ Upgrade\ ratio \qquad Equation\ 15$$

Where:

c_g is the concentrate grade (g/t or %)

f is the feed grade (g/t or %)

C_m is the concentrate mass produced (kg or tons)

F is the feed mass treated (kg or tons)

Mass Pull can be defined as C_m/F; and upgrade ratio as c_g/f.

As much as the graphical comparison can be used with confidence to compare the metallurgical performance between the two processes, it is vital to quantify the difference statistically. The technique used for the statistical comparison is well documented by Napier-Munn (1998). This methods provides a guide to make statistically valid decisions when comparing cumulative data.

3.6 Data validation

Project validation is vital as key decisions are made based on the insights drawn from the test-work. A rigorous approach was be taken to ensure the validation of this project. The following measures were be taken:

- Run a number of trials on the same circuit configuration and check for repeatability
- Statistical Analysis of the data using the 2-sample t-test tool and the Mann-Whitney test for the two different circuits in order to make robust decisions
- Comparing experimental data with the fundamental supporting theories in literature (recovery vs time, grade recovery relationship)

3.7 Assumptions

The flexi-float plant is technically a pilot plant thus it can be assumed that the results obtained are a good representation of the plant performance if the proposed changes are implemented.

When modelling the flotation rate constants, it was assumed that the components can be split into three categories, fast floating, slow floating and non-floating species.

CHAPTER FOUR

RESULTS AND DISCUSSION

“Science is not all about making predictions or performing experiments. Science is about explaining”.~ Bill Gaede

4.1 Ore characterization

The ore specific gravity was measured using the pycnometer and the results are shown in the Table 4.1 below. The average specific gravity was found to be 3.00. These results were in line with data available in the Anglo archives.

Table 4.1: Flexi-float feed ore SG

SG 1	3.03
SG 2	2.99
SG 3	2.91
SG 4	3.05
SG 6	3.05
SG 7	2.96

Table 4.2 below summarizes the results of the Bond Work Index test which were carried out.

Table 4.2: Bond Work Index determination

CYCLE	TIME		REVS	FEED U/S	PROD U/S	NET U/S	Gms/Rev	NEW U/S	REQ U/S
	Min	Sec							
0				185.57					
1	5	12	364	185.57	500.89	315.32	0.87	65.84	337.9
2	5	34	390	65.84	413.89	348.05	0.89	54.41	349.3
3	5	41	397	54.41	410.99	356.58	0.90	54.02	349.7
4	5	35	391	54.02	411.99	357.97	0.92	54.16	349.6
5	5	30	386	54.16	410.89	356.73	0.93	54.01	349.7
6	5	26	380	54.01	408.09	354.08	0.93	53.64	350.1
7	5	23	377	53.64	405.39	351.75	0.93	53.29	350.5
8	5	22	376	53.29	406.39	353.10	0.94	53.42	350.3
9	5	21	374	53.42	402.49	349.07	0.93	52.91	350.8

Figure 4.1 shows the particle size distribution of the feed sample which was submitted for the abrasion test and the product size distribution profile.

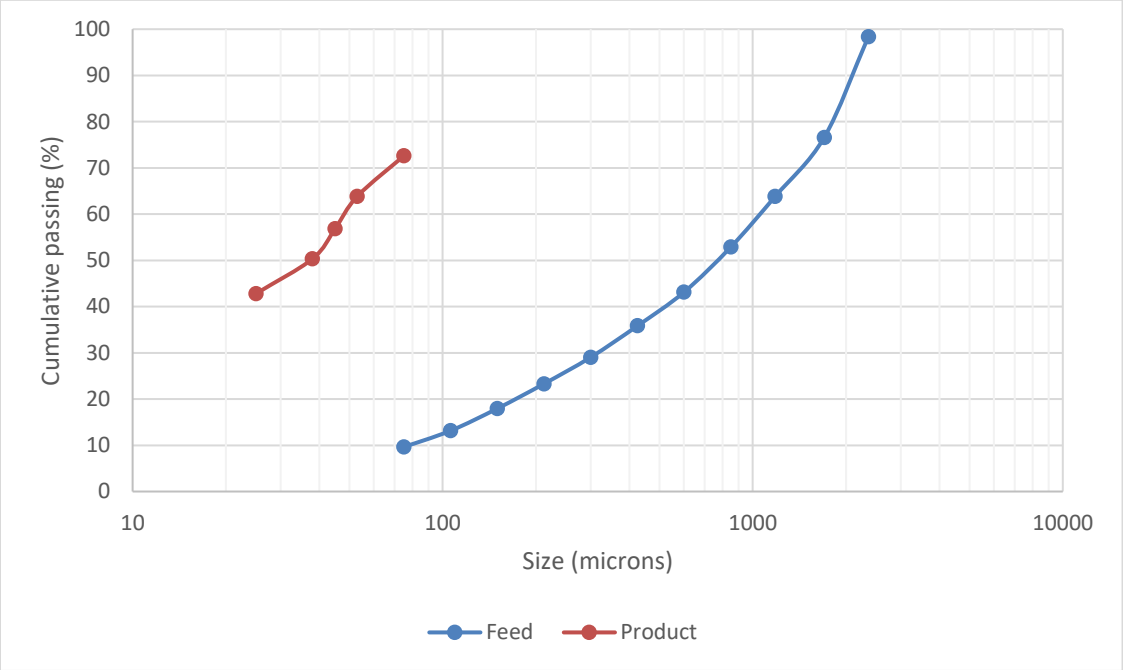

Figure 4.1: Feed and product size distribution profile

Table 4.3: Bond Work Index

			No of Cycles	7	10	
Type of Test	BWI 106		Bond grindability	0.939	0.933	g/rev
Sample Description	MNC		Final test CLR	233.3	250.5	%
Sample ID	MINTEK		F80	1803.48	1803.48	µm
			P80	84.77	84.82	µm
			BWI	21.79	21.91	kWhr/t

The bond work index was conducted using a closing screen of 106 microns. The bond work index was found to be 21.79 kWh/t and 21.91 kWh/t. This was in line with historical measurements available in the Anglo archives for the Platreef ore as shown by the bond work index for the drill core samples in Appendix A.

After crushing and splitting the sample at Mintek, the efficiency of the split was assessed by measuring the particle size distribution of the different portions. Figure 4.2 indicates the particle size distribution of the different portions.

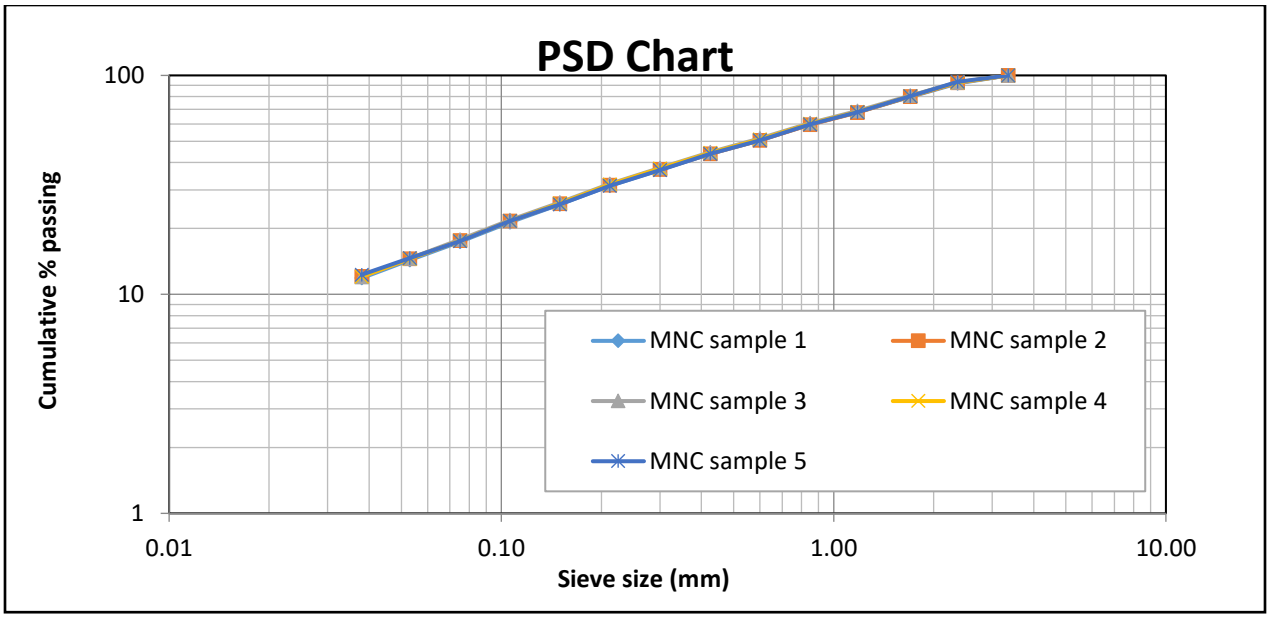

Figure 4.2: Particle size distribution of flexi-float feed

The chart indicates that the PSD of the sub-samples is comparable. This indicates that the splitting process was efficient thus the feed composition of the different runs was consistent. Any differences in metallurgical performance observed for the different runs cannot be attributed to particle size variability of the feed. The individual particle size distribution data is presented in Appendix A.

The bulk mineralogy of the feed is shown in the Table 4.4 below. This is typical of Platreef ore based on the results available in the Anglo Archives.

Table 4.4: Flexi-float feed bulk mineralogy

Mineral	PFF-1403
Pyroxene	56.1
Feldspar	19.2
Alteration Minerals	16.2
Talc	4.9
Serpentine	2.1
Amphibole	3.5
Chlorite	5.8
Mica	1.7
Carbonates	0.3
BMS	1.2
Other	5.3
Total	100.0

The base metal distribution in the feed is shown in the Table 4.5 below. This is typical of Platreef ore based on the results available in the Anglo Archives.

Table 4.5: Flexi-float feed base metal distribution

	PFF-1403
Pentlandite	30.4
Millerite	0.0
Pyrite	10.7
Pyrrhotite	38.7
Chalcopyrite	20.1
Bornite	0.0
Total:	100.0

The base metal grain size and PGM grain size distributions results for the feed are shown in the Table 4.6 and Table 4.7

Table 4.6: Flexi-float feed base metal grain size distribution

	PFF-1403
<10	8.2
<20	12.8
<40	19.2
<80	25.9
<160	23.4
<320	5.4
>320	5.1
Total:	100.0
BMS d_{50}	60
Number of particles	9363

Table 4.7: Flexi-float feed PGM grain size distribution

Grain size (µm)	Feed
<4.1	31.0
5.7	14.9
9.6	21.2
13.5	14.6
19.0	0.0
27.0	18.2
38.0	0.0
53.0	0.0
75.0	0.0
106.0	0.0
212.0	0.0
Total	100.0
p50	6.4

One feed sample was taken for mineralogical analysis based on the observation that the splitting process was efficient in producing consistent smaller representative samples. It was therefore assumed that the feed sample for each run should exhibits the same mineralogy. The ore sample exhibits the same characteristics as the feed to the plant thus it can be concluded that the ore sample used for the trial on the flexi-float test rig is representative of the plant actual plant feed. From the grain size analysis, it is apparent that the PGM grains are very fine compared to the base metal grain sizes. This supports the need to adjust the circuit configuration to minimize overgrinding of the base metals but at the same time ensuring liberation of the PGMs.

4.2 Campaign number 1

A comparison of the comminution power intensity is shown below. A t-test analysis was conducted to compare the means of the power used at the different comminution stages for data exhibiting normal distribution and the Mann-Whitney test was used for non-normal data.

Table 4.8: Campaign 1 Power Intensity comparison

	MF2 (kWhr/t)	MF3 (kWhr/t)	t-test p value
Primary mill	30.05	32.82	0.01
Secondary mill	20.94	21.29	0.79
IsaMill	16.09	15.98	0.16

The grind comparison for the different comminution stages is shown in Table 4.9 below. It was evident that the for the MF3 circuit configuration the secondary rougher tail was coarser due to decoupling the secondary milling stage and the tertiary mill stage.

Table 4.9: Campaign 1 Grind comparison

Stream	PFF		PRT		SRT		TRT	
	(Primary Float Feed)		(Primary Rougher Tail)		(Secondary Rougher Tails)		(Tertiary Rougher Tails)	
Parameter	MF2	MF3	MF2	MF3	MF2	MF3	MF2	MF3
<75 µm	48%	50%	42%	42%	89%	69%	89%	88%
P80 (µm)	198	187	227	224	61	100	61	63
P50 (µm)	81	76	97	96	31	45	32	29
P25 (µm)	25	24	27	28	14	18	15	14

A graphical comparison of the -75 micron size class was conducted and the results are depicted in Figure 4.3 and Figure 4.4.

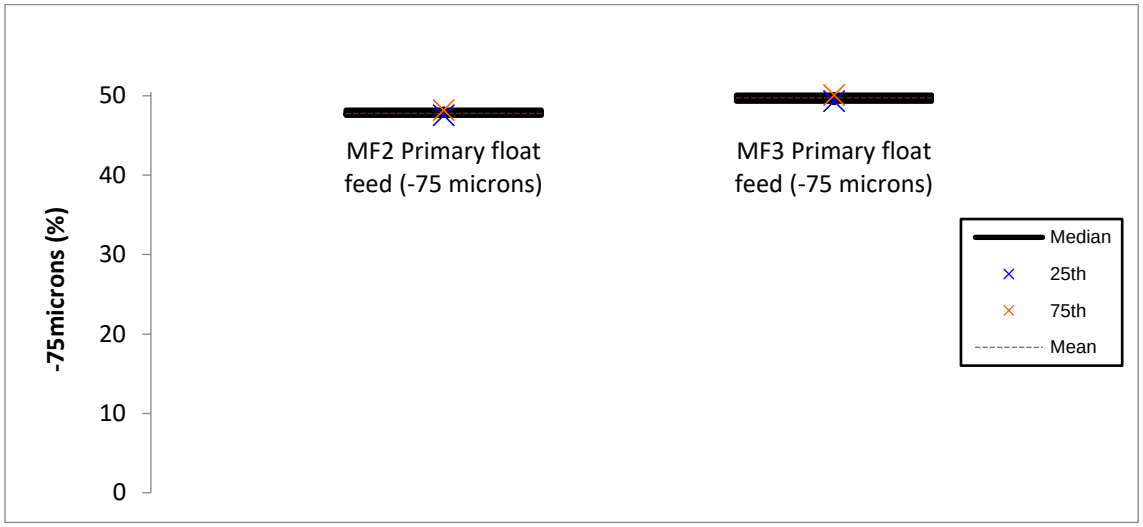

Figure 4.3: Primary mill grind cumulative passing 75 microns

Looking at Figure 4.3, the primary grind for the MF3 circuit was finer compared to the MF2 circuit.

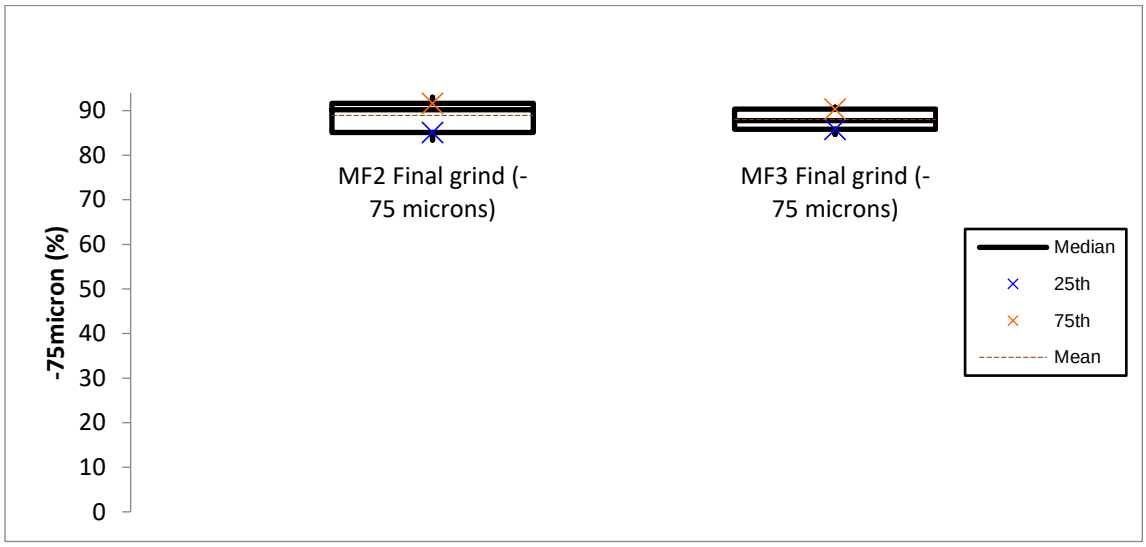

Figure 4.4: Final grind cumulative passing 75 microns

The graphical analysis for the final grind indicated that the grind was comparable for this back to back campaign. A statistical analysis was conducted to evaluate if the grind was comparable for the back to back survey.

Table 4.10: Campaign 1 Grind Statistical Analysis

	MF2	MF3	t-test p value
Primary float feed (-75 microns)	47.8	49.8	0.00
Final grind (-75 microns)	88.9	88.0	0.59

The statistical analysis on the grind indicated that the difference in the primary grind was statistically significant for the two surveys. This was in line with the observation made on the specific energy intensity comparison and the box plot in Figure 4.3. The final grind however was comparable for the two survey results. A detailed analysis of the power intensity and particle size analysis is available for reference in Appendix C.

In order to evaluate the metallurgical performance for the two trial conditions, a mass balance was conducted across the mainstream circuit units that is the primary, secondary and the tertiary roughers. The impact of decoupling the secondary milling stage and the tertiary milling stage was expected to manifest in the mainstream metallurgical performance as the flotation cells in the mainstream treat the product from the comminution circuit. The cleaner circuit mass balance was not included in this exercise. The mass balance was conducted using the matrix method. The flotation mass balance data integrity is represented in the form of parity charts.

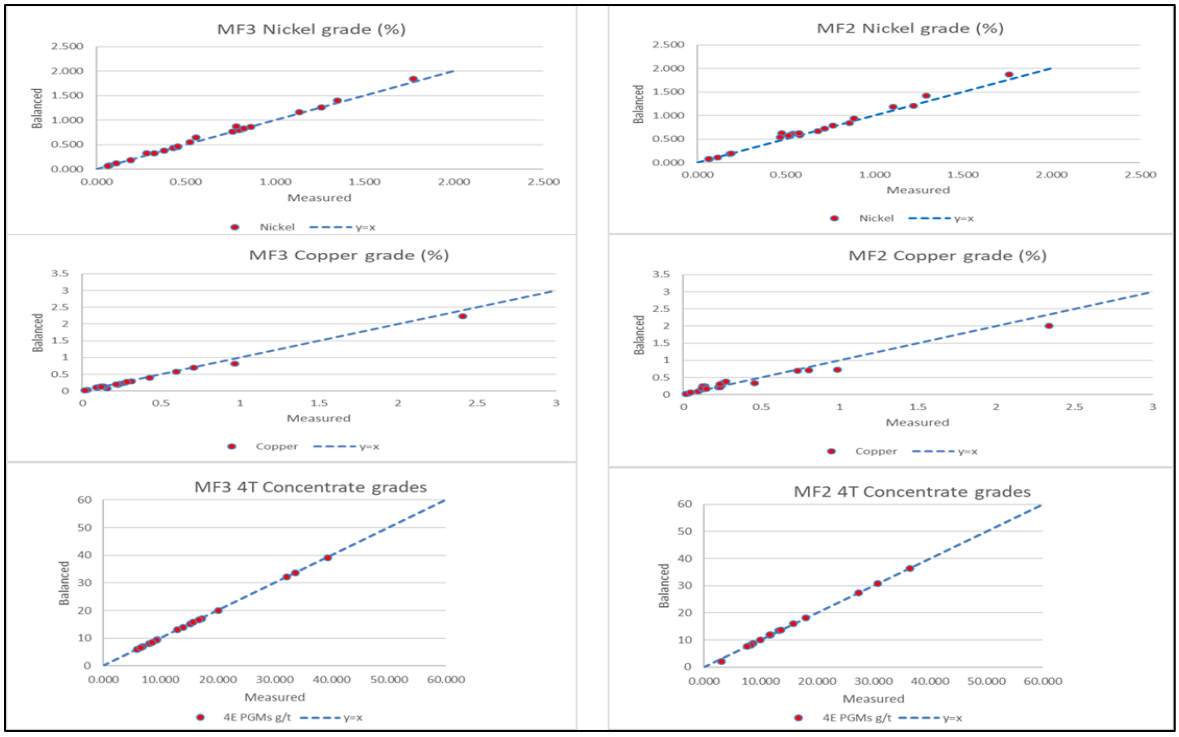

Figure 4.5: Campaign 1 mass balance data integrity

The parity charts indicated a good correlation between the measured and balanced data because most of the data points were on the line y=x. This was an indication that the reconciliation process resulted in data of good integrity.

The flotation kinetics for the base metals is shown in Figure 4.6 below. The cumulative recovery curve was split into three sections, the primary rougher circuit, the secondary rougher circuit and the tertiary rougher circuit. The recovery was calculated as the cumulative recovery down the bank. This was based on the mass balance conducted using the matrix method. The mass balance was conducted making use of the assay results of the concentrate samples collected from each flotation cell and the tailings streams samples. This enabled one to calculate the recovery of each flotation cell down the bank.

$$R_c = \frac{\sum C_j c_{gij}}{F f_i} \qquad \textit{Equation 14}$$

Where:

R_c is the cumulative recovery

C_j is the mass flow of concentrate for flotation unit j

c_{ij} is the grade of component i in the concentrate of flotation unit j

F is the feed flow

f_i is the grade of component i in the feed

The sharp gradient in the recovery when moving from one flotation stage to the other was due to the introduction of a milling stage which changed the particle flotability.

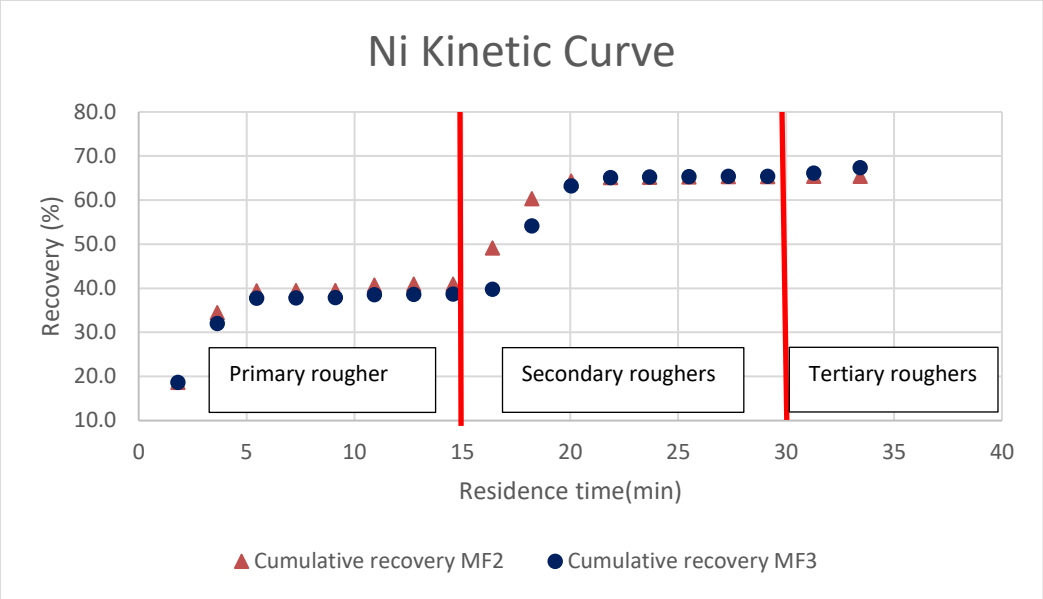

Figure 4.6: Nickel kinetic curve for the different configurations

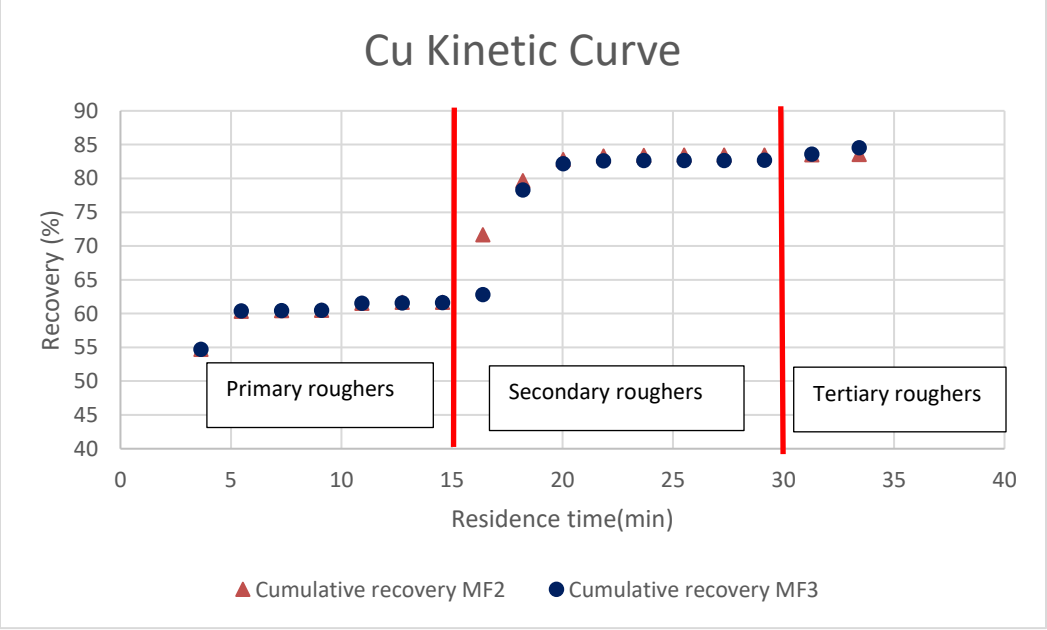

Figure 4.7: Copper kinetic curve for the different configurations

The milling stage changed the particle identity by liberating the material of value thereby resulting in the step change in recovery due to improved kinetics The work conducted by Steyn (2012) supports these observations. The difference between the MF2 and the MF3 circuit was well pronounced in the kinetic curves looking at the performance in the tertiary rougher circuit. The MF2 circuit cumulative grind reached a plateau in the secondary rougher stage after which there is minimal gain in recovery in the tertiary rougher stage. The gain in recovery in the tertiary flotation stage for the MF3 circuit was attributed to liberation as a result of grinding the secondary rougher tailings. The MF3 circuit configuration decoupled the secondary milling stage and the tertiary milling stage which meant that the tertiary grinding circuit treated the secondary rougher tailings stream. The recovery improvement observed thus can be attributed to this change in circuit configuration. Table 4.11 below summarizes the bank recoveries achieved for the different circuit configurations.

Table 4.11: Run 1 bank recoveries

	MF2			MF3		
	4T	Cu	Ni	4T	Cu	Ni
Rougher recovery	58.59	61.68	40.95	60.18	69.14	38.66
Secondary rougher recovery	23.42	21.80	24.36	21.08	13.82	26.74
Tertiary rougher recovery	**0.06**	**0.06**	**0.09**	1.98	1.56	1.91

Table 4.11 reinforced the observation mentioned earlier pertaining to the minimal recovery change when moving from the secondary roughers to the tertiary roughers for the MF2 circuit configuration.

In order to quantify the metallurgical benefit of the circuit change a relationship between upgrade ratio and mass pull was used as defined in the literature review. This enabled one to then compare the performance of the two processes at the same mass pull thus standardizing the comparison. This comparison was conducted for the mainstream flotation units using data obtained from the mass balancing process. The enrichment ratio was calculated as the cumulative concentrate grade down the bank divided by the feed grade. The mass pull was calculated as the cumulative mass pull down the bank. The concentrate grade showed a decreasing trend down the bank due to the reduction in the concentration of material of value moving from one flotation cell to the next. This resulted in a decrease in the enrichment ratio with increase in the mass pull down the bank.

Figure 4.8 and Figure 4.9 are graphs illustrating the enrichment ratio against mass pull relationship for the base metals. The analysis to quantify the size of the benefit focused on base metals only and not platinum group metals because floating the secondary mill product in the MF3 treats a coarser product stream compared to the finer product from the tertiary circuit. The hypothesis therefore was that this will benefit the coarser grained base metal sulphides. There was however a benefit in the PGM recovery due to the association of the PGMs with base metal sulphides in the Platreef ore this however was not considered in quantifying the size of the benefit.

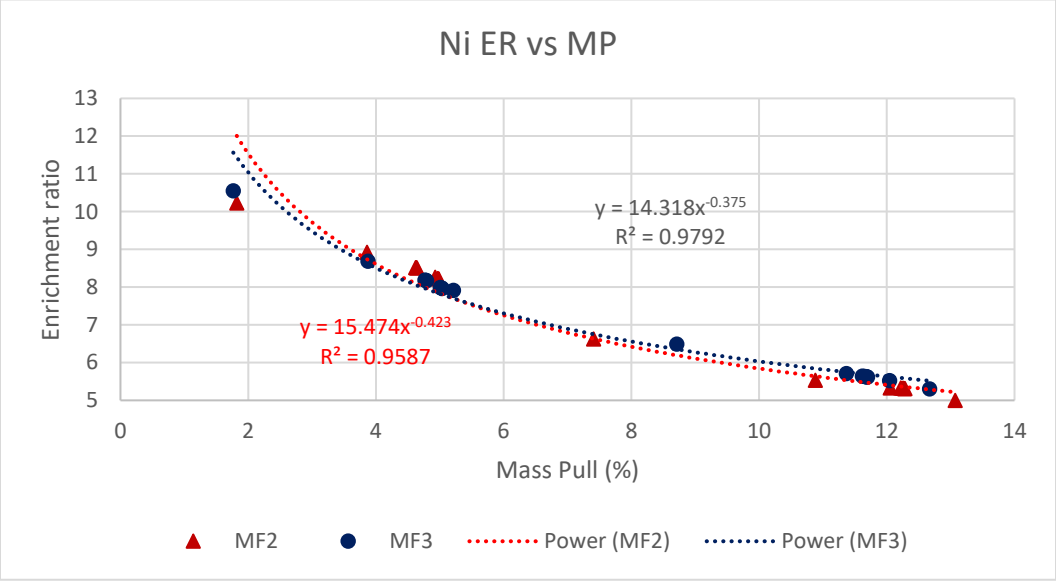

Figure 4.8: Enrichment ratio vs mass pull relationship

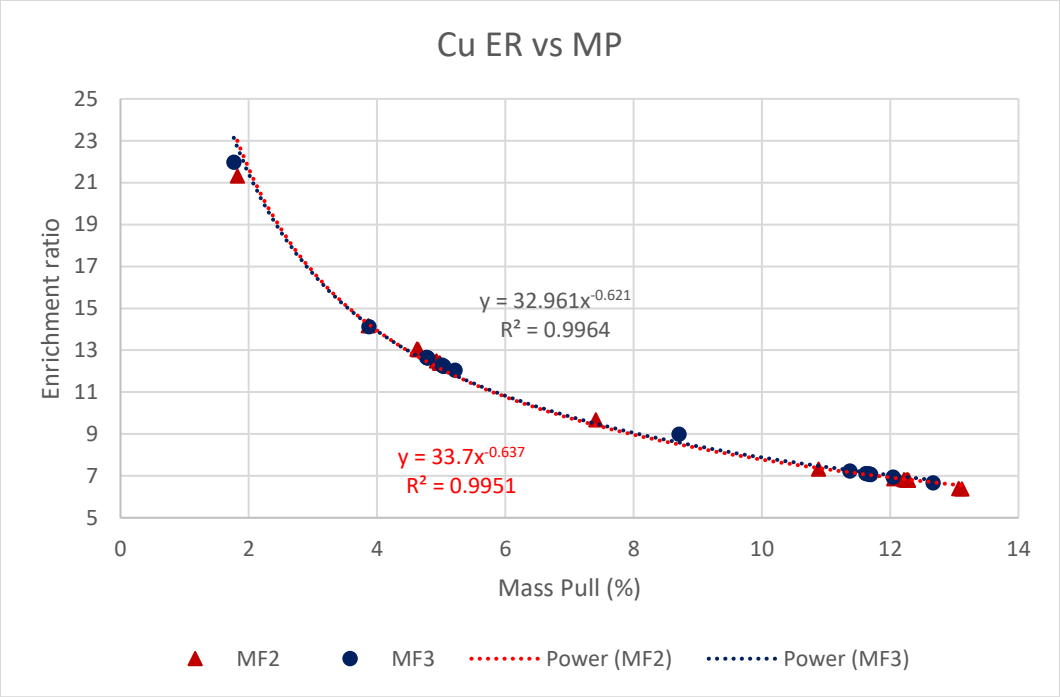

Figure 4.9: Enrichment ratio vs mass pull relationship

A power model fitted and defined the profile well for both MF2 and MF3 configurations as indicated by the R^2 values. The general trend indicated that at mass pulls beyond 8%, the MF3 circuit yielded a better concentrate grade compared to the MF2 circuit at the same mass pull for nickel. This indicated the poor selectivity of the MF2 process after the tertiary grinding circuit. This was also observed visually during the trial when looking at the bubble loading. The bubbles had a high solids loading which was attributed to a higher entrainment rate for the MF2 circuit. The work done by Engelbrecht and Woodburn (1975) confirmed these observations. The recovery comparison was then conducted at 12% mass which is comparable to the plant mainstream mass pull. The table below summarizes the recovery comparison based on the enrichment ratio vs mass pull models.

Table 4.12: Campaign 1 recovery comparison

	MF2			MF3			
	A	b	Recovery (%)	A	b	Recovery (%)	Δ Recovery (%)
Copper	33.7	-0.6	83.1	33.0	-0.6	84.5	1.5
Nickel	15.5	-0.4	64.9	14.2	-0.4	66.9	2.0

The results indicated that the MF3 circuit outperforms the MF2 circuit configuration yielding an improvement in nickel recovery of 2.0% and an improvement in copper recovery of 1.5%.

The final tailings samples for the different circuit configurations were taken for mineralogical analysis. The figure below depicts the PGM association in different size classes.

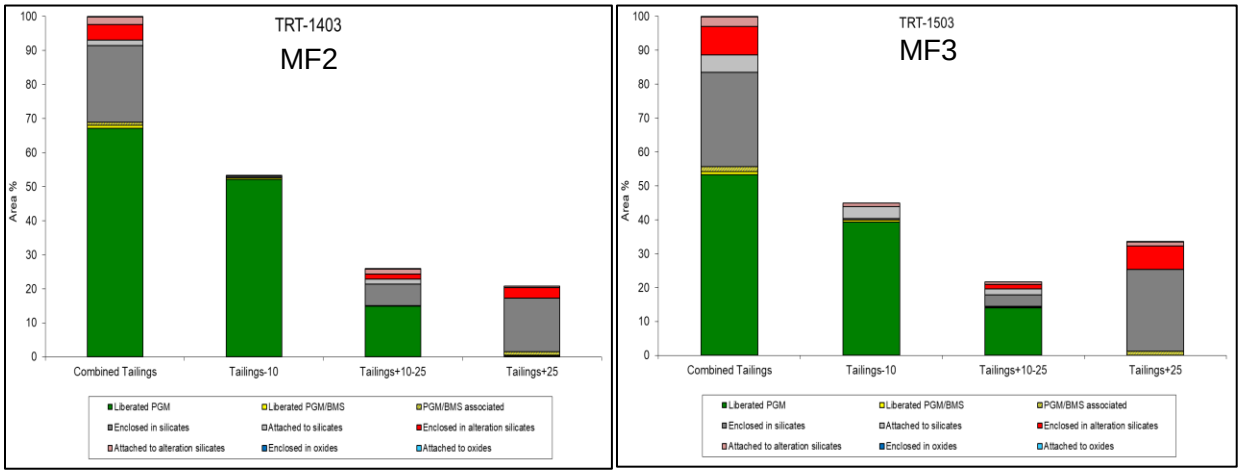

Figure 4.10: PGM association for sized tailings from different circuit configurations

Figure 4.10(a) is a bar graph of the PGM association of the tailings from the current circuit configuration (MF2) whereas Figure 4.10(b) indicated the PGM association of the tailings from the proposed MF3 circuit which involves the decoupling of the secondary milling circuit and the tertiary milling circuit. It was evident that the current circuit configuration (MF2) has more losses of PGMs to the -10 micron size fraction despite that there was no statistically significant difference in the final grind for the two circuit configurations. This indicated that the stage wise flotation of material after every milling stage has the potential to minimize overgrinding and the benefits manifest in the downstream flotation process. This validated the anticipated benefits of improved metallurgical performance by minimizing overgrinding by decoupling the two milling stages, and this was underpinned by the literature on the challenges associated with the recovery of fines. Despite the pronounced difference observed between the two circuits in favor of the MF3 circuit configuration, the two circuit configurations both had a significant amount of material of value in the -10 micron size fraction, this presents a potential opportunity to coarsen the grind upfront in the primary and secondary milling circuit and ultimately minimize overgrinding.

Table 4.13 represents the percentage of liberated PGMs per size fraction in the tailings. It was evident that the MF2 circuit configuration had a higher percentage of liberated fines in the -10 micron size fraction compared to the MF3 circuit configuration which again was an indicator of overgrinding of liberated material considering that the final grind level was comparable for the back to back campaign.

Table 4.13: Percentage liberated PGMs per size fraction in the tailings

	Tailings-10	Tailings+10	Tailings+25
MF2 Liberated PGM in tailings %	77.8	22.1	0.2
MF3 Liberated PGM in tailings %	73.8	26.2	0.0

The detailed mineralogy report is available for reference in Appendix F.

4.3 Campaign number 2

A comparison of the comminution power is shown below. A t-test analysis was conducted to compare the power used at the different comminution stages.

Table 4.14: Campaign 2 Power intensity comparison

	MF2 (kWhr/t)	MF3 (kWhr/t)	t-test p value
Primary mill	31.77	31.49	0.84
Secondary mill	22.34	22.31	0.98
IsaMill	29.04	29.58	0.30

It was evident that there was no statistically significant difference in the comminution power used at the different stages for the two trial conditions.

The grind comparison is shown in the Table 4.14. The objective of decoupling the secondary milling circuit and the tertiary milling circuit was to feed a coarser feed to the secondary roughers when running the MF3 circuit configuration. The secondary rougher tail particle size distribution indicated that the particle size distribution of the feed to the secondary roughers was indeed coarser when running the MF3 circuit.

Table 4.15: Campaign 2 Grind comparison

Stream	PFF (Primary Float Feed)		PRT (Primary Rougher Tail)		SRT (Secondary Rougher Tails)		TRT (Tertiary Rougher Tails)	
Parameter	MF2	MF3	MF2	MF3	MF2	MF3	MF2	MF3
<75 µm	49%	48%	44%	44%	95%	74%	94%	95%
P80 (µm)	202	189	209	209	48	90	46	43
P50 (µm)	82	76	90	90	24	39	22	20
P25 (µm)	25	24	30	29	12	16	11	10

In order to be able to compare the impact of the circuit configuration only, the overall grind for the two circuit configurations was maintained the same as shown by the comparison of the secondary rougher tail grind of the MF2 circuit and the tertiary rougher tail grind of the MF3 circuit. A statistical comparison of the particle size distribution is shown in Table 4.15.

Table 4.16: Campaign 2 Grind statistical analysis

	MF2	MF3	t-test p value
Primary float feed (-75 microns)	48.6	47.7	0.31
Final grind (-75 microns)	95.2	95.6	0.49

The t-test conducted showed that there is no statistically significant difference in the grind between the two trial conditions. This was in line with the comparison conducted for the comminution power intensity. At the same comminution power intensity utilized and same feed ore characteristics, it was expected that the comminution circuit will yield the same grind provided the efficiency of the classification units is comparable for the two trial conditions. From the grind comparison, a conclusion can be drawn that the overall grind was the same despite decoupling the secondary and tertiary milling stages. Any change in the metallurgical performance between

the two processes therefore could not be attributed to particle size distribution of the flotation feed. The detailed statistical analysis on the grind and power intensity is presented in Appendix D.

The mass balancing process was conducted using the matrix method. After conducting the mass balance, parity charts were plotted to assess the deviation between measured data and balanced data. The line y=x was also plotted on the same axis. The parity charts are shown below.

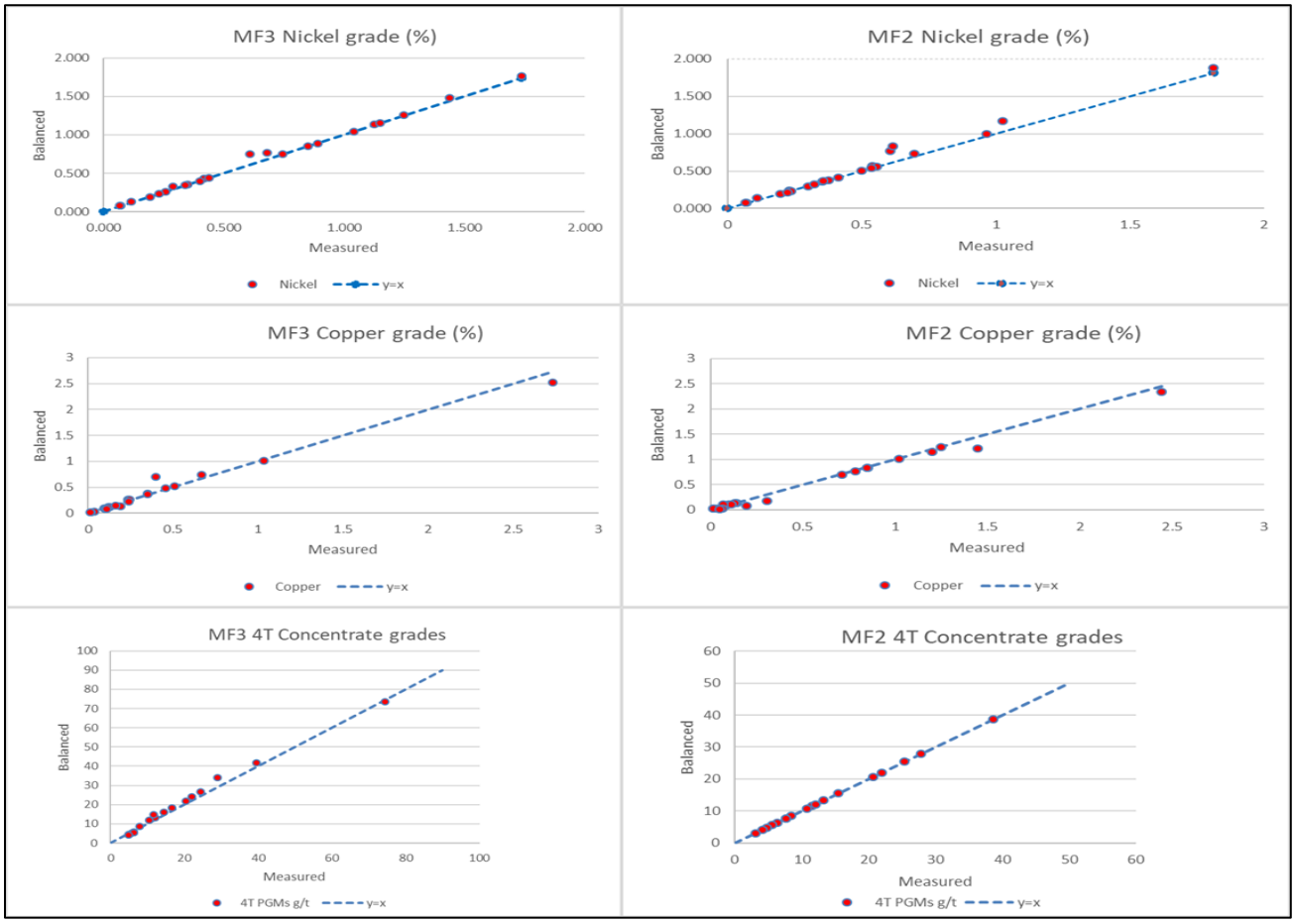

Figure 4.11: Campaign 2 mass balance data integrity

The parity charts indicated a good correlation between the measured and balanced data because most of the data points are on the line y=x. This was an indication that the reconciliation process which is the mass balancing method using the matrix method resulted in data of good integrity.

The nickel and copper kinetic curves below show the flotation response with time for the two back to back campaigns. The kinetic curves followed a similar trend as observed for the first campaign. The analysis was conducted over the primary, secondary and tertiary roughers. The impact of

introducing a grinding stage after each flotation stage is shown by the change in kinetics when moving from one flotation stage to the other. The difference between the two circuit configurations is observed on the tertiary rougher bank as hypothesized.

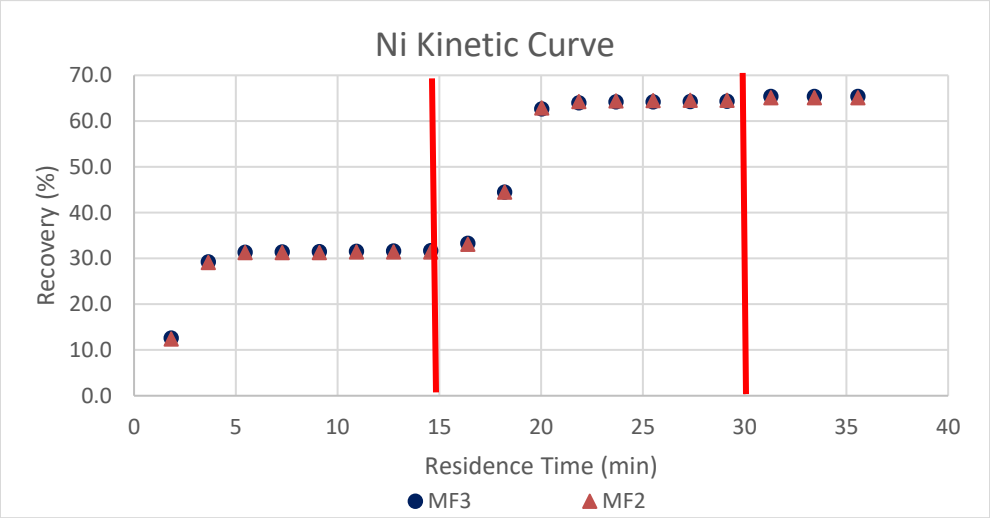

Figure 4.12: Campaign 2 Nickel kinetic curve for the different configurations

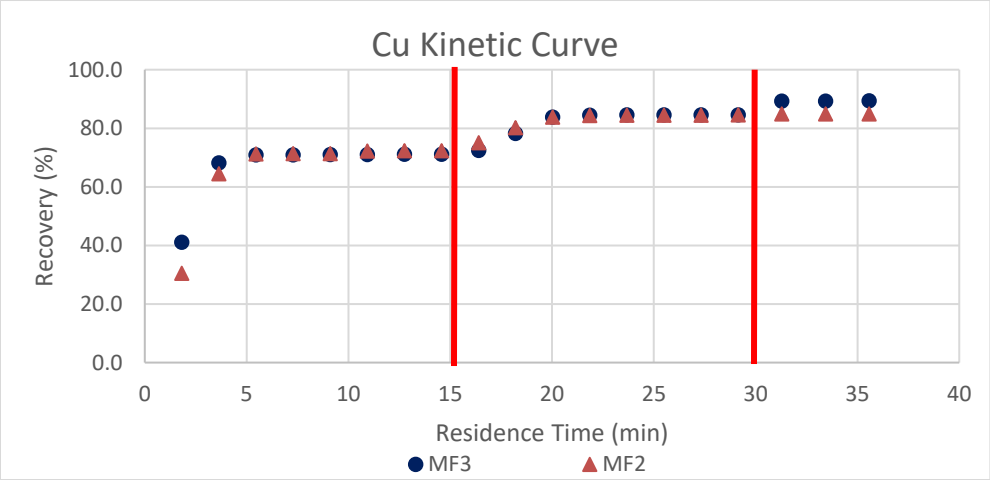

Figure 4.13: Campaign 2 Copper kinetic curve for the different configurations

As observed in the results of the first campaign, the decoupling of the secondary mill and the tertiary mill was responsible for the difference in recovery observed in the tertiary roughers making the MF3 configuration to record a superior metallurgical performance. The kinetic response profiles matched each other closely until the end of the secondary rougher bank, the tertiary rougher profile distinguished the performance of the two circuits. This was achieved without any additional comminution power but by redistributing the available power.

The enrichment ratio vs mass pull relationship for the base metals was used to quantify the metallurgical performance of each circuit configuration. This down the bank analysis was conducted using the reconciled data obtained from the mass balance. Figure 4.14 and Figure 4.15 are graphs showing the enrichment ratio against mass pull relationship for the down the bank analysis.

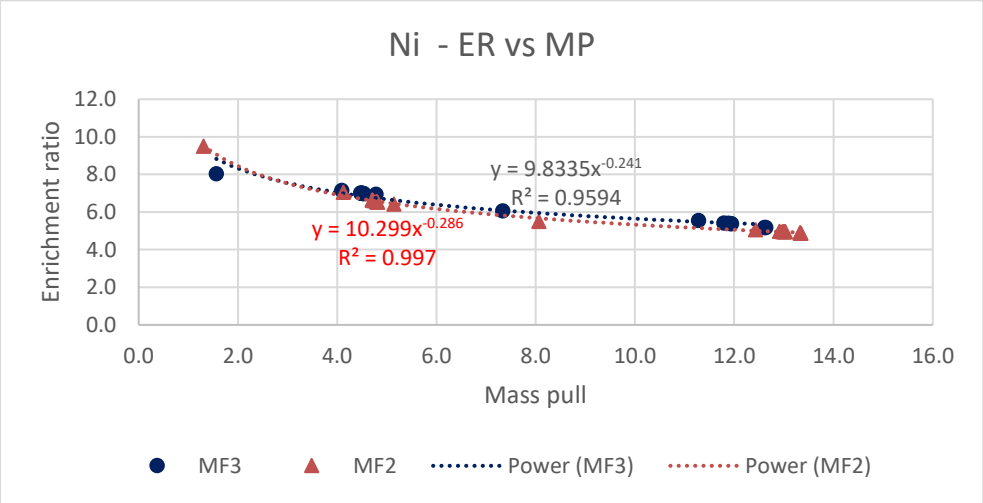

Figure 4.14: Nickel Enrichment ratio vs mass pull relationship

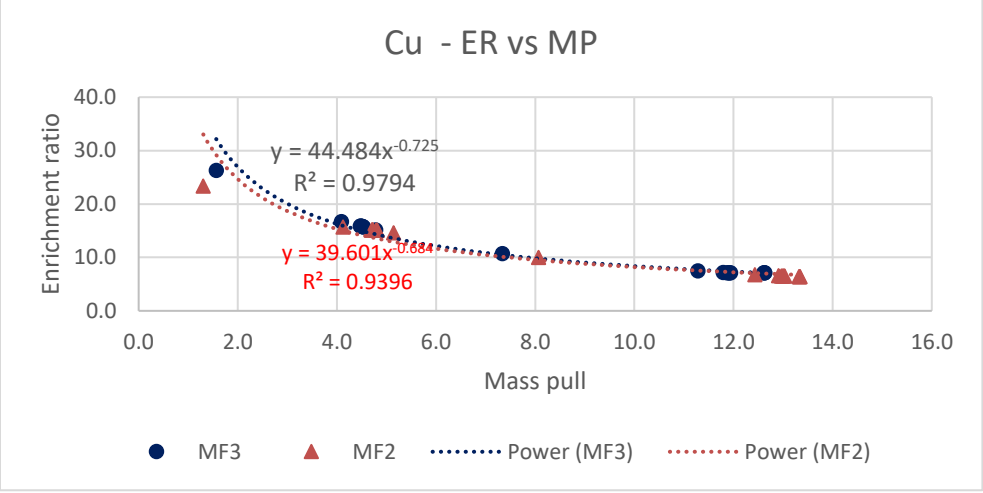

Figure 4.15: Copper Enrichment ratio vs mass pull relationship

The MF3 circuit exhibited a superior metallurgical performance compared to MF2 circuit. These observations supported the findings by Steyn (2012) which indicated that the introduction of multiple mill-float stages has the potential to increase recovery. At the same mass pull, the MF3 circuit yielded higher grades compared to the MF2 circuit (higher enrichment ratio). This proved the theory of entrainment documented by Engelbrecht and Woodburn (1975). Despite the similar

grind level for the two circuit configurations, the ultrafine product from tertiary milling stage for the MF2 circuit configuration had a longer residence time in the circuit (secondary roughers and tertiary roughers) compared to the MF3 circuit configuration where the ultrafine product only had to go through the tertiary roughers. The longer residence times provided a platform for the gangue to be recovered by entrainment and in the process diluting the product grade.

The power model described the enrichment ratio vs mass pull relationship well for copper and nickel metallurgical performance. This model fit is good as seen from the R squared values. A comparison of the recovery at the same mass pull was conducted using the models for the enrichment ratio vs mass pull. The MF3 yielded a 4.1% and 1.3 % increase in recovery for nickel and copper respectively. The detailed mass balance report is presented in Appendix E.

Table 4.17: Campaign 2 recovery comparison

	MF2			MF3			Δ Recovery (%)
	A	b	Recovery (%)	A	b	Recovery (%)	
Copper	39.6	-0.7	86.8	44.5	-0.7	88.1	1.3
Nickel	10.3	-0.3	60.7	9.8	-0.2	64.8	4.1

In order to test the hypothesis of overgrinding of material of value in the MF2 circuit configuration, a mineralogical analysis of the tailings stream was conducted. The PGM grain size distribution comparison of the tailings stream is shown in the Figure 4.16.

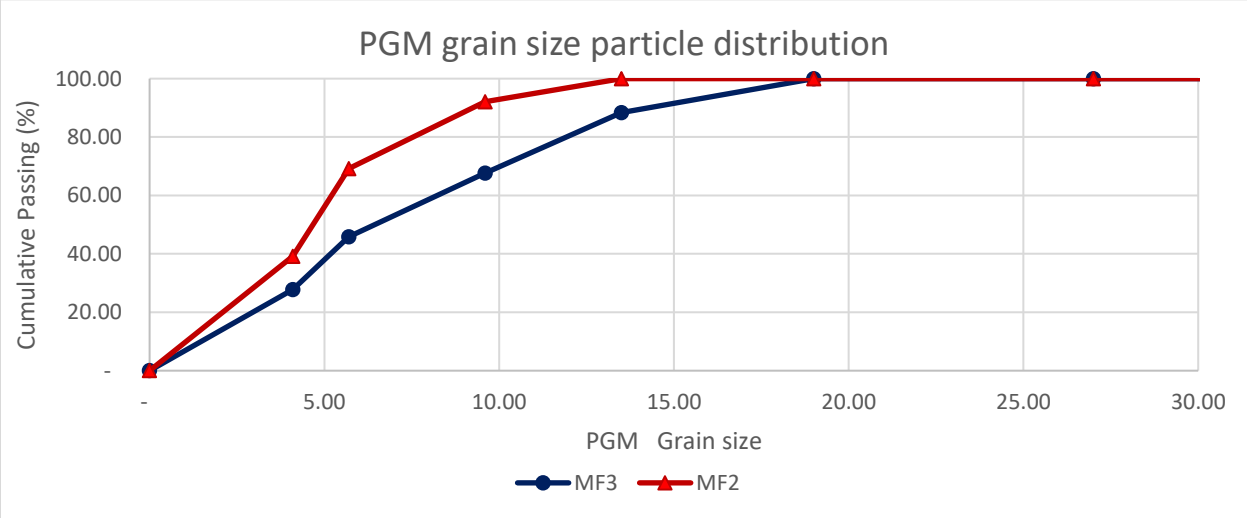

Figure 4.16: Particle size distribution comparison of the tailings streams

The MF2 tailings stream had a finer PGM grain size compared to the MF3 PGM grain size despite the same grind level. This validated the findings of the first survey campaign. The MF2 circuit configuration resulted in overgrinding as indicated by the finer grain size of the material of value in the tailings stream. An analysis of the liberation indices in the tailings was also conducted.

Table 4.18: Percentage liberated PGMs per size fraction in the tailings

	Tailings-10	Tailings+10	Tailings+25
MF2 Liberated PGM in tailings %	89.7	9.7	0.5
MF3 Liberated PGM in tailings %	78.4	21.3	0.3

The percentage of liberated PGMs in the -10 micron size class was higher for the MF2 compared to the MF3. This was an indicator of overgrinding of liberated material resulting in fines which were difficult to recover by conventional flotation thereby reporting to the tailings stream. This finding on trans-granular breakage was in line with the mineralogy results for the March 2018 depicted in Figure 2.3, which indicated evidence of trans-granular breakage in the process. The detailed mineralogy report is available for reference in Appendix F.

4.4 Campaign number 3

The flotation performance of the third back to back campaign is presented in this section. A similar comparison technique as in campaign one and campaign two was used. The results followed a similar trend as those observed in campaign one and campaign two. The enrichment ratio vs mass pull relationship for nickel and copper is shown in Figure 4.17 and Figure 4.18.

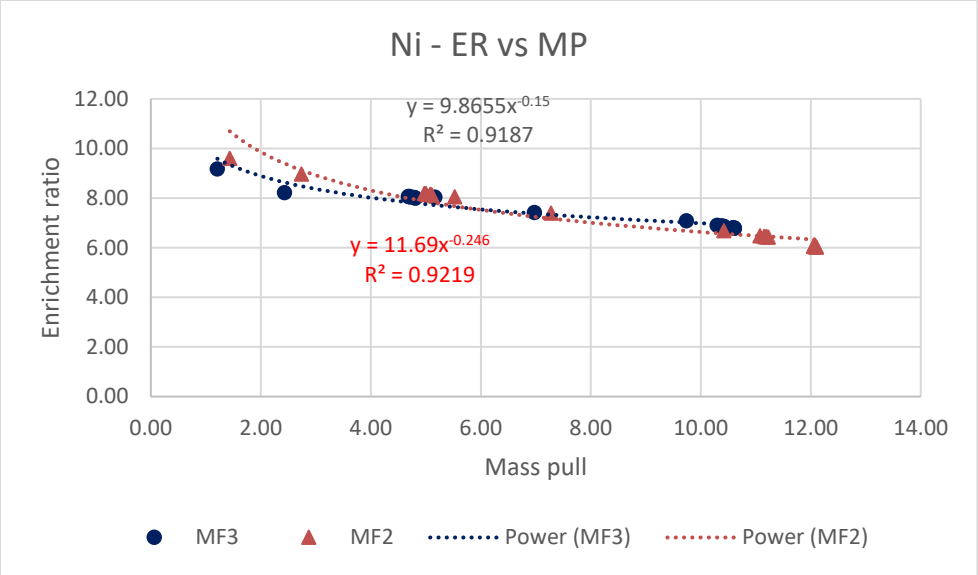

Figure 4.17: Nickel Enrichment ratio vs mass pull relationship

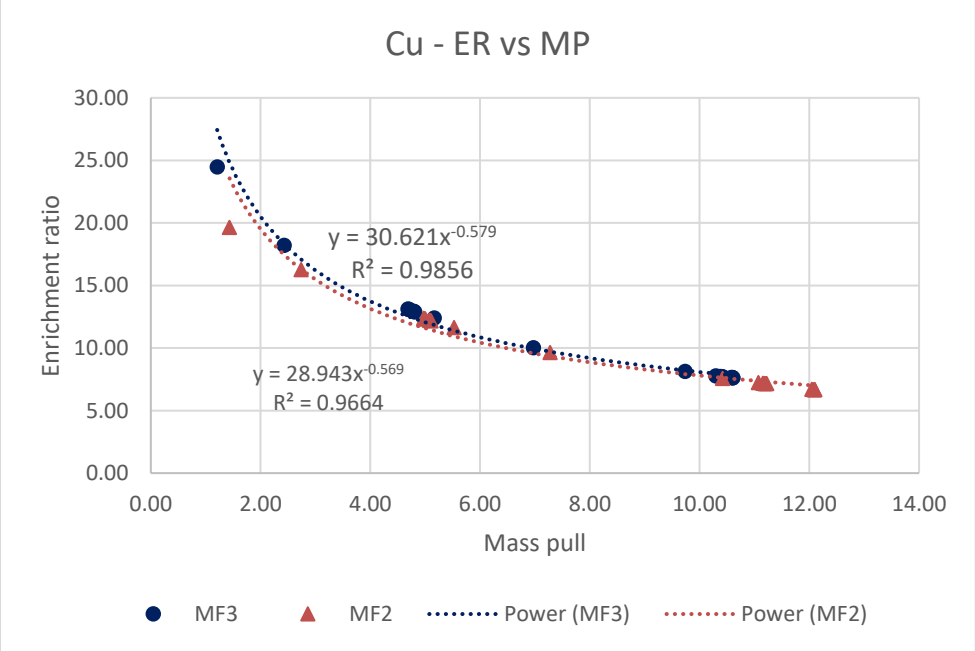

Figure 4.18: Copper Enrichment ratio vs mass pull relationship

The recovery comparison was conducted at mass pull of 10% due to the MF3 operating at a lower total mass pull. Table 4.19 shows a comparison of the two circuits at the same mass pull.

Table 4.19: Campaign 3 recovery comparison

	MF2			MF3			Δ Recovery (%)
	A	b	Recovery (%)	A	b	Recovery (%)	
Copper	28.9	-0.6	78.1	30.6	-0.6	80.7	3.5
Nickel	11.7	-0.2	66.3	9.9	-0.2	69.8	2.6

The MF3 circuit yielded a superior metallurgical performance compared to the MF2 circuit configuration. This was attributed to the reasons explained earlier. The detailed mass balance is available is Appendix E.

The findings from the campaigns conducted on the flexi-float indicated that the MF3 yields a superior performance compared to the MF2 circuit. It was however observed that the nickel recovery had the highest improvement in recovery compared to copper. In order to understand why the difference in recovery was more pronounced for nickel than copper it was important to look at the flotation kinetics. Figure 4.19 shows the difference in flotation kinetics between copper and nickel for the MF3 campaign. Copper flotation kinetics appeared to be significantly faster than that of nickel. The difference observed in the kinetics was in line with the findings by Sabau (1998) which indicated that under normal aeration rates, the ease of flotability of individual elements follows the order chalcopyrite>pentlandite> pyhrrotite. Looking at the feed mineralogy, copper was present in the ore in the form of chalcopyrite while the nickel was present mainly in the form of pentlandite. Both these base metal sulphides have a hardness of between 3.5- 4.0 based on Moh's Scale thus looking at the comminution power intensity utilized the two should experience the same level of grinding. A higher proportion of the nickel however stood a chance to be over ground compared to copper due to the slower kinetics of the nickel. In addition, the nickel head feed grade was double that of copper, this combined with the lower kinetics resulted in a significantly higher amount of nickel exposed to secondary and tertiary grinding compared to copper hence the higher chances of being over ground.

Figure 4.19 shows the difference in kinetics for the two base metals for the first campaign.

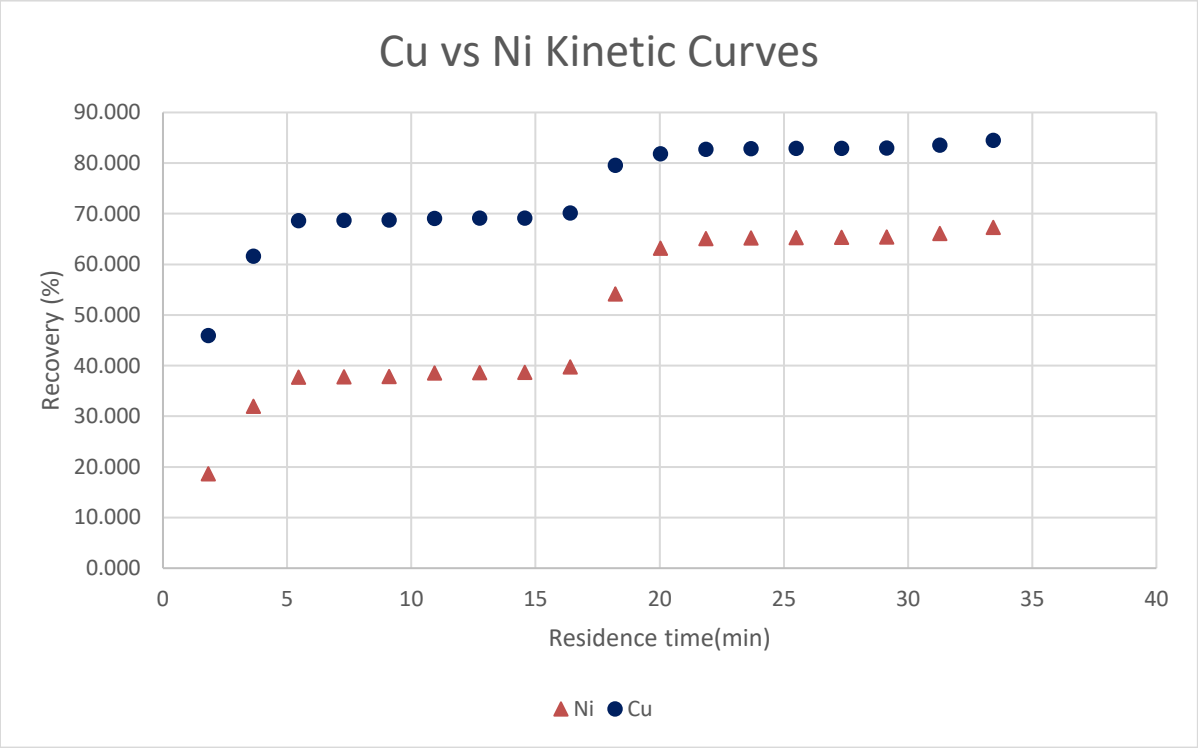

Figure 4.19: Comparison of copper and nickel kinetics

The primary rougher bank was then modelled from first order kinetics to validate the difference in kinetic response between copper and nickel.

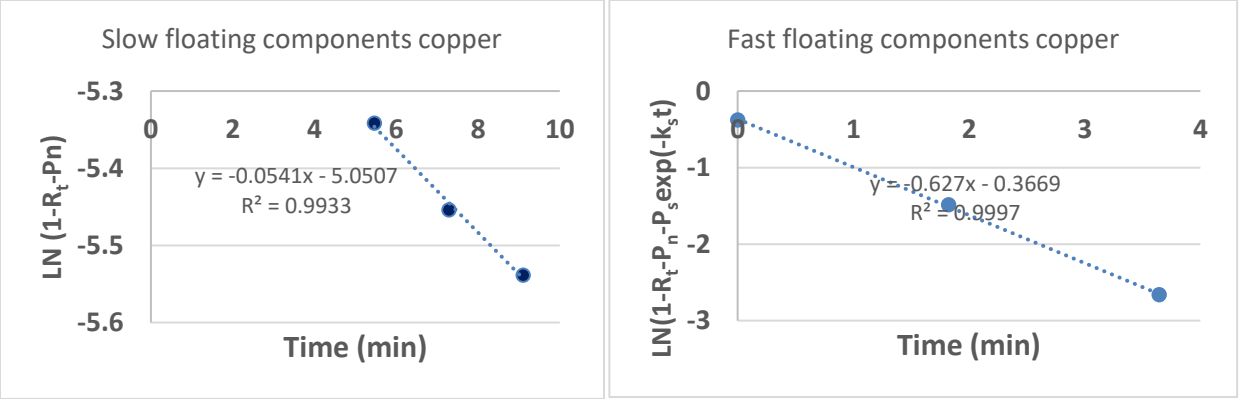

Figure 4.20: Copper flotation rate constants

The mass fractions for the fast, slow and non floating copper were found to be 0.699, 0.006 and 0.300 respectively. The flotation constants were found to be 0.595 min^{-1} and 0.029 min^{-1} for the fast and slow floating components respectively.

The nickel kinetics were also modelled using first order kinetics using the three component model.

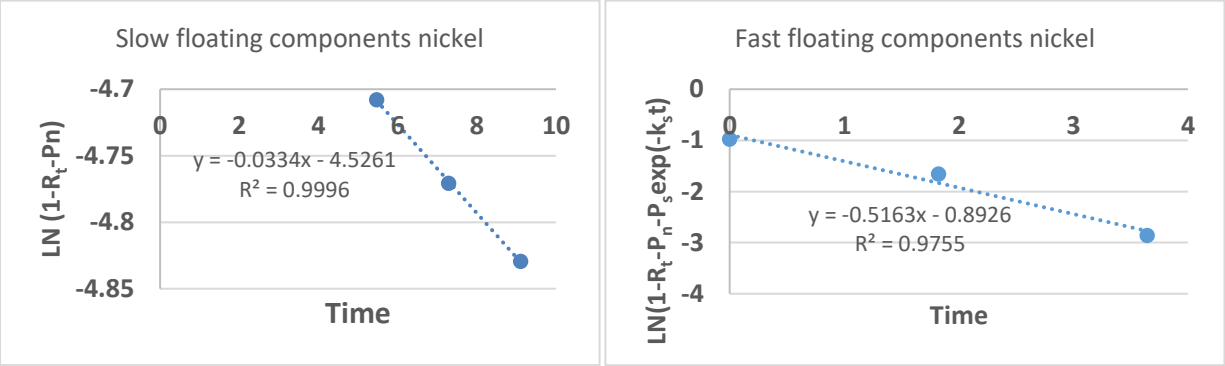

Figure 4.21: Nickel flotation rate constants

The mass fractions for the fast, slow and non floating nickel were found to be 0.404, 0.011 and 0.595 respectively. The flotation constants were found to be 0.395 min^{-1} and 0.013 min^{-1} for the fast and slow floating components respectively.

A quantitative comparison of the flotation constants is shown in the Table 4.20 below.

Table 4.20: Proportions and flotation constants in the rougher feed

	Cu	**Ni**
Pn	0.300	0.595
Ps	0.006	0.011
Pf	0.699	0.404
ks	**0.029**	**0.013**
kf	**0.595**	**0.395**

The copper flotation rate was faster compared to the nickel as seen in Table 26. The difference observed in the kinetics was in line with the findings of Sabau (1998). This substantiates the hypothesis why nickel was more prone to overgrinding in the MF2 circuit as a significant amount reported to the secondary and tertiary milling circuits due to the slower kinetics in the rougher bank compared to copper. This phenomenon also explained the higher benefit in the nickel recovery compared to copper when the secondary milling circuit is decoupled from the tertiary milling circuit.

Another measurement taken during the flexi-float first campaign was the pulp chemistry. Figure 4.22 depicts the oxygen demand results obtained from the measurements taken using the TPS meter. The pulp chemistry sampling process was supervised by an expert in the field working for Magotteaux.

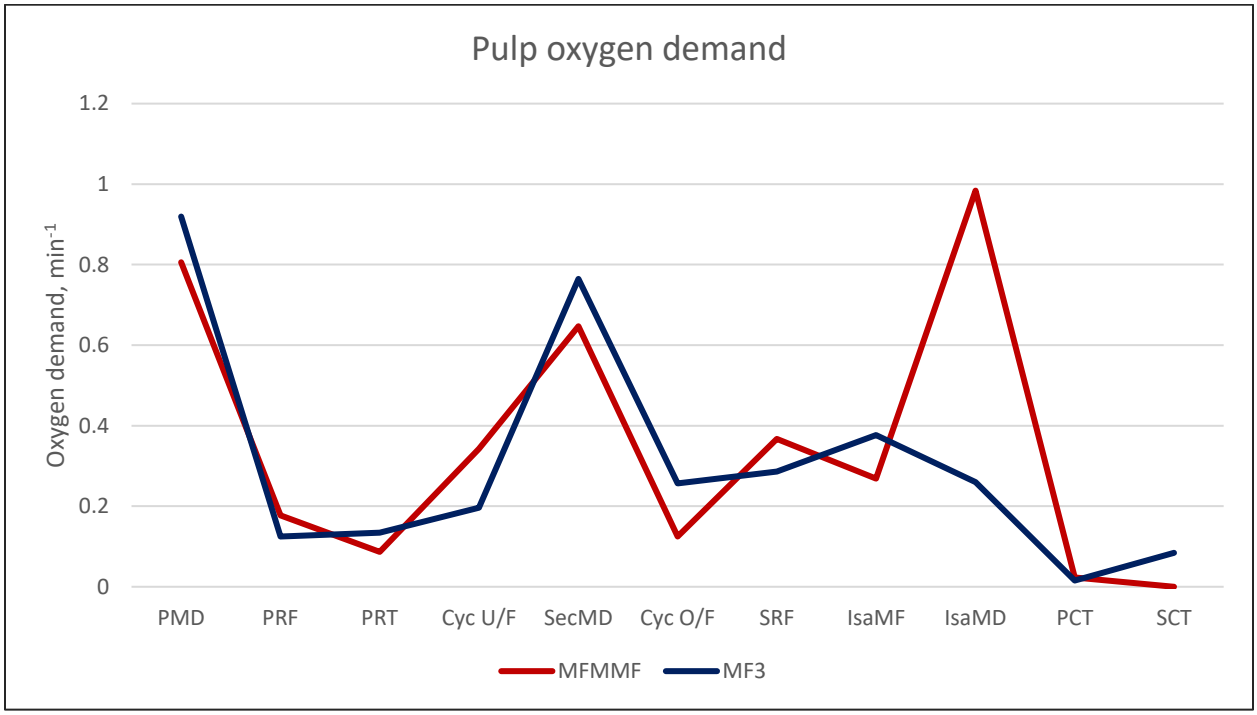

Figure 4.22: Oxygen demand of the different process streams

Oxygen Demand is a measure on how quickly the pulp consumes oxygen and can be referred to the reactivity of the pulp. The decay of Oxygen Demand was recorded over 2 minutes and the rate (K) determined. The pulp chemistry results indicated the change in process from the base case to the MF3 configuration. The results indicated a decrease in oxygen demand for the IsaMill discharge when running the MF3 configuration. This was a good indication that some of floatable material was recovered after the secondary milling stage hence less mineral exposed surfaces after the IsaMills when running this configuration. The spike observed for the base case on the IsaMill discharge indicated that there was a significant amount of exposed mineral surfaces in the IsaMill product which are prone to oxidation and hence flotation inefficiency. Also the fine nature of the material increased the available surface area for oxidation hence the high oxygen demand. This was in line with the observation of Clarke et al (1995) which indicated that the rate of oxidation is higher in fine particles. The Oxygen Demand was highest on the Mill discharge and very well pronounced for MF2 on the IsaMill discharge and not so much for MF3 IsaMill discharge. It is important also to note that the IsaMill feed and product had the same grade (same amount of

material of value) however the oxygen demand for the IsaMill product was significantly higher. This was in line with the results by Lu et al (2018) which highlighted that the amount of oxidation products extracted using EDTA increased with the decrease of particle sizes indicating a higher rate of oxidation with decrease in particle size. For the same grade, overgrinding increased the rate of oxidation. The reason for the difference between the circuits was that for MF2 the IsaMill was still grinding material that contains substantial sulphide minerals while for MF3 the secondary flotation had recovered some of the sulphide minerals to a point that there was a minimal amount requiring oxygen for oxidization. For this reason, the competitive advantage of the MF3 based on this aspect was clear although both systems were running at the same grind level.

A summary of the metallurgical performance for the back to back campaigns is presented below.

Table 4.21: Recovery comparison summarized

		Recovery (%) first campaign	Recovery (%) second campaign	Recovery (%) third campaign	Average Recovery (%)	Δ Recovery (%)
Nickel	MF2	64.9	60.7	66.3	64.0	3.20
	MF3	66.9	64.8	69.8	67.2	
Copper	MF2	83.1	86.8	78.1	82.7	1.78
	MF3	84.5	88.1	80.7	84.4	

4.5 Mogalakwena North Concentrator circuit retrofit

The positive results from the concept study prompted the need to evaluate the feasibility of converting the circuit configuration at Mogalakwena North Concentrator to enable the decoupling of the secondary and tertiary milling circuits. MNC engaged the services of its flotation original equipment manufacturer (FLSmidth) to investigate ways of implementing the proposed circuit configuration on full scale. Three options were considered namely:

Option 1: New Flotation Cells

The first option was to add an additional 8 flotation cells to treat the secondary mill product. This required a new surge tank to be installed after the secondary mill to pump to the new secondary rougher flotation bank. The final tailings from these cells would then be pumped to the tertiary mills and the rest of the process remains unchanged.

Option 2: Convert Bank #1 to Secondary rougher Bank prior to tertiary milling

A new surge tank is installed after the secondary mill. Slurry is pumped to the first bank of existing secondary rougher flotation cells. The concentrate line configuration remains as is. The final tailings from this one secondary rougher bank is then pumped to the tertiary mills. The tertiary mills product is then redirected to the second bank of the existing secondary rougher cells. A new tailings collection tank is required to split the tailings from the two existing flotation banks.

Option 3: Convert Cells #1 to 3 of both banks to Secondary rougher step prior to tertiary milling

Slurry is pumped to the first three secondary rougher flotation cells of banks. The concentrate line configuration remains as is in the current wet section configuration. A new tailings tank is added to redirect the tailings from the third set of flotation cells to the tertiary mill. The tertiary mills product is then redirected to the last five set of the existing secondary rougher cells, which will require a new feed arrangement for these cells. The rest of the circuit remains unchanged.

The factors considered in choosing the best option were as follows:

- Layout (space constraints)
- Accessibility of the units
- Maintainability
- Cost

The best option is Option 3 which involves the use of the first three cells on each secondary rougher bank as flash float cells to treat the secondary mill product. The tailings of these cells report to the tertiary grinding circuit and the product from the tertiary grinding circuit reports to the fourth cell of the secondary rougher bank. The conceptual design for the plant retrofit is shown in Appendix G. The value proposition was then estimated based on this option.

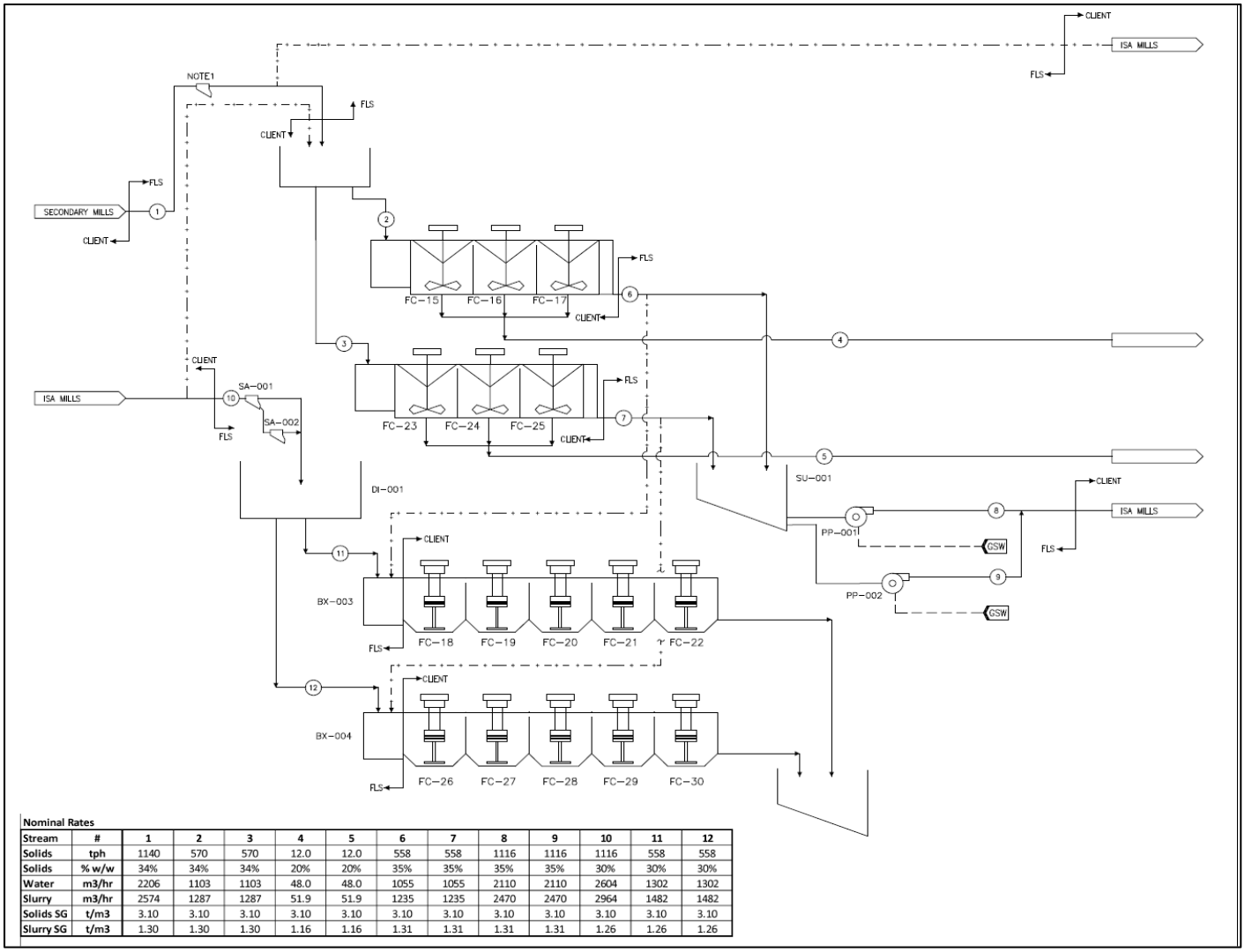

Nominal Rates

Stream	#	1	2	3	4	5	6	7	8	9	10	11	12
Solids	tph	1140	570	570	12.0	12.0	558	558	1116	1116	1116	558	558
Solids	% w/w	34%	34%	34%	20%	20%	35%	35%	35%	35%	30%	30%	30%
Water	m3/hr	2206	1103	1103	48.0	48.0	1055	1055	2110	2110	2604	1302	1302
Slurry	m3/hr	2574	1287	1287	51.9	51.9	1235	1235	2470	2470	2964	1482	1482
Solids SG	t/m3	3.10	3.10	3.10	3.10	3.10	3.10	3.10	3.10	3.10	3.10	3.10	3.10
Slurry SG	t/m3	1.30	1.30	1.30	1.16	1.16	1.31	1.31	1.31	1.31	1.26	1.26	1.26

Figure 4.23: MF3 Secondary rougher setup at Mogalakwena North Concentrator

4.6 Economic evaluation

The additional cost of maintenance associated with the additional pumping stage was calculated based on historical maintenance data on a similar size pump handling the same duty as desired for this retrofit. The runtime of the pump was used together with the tonnage treated to normalize the data for the period considered. The power consumption in kilowatt-hours was calculated based on the runtime and the motor rating. Unit cost 1 caters for the maintenance costs while unit cost 2 indicates the additional cost of power.

Table 4.22: Additional pumps operating cost

Date	Task	Spares Used	Part Number	Quantity	Price
16-12-16	Complete Overhaul Pump	Volute Liner	H14110-A05A	1	R 139,843
		Throatbush	H14083MA05	1	R 66,686
		Impeller	GAM14147-A05A	1	R 121,703
		Frame Plate Liner Insert	H14041M-A05A	1	R 115,651
		Shaft Sleeve	GAM076-2-C23	1	R 3,276
		Shaft Oring	G109-S10	2	R 16
25-10-17	Replace Motor & Upgrade Pulleys	500 kW motor	WEG 500kW motor	1	R 437,190
22-05-18	Replace Pump	Complete Pump	16/14-G-AH-MM	1	R 912,612
18-06-18	Replace Motor	500 kW motor	WEG 500kW motor	1	R 437,190

Tons milled	12,745,925	tons
Plant productive time	11,858	hrs
Pump runtime	10,515	hrs
Proportion of tons through pump	11,302,706	tons
Operational costs	2,234,167	ZAR
Unit cost 1	0.20	ZAR/ton
Rand per kWhr	0.96	ZAR/kWhr
Pump motor rating	500	kW
Power cost	5,047,354	ZAR
Unit cost 2	0.45	ZAR/ton
Total unit cost	**0.64**	ZAR/ton

A detailed estimate for the cost of implementation was conducted by FLSmidth. The estimate cost of implementation amounted to R72 100 000.

Table 4.23: Bill of quantities for circuit conversion (Smith, 2019)

PROJECT MANAGEMENT	ZAR 6,000,000
ENGINEERING	ZAR 4,020,000
PUMPS	ZAR 3,060,000
INSTRUMENTS	ZAR 1,670,000
EC&I	ZAR 11,250,000
EC&I - INSTALL	ZAR 3,690,000
AUTOMATION	ZAR 380,000
STRUCTURAL SUPPLY	ZAR 6,570,000
STRUCTURAL AND MECHANICAL INSTALLATION	ZAR 14,860,000
PIPING SUPPLY	ZAR 5,080,000
PIPING INSTALLATION	ZAR 4,470,000
CONTROL VALVES	ZAR 5,040,000
SAMPLER	ZAR 1,190,000
CIVIL WORKS	ZAR 3,700,000
LOGISTICS	ZAR 260,000
PAYMENT TERMS & BONDS	ZAR 860,000
BUDGET ESTIMATE	ZAR 72,100,000

The benefit of operating the MF3 was calculated based on the recovery improvement associated with this circuit. The downstream processing cost associated with the production of the additional

metal were taken into consideration. The model used was subject to key assumptions of the processing steps such as fixed losses of PGMs and base metals in downstream of concentrator processing and no buffering or stockpiling between each unit operation. In reality, this is not the case but for the purposes of understanding the impact on the value chain, it was sufficient to provide a useful methodology for combining a metallurgical model into a financial calculation to understand value creation across the value chain from mining to final product. For the smelting costs, the unit cost driver was tonnes of concentrate produced which was determined by the mass yield or mass pull multiplied by tonnes milled. For refining costs at the precious metals refinery, the unit cost driver was Pt ounces produced which was calculated from the recovery model for the concentrator. For the base metal costs, due to a suite of several base metals, nickel tonnes refined was used as a key driver due to nickel being the highest volume produced. The costs used in the analysis were purely processing costs and did not included any stay in business capital, or amortization costs which could be factored in to further improve the accuracy of the model. Table 4.23 shows the assumptions made in calculating the net revenue associated with the increase in metallurgical performance. These assumptions included the following:

- Yearly tonnage profile
- Nickel and Copper head grade profile
- Downstream recovery efficiencies

Table 4.24: Assumptions for Net Revenue Calculation

	2021	2022	2023	2024	2025
Tons milled	8,875,000	8,965,000	9,020,000	8,950,000	8,950,000
Ni feed grade (%)	0.1870	0.1855	0.2263	0.2480	0.2730
Cu feed grade (%)	0.0919	0.0917	0.1161	0.1287	0.1417
Additional Ni recovery (%)	3.20%	3.20%	3.20%	3.20%	3.20%
Additional Cu Recovery (%)	1.78%	1.78%	1.78%	1.78%	1.78%
Smelter Ni efficiency	0.9203	0.9203	0.9203	0.9203	0.9203
Smelter Cu efficiency	0.8965	0.8965	0.8965	0.8965	0.8965
Refinery Ni efficiency	0.9891	0.9891	0.9891	0.9891	0.9891
Refinery Cu efficiency	0.9719	0.9719	0.9719	0.9719	0.9719
Additional Ni (tons)	513.6	514.6	631.7	686.9	756.1
Additional Cu (tons)	145.7	146.9	187.1	205.8	226.6

The NPV and IRR were calculated based on the estimate cost of implementation and net revenue resulting from the improvement in process efficiency. A benefit of 3.20% in nickel recovery and 1.78% in copper recovery results yielded a payback period of 1 yr 5 months for the project calculated at a discount rate of 11.5%. A pessimistic approach was also considered whereby the cost of implementation was escalated 1.5 times. This also revealed that the project was cash positive with a payback period of 2 yrs 3 months. It was therefore concluded that the risk associated with the project is low. The different scenarios are shown in Appendix H.

Table 4.25: Economic Evaluation

Financial Item	Units	Results
Payback	Years	1 yr 5 months
Profitability Index	NPV / I	240%
IRR	%	80%
Discount Rate	%	11.5%
Cumulative Cash Flow	ZAR (m)	272.5
NPV@11.5%	ZAR (m)	173.1

4.7 Implementation schedule

Anglo American Platinum follows a rigorous exercise to evaluate possible projects for implementation. The key drivers in this evaluation are safety, environmental impact, capital requirements, payback period and return on investment. The conversion of the circuit configuration at Mogalakwena North Concentrator from MF2 to MF3 has been identified as one of the projects that will yield value for the organization. Figure 4.24 shows the project implementation schedule.

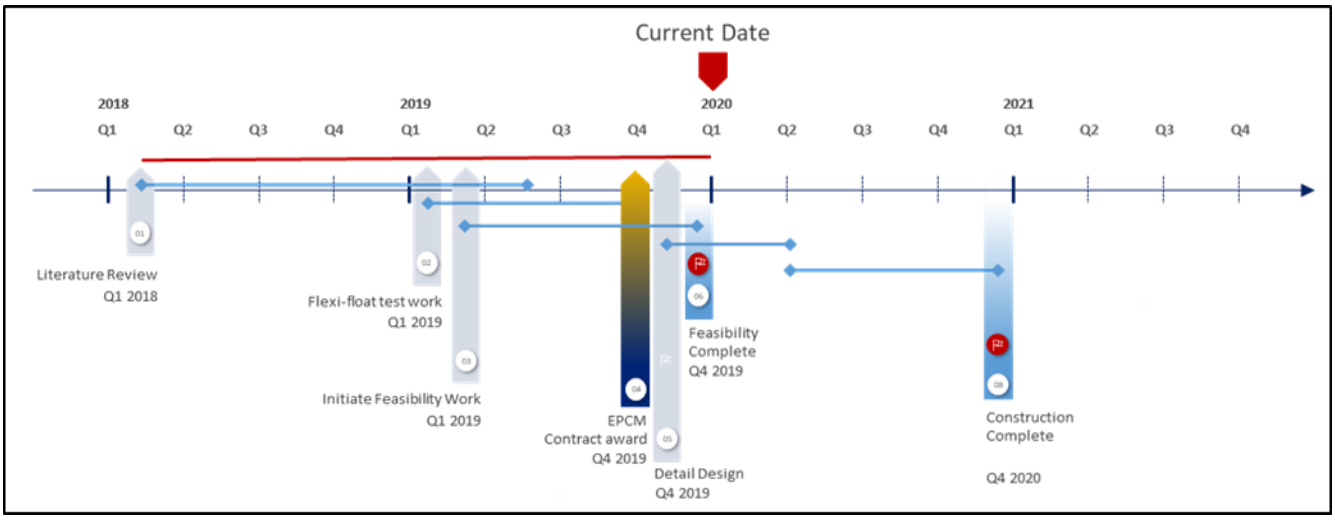

Figure 4.24: Project implementation schedule

CHAPTER FIVE

CONCLUSION AND RECOMMENDATIONS

“Any new fact or insight that I may have found has not seemed to me as a ‘discovery’ of mine, but something that has been there and I had a chance to pick up” ~Subrahmanyan Chandrasekhar

The MF3 circuit yielded a superior metallurgical performance compared to the MF2 circuit for all the runs that were conducted. This indicated that the MF3 configuration systematically outperforms the MF2 circuit configuration. This was attributed to the circuit configuration which incrementally recovers material of value after each milling stage thereby minimizing both overgrinding and oxidation of material value. An improvement in copper recovery by 1.78% was observed when running the MF3 circuit configuration and an improvement in nickel recovery of 3.20% was realized. Nickel recovery showed the highest benefit compared to copper due to slower kinetics of the nickel which made it prone to overgrinding and oxidation after it was subjected to a succession of secondary and tertiary milling. The difference in kinetics was validated graphically and by modelling the rate constants from first order kinetics.

The MF3 circuit configuration yielded a better product quality for the same mass pull due to the circuit configuration not exposing ultrafine material to extended residence time conditions which promotes entrainment. This was validated by the enrichment ratio vs mass pull relationship comparison of the two circuit configurations.

The pulp chemistry data indicated a significant difference in the oxygen demand for the two circuit oxygen configurations particularly considering the IsaMill discharge stream. The lower oxygen demand for the MF3 circuit at the same grind level indicated less material available for oxidation compared to the MF2, this highlighted the superior performance of the MF3 circuit configuration.

Redistributing the applied comminution power resulted in an improvement in metallurgical performance. This phenomenon observed highlighted the importance of circuit configuration on metallurgical performance. The mineralogy analysis indicated a finer grain size in the tailings stream for the MF2 circuit configuration due to overgrinding of the material of value already liberated in the secondary milling stage. This contributed to the poor metallurgical performance of the MF2 circuit.

An economic evaluation on converting the current circuit configuration to MF3 was conducted looking at the production profile for the next 5 years. The analysis indicated that converting the circuit to MF3 at Mogalakwena North Concentrator will be cash positive. The project has a payback period of 2 years 3 months and internal rate of return of 80%.

The infrastructure assessment conducted indicated that the conversion of Mogalakwena North Concentrator to MF3 configuration was feasible. The proposed changes to the circuit were of

relatively low complexity and risk. The implementation thereof has the potential to generate considerable value for Mogalakwena over the life of the asset.

New knowledge has been developed for the handling of Platreef ore which Anglo American Platinum has embraced, this will definitely be considered for future design.

The power intensity for the back to back campaigns was kept comparable in order to keep the final grind also comparable. The MF3 circuit configuration reduced overgrinding by recovering the material of value liberated in the secondary grinding circuit before it reported to the tertiary grinding circuit. It is recommended that further testwork is conducted at higher tertiary grinding circuit energy intensity for the MF3 circuit configuration. This has the potential to liberate material of value which is locked without overgrinding the secondary mill product.

Despite the pronounced difference observed between the two circuits in favor of the MF3 circuit configuration, both circuit configurations had liberated material of value in the -10 micron size fraction. It is recommended to assess the feasibility of coarsening the grind upfront in the primary and secondary milling circuit coupled with precision classification in bid to minimize overgrinding. This will also present an opportunity to explore the feasibility of having four stages of milling with each stage of milling followed by a flotation stage for incremental recovery. It is also recommended to explore alternative flotation technologies at the back end of the circuit to target fines recovery at a saleable concentrate grade. High energy intensity flotation mechanisms have the potential to improve recovery of fines however the challenge is the poor selectivity due to increased entrainment rates at high energy input. It is also recommended to investigate technologies that can be used to agglomerate fine particles such as magnetism, agglomeration of the liberated particles in the -10 micron size fraction has the potential to increase the probability of collision and attachment in the flotation process resulting in enhanced flotation performance.

CHAPTER FIVE

REFERENCES

“If I have seen further it is by standing on the shoulders of Giants”. ~Isaac Newton

Aldrich, C., Feng, D. 1999. Effect of particle size on flotation performance of complex sulphide ores. Minerals Engineering, Vol 12. 721-731

Albijanic, B., Nimal Subasinghea, G.K., Bradshaw, D.J., Nguyen, A.V. (2015) Influence of liberation on bubble-particle attachment time in flotation. Minerals Engineering. 74. 156-162

Anyimadu, A.K., Rule, C., Knopjes, L. 2006. The development of ultra fine-fine grinding at Anglo American Platinum. The Southern African Institute of Mining and Metallurgy.107.15-22

Basaova, P., Hubicka , M. 2014. The collision efficiency of small bubbles with large particles. Minerals Engineering. 66-68. 230-233.

Baxter, R., 2014. Platinum State of the Nation. Chamber of Mines

Blom, A., 2018. Mogalakwena North Concentrator Management Strategy. Internal Anglo American Platinum Report. Unpublished.

Bisshop, J.P. 1974. A study of particle entrainment in flotation froths . BSc Thesis. The University of Queensland, Brisbane. Australia.

Cheng, G., Shi, C., Yan, X., Zhang, Z., Xu, H., Lu, Y. 2017. A study of bubble particle interaction in a column flotation process. Mineral Processing. 53 (1).17-33.

Clarke, P., Fornasiero, D., Ralston, J., Smart, R.St.C. 1995. A study of the removal of oxidation products from sulfide mineral surfaces. Minerals Engineering. 8. 1347-1357.

Deglon, D.A., Egya-Mensah, D., Franzidis, J.P. 2000. Review of hydrodynamics and gas dispersion in flotation cells on South African platinum concentrators. Minerals Engineering, 13. 235-244.

Dobby, G.S., Falutsu, M. 1989. Direct measurement of froth drop back and collection zone recovery in a laboratory flotation column. University of Toronto Department of Metallurgy and Material Science.

Engelbrecht, J., Woodburn, E. 1975. The effects of froth height, aeration rate and gas precipitation on flotation. Journal of the Southern African Institute of Mining and Metallurgy 76, 125–132.

Falutsu, M., Dobby, G. S. 1989. Direct Measurement of Froth Zone Performance in a Laboratory Flotation Column. Processing of Complex Ores, Proceedings of an International Symposium, Halifax, Nova Scotia - Canada, Pergamon Press.

Gorain,B.K., Franzidis, J-P., Manlapig, E.V., Napier-Munn, T.J. 1998. Studies on impellor type, impellor speed and air flow rate in an industrial scale flotation cell. Part 1: Effect on bubble size distribution. Minerals Engineering (8). 615-635.

Greet, C. 2019. Meeting. Magotteaux: Pulp Chemistry and its influence on flotation. Mogalakwena Concentrators, delivered 16 July 2019.

Hadler, K., Cilliers, J.J., 2009. The relationship between the peak in air recovery and flotation bank performance. Minerals Engineering 22(5).451-455.

Henley, K.I. 1983. Ore-dressing mineralogy: A review of techniques, applications and recent developments. Geology Society South Africa 7. 175-200.

Harris, G.H., Jia, J. 2000. International Journal of Mineral Processing, Vol 58, 35.

Harris, M.C., Runge, K.C., Whiten, W.J., Morrison, R.D. 2002. JKSimFloat as a practical tool for flotation process design and optimization. Mineral Processing Plant Design, Practical and Control. SME. 461-478.

Hewitt, D., Fornasiero, D., Ralston, J. 1995. Bubble–particle attachment. Chemical Society Faraday Transactions 91. 1997–2001.

Holwell, D.A., McDonald, I. 2006. Petrology, geochemistry and the mechanisms determining the distribution of platinum-group element and base metal sulphide mineralization in the Platreef at Overysel, northern Bushveld Complex, South Africa. Mineralium Deposita.41.575-598.

Kelebek S. 1993. The Effect of Oxidation on the Flotation Behaviour of Nickel-Copper Ores. XVIII International Mineral Processing Congress. Page 999 - 1005.

Klimpel, R. 1984. Froth Flotation: The Kinetic Approach. Johannesburg, South Africa: Proceedings of Mintek 50

Lu, Y., Tong, X., Xie, X., Yang, B., Hua, Z. 2018. Effect of particle size on the oxidation and flotation behavior of galena particles. Physicochemical Problems of Mineral Processing. 55. 208-216.

Mugadza, M. 2015. Investigating ways of improving recovery of slow floating PGM Minerals at Zimplats. A research report submitted to the Faculty of Engineering and the Built Environment, University of the Witwatersrand.

Napier-Munn, T. 1998. Analysing plant trials by comparing recovery-grade regression lines

Napier-Munn, T. 2010. An introduction to Comparative statistics and experimental design for minerals engineers. Course Notes, 2nd version 6.4. University of Queensland.

Napier-Munn, T.J, Morrell, S., Morrison, R.D., Kojovic, C. 2005. Mineral Comminution Circuits: Their Operation and Optimization. Julius Kruttschnitt Mineral Research Centre. Queensland.

Pease, J., Curry, D., Young, M. 2006. Designing flotation circuits for higher fines recovery. Minerals Engineering 19.831-840.

Pyke, B., Fornasiero, D., Ralston, J. 2003. Bubble particle hetero coagulation under turbulent conditions. Journal of Colloid and Interface Science 265. 141–151.

Rixom, P.M. 2015. Short Course on Geology and Mineralogy for Anglo Platinum Metallurgists. Anglo Research, Crown Mines, Johannesburg.

Rule, C.M. 2009.Energy considerations in the current PGM processing flowsheet utilizing new technologies. SAIMM. 109(1).39-45.

Rule, C.M. 2011. Stirred milling –new comminution technology in the PGM industry. SAIMM. 111(2).101-107.

Sabau A. 1998. Laboratory Studies on Magnetoflotation of Falconbridge Nickel Ore. Mineral Resources Engineering, Laurebtian University, Sudbury, Ontario.

Shamaila, S., O'Connor C.T. 2008. The role of synthetic minerals in determining the relative flotation behavior of Platreef PGE tellurides and arsenides. Minerals Engineering.899-904.

Steyn, J.J. 2012. Developing a framework for the design of the milling and rougher circuits for a Platinum-bearing UG2 ore. Thesis Presented for the Degree of Doctor of Philosophy. Department of Chemical Engineering. University of Capetown.

Sylvester, P.J. 2012. Chapter 1: Use of the mineral liberation analyzer for mineralogical studies

of sediments and sedimentary rocks. Mineralogical Association of Canada Short Course 42. St John's. Newfoundland and Labrador.

Valenta, M.M. 2007.Balancing the reagent suite to optimize grade and recovery. Mineral Engineering, Vol 20. 979-985.

Verrelli, D.I., Koh, P.T.L., Nguyen, A.V. 2011. Particle-bubble interaction and attachment in flotation. Chemical Engineering Science, Vol. 66. 5910-5921.

Vinnett, L., Alvarez-Silva, M., Jaques, A., Hinojosa, F. & Yianatos, J. 2015. Batch flotation kinetics: Fractional calculus approach. Minerals Engineering, Vol. 77. 167-171.

Wang, G., Nguyen, A.V., Mitra. S., Joshi, J.B., Jameson, G.J., Evans, G.M. 2016. A review of the mechanisms and models of bubble-particle detachment in froth flotation. Separation and Purification Technology 170. 155–172.

Weber, M.E., Paddock, D. 1983. Interceptional and gravitational collision efficiencies for single collectors at intermediate Reynolds numbers. Journal of Colloid and Interface Science 94. 328–335.

Wills, B.A., Napier-Munn, T., 2006. Mineral Processing Technology. 7nth Ed. Elsevier Science and Technology Books. Queensland.

Woodburn, E.T.1971. The effect of particle size distribution on the performance of phosphate flotation process. Metallurgy Transcript, Volume 75. 3163-3174.

Zongfu, D., Daniel, F., Ralston, J. 1999. Particle-bubble attachment in Mineral Flotation. Ian Wark Research Institute. University of South Australia. Australia.

CHAPTER SEVEN

APPENDICES

APPENDIX A

ORE CHARACTERIZATION

Table 7.1: Sample Splitting efficiency

Sieve Size	MNC sample 1			MNC sample 2			MNC sample 3			MNC sample 4			MNC sample 5		
(mm)	Mass (g)	Mass %	Cum% passing	Mass (g)	Mass %	Cum% passing	Mass (g)	Mass %	Cum% passing	Mass (g)	Mass %	Cum% passing	Mass (g)	Mass %	Cum% passing
3.350	0.00	0.00	100.00	0.00	0.00	100.00	0.00	0.00	100.00	0.00	0.00	100.00	0.00	0.00	100.00
2.360	89.50	7.92	92.08	80.70	7.36	92.64	76.30	7.04	92.96	79.10	7.11	92.89	85.20	6.58	93.42
1.700	138.50	12.25	79.83	137.80	12.57	80.06	130.80	12.07	80.89	139.00	12.49	80.40	169.80	13.11	80.31
1.180	134.40	11.89	67.95	134.60	12.28	67.78	131.70	12.15	68.75	136.10	12.23	68.17	159.00	12.28	68.03
0.850	92.90	8.22	59.73	89.10	8.13	59.65	87.80	8.10	60.65	89.70	8.06	60.11	107.80	8.32	59.71
0.600	103.40	9.15	50.59	99.30	9.06	50.59	99.50	9.18	51.47	101.00	9.08	51.03	117.90	9.10	50.60
0.425	75.20	6.65	43.94	73.30	6.69	43.91	73.60	6.79	44.68	74.80	6.72	44.31	88.20	6.81	43.79
0.300	77.70	6.87	37.06	73.40	6.70	37.21	74.40	6.86	37.81	75.40	6.78	37.54	88.60	6.84	36.95
0.212	64.40	5.70	31.37	62.50	5.70	31.51	63.10	5.82	31.99	64.30	5.78	31.76	73.10	5.64	31.31
0.150	63.10	5.58	25.79	60.80	5.55	25.96	62.00	5.72	26.27	63.20	5.68	26.08	71.50	5.52	25.79
0.106	49.90	4.41	21.37	47.40	4.32	21.63	47.60	4.39	21.88	49.70	4.47	21.61	54.00	4.17	21.62
0.075	45.30	4.01	17.37	44.20	4.03	17.60	44.40	4.10	17.79	45.10	4.05	17.56	53.40	4.12	17.49
0.053	34.30	3.03	14.33	33.70	3.07	14.53	34.70	3.20	14.58	33.30	2.99	14.57	37.10	2.86	14.63
0.038	27.80	2.46	11.87	26.90	2.45	12.07	27.80	2.56	12.02	27.90	2.51	12.06	30.10	2.32	12.30
-0.038	134.26	11.87		132.30	12.07		130.29	12.02		134.19	12.06		159.33	12.30	
Total	**1130.66**	**100.00**		**1096.00**	**100.00**		**1083.99**	**100.00**		**1112.79**	**100.00**		**1295.03**	**100.00**	

Table 7.2: Typical BWI from drill core samples

SAMPLE_ID	FROM	TO	GPR mini bond (gram)	WI mini bond [kWh/mt]
GM-ZN944D0-001	247	262	0.22	22.24
GM-ZN944D0-002	262	277	0.25	20.76
GM-ZN944D0-003	277	292	0.3	18.93
GM-ZN944D0-004	292	307	0.29	19.25
GM-ZN944D0-005	307	322	0.24	21.07
GM-ZN944D0-006	322	337	0.26	20.63
GM-ZN944D0-008	351	367	0.29	19.33
GM-ZN944D0-009	367	382	0.36	17.46
GM-ZN944D0-010	382	397	0.38	16.91
GM-ZN944D0-011	397	412	0.39	16.85
GM-ZN944D0-012	412	427	0.38	16.96
GM-ZN910D0-002	270	285	0.23	21.73
GM-ZN910D0-003	285	300	0.29	19.5
GM-ZN910D0-006	335	350	0.36	17.38
GM-ZN910D0-007	350	365	0.32	18.49
GM-ZN903D0-001	399	415	0.22	21.99
GM-ZN903D0-002	415	430	0.26	20.27

APPENDIX B

FLEXI-FLOAT PUMPS AND AIR RATE CALIBRATIONS

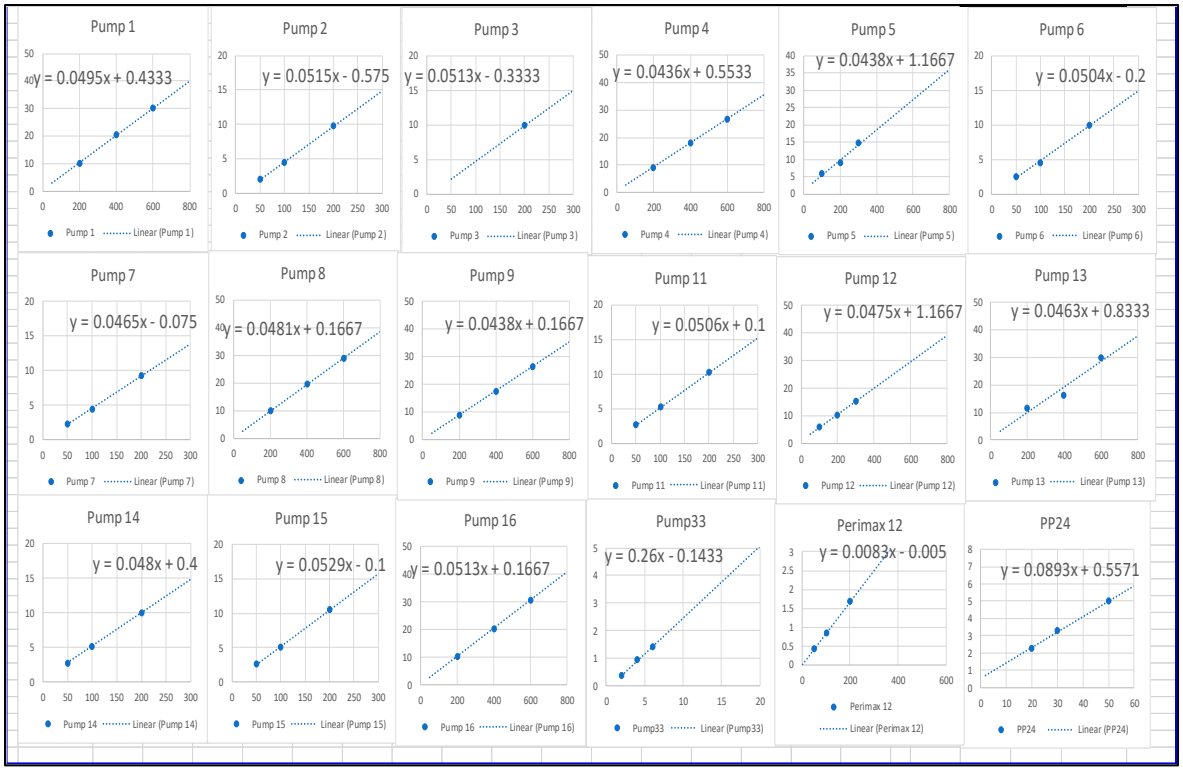

Figure 7.1: Flexi-float pump calibration

Table 7.3: Air rate calibration at different supply pressure

Flow meter *Reading*	**@4 bar**	**@4.5 bar**	**@5 bar**
	Flowrate (Nl/min)		
1	2	2.1	2.3
2	4.0	4.3	4.5
3	6.4	6.7	7.1
4	8.8	9.2	9.6
5	11.2	11.9	12.6
6	13.5	14.5	15.5
7	16.3	17.4	18.5
8	19.0	20.3	21.5
9	22.0	23.4	24.8
10	25.0	26.5	28
11	28.0	29.5	31.0
12	31.0	32.5	34
13	34.0	35.8	37.5
14	37.0	39.0	41
15	40.0	42.3	44.5
16	43.0	45.5	48
17	46.0	48.8	51.5
18	49.0	52.0	55
19	52.5	55.5	58.5
20	56.0	59.0	62

APPENDIX C

CAMPAIGN ONE DATA COLLECTION

Table 7.4: Primary mill energy intensity

14-Mar	15-Mar
MF2 Primary mill kWhr/t	MF3 Primary mill kWhr/t
31.12	28.54
30.05	35.39
30.05	33.11
31.12	34.25
28.97	33.11
30.05	33.11
31.12	33.11
28.97	31.96
28.97	

Table 7.5: Primary mill energy intensity normality test

Descriptive Statistics	MF2 Primary mill kWhr/t	MF3 Primary mill kWhr/t
Count	9	8
Mean	30.05	32.82
StDev	0.93	2.00
Range	2.15	6.85
Minimum	28.97	28.54
25th Percentile (Q1)	28.97	32.25
50th Percentile (Median)	30.05	33.11
75th Percentile (Q3)	31.12	33.96
Maximum	31.12	35.39
95.0% CI Mean	29.331 to 30.76	31.147 to 34.492
95.0% CI Sigma	0.62769 to 1.7803	1.3228 to 4.0718
Anderson-Darling Normality Test	0.66	0.68
P-Value (A-D Test)	0.06	**0.05**
Skewness	0.00	-1.41
P-Value (Skewness)	1.00	
Kurtosis	-1.71	3.32
P-Value (Kurtosis)	0.12	

Table 7.6: Primary mill energy intensity variance test

Levene's Test For Equal Variance: MF2 Primary mill kWhr/t - MF3 Primary mill kWhr/t		
(Use with non-normal data)		
Test Information		
H_0: Variance 1 = Variance 2 = ... = Variance k		
Ha: At least one pair Variance i ≠ Variance j		
Results	**MF2 Primary mill kWhr/t**	**MF3 Primary mill kWhr/t**
Count	9	8
Mean	30.05	32.82
Median	30.05	33.11
StDev	0.93	2.00
AD Normality Test P-Value	0.06	**0.05**
Levene's Test Statistic	0.56	
DF Num	1	
DF Den	15	
P-Value	0.47	

Table 7.7: Primary mill energy intensity Mann-Whitney test

2 Sample Mann-Whitney		
Test Information		
H_0: Median Difference = 0		
H_a: Median Difference ≠ 0		
Results:	**MF2 Primary mill kWhr/t**	**MF3 Primary mill kWhr/t**
Count	9	8
Median	30.05	33.11
Mann-Whitney Statistic	54.00	
P-Value (2-sided, adjusted for ties)	**0.0102**	

Table 7.8: Primary rougher float feed particle size distribution normality test

Descriptive Statistics	MF2 Primary float feed (-75 microns)	MF3 Primary float feed (-75 microns)
Count	4	4
Mean	47.80	49.75
StDev	0.36	0.42
Range	0.78	0.93
Minimum	47.54	49.17
25th Percentile (Q1)	47.54	49.31
50th Percentile (Median)	47.67	49.87
75th Percentile (Q3)	48.18	50.07
Maximum	48.32	50.10
95.0% CI Mean	47.222 to 48.378	49.089 to 50.412
95.0% CI Sigma	0.20579 to 1.3545	0.23546 to 1.5497
Anderson-Darling Normality Test	0.41	0.31
P-Value (A-D Test)	0.16	0.33
Skewness	1.51	-1.28

Table 7.9: Primary rougher float feed particle size distribution variance test

Bartlett's Test For Equal Variance: MF2 Primary float feed (-75 microns) - MF3 Primary float feed (-75 microns)		
(Use with normal data)		
Test Information		
H_0: Variance 1 = Variance 2 = ... = Variance k		
Ha: At least one pair Variance i ≠ Variance j		
Results	MF2 Primary float feed (-75 microns)	MF3 Primary float feed (-75 microns)
Count	4	4
Mean	47.80	49.75
Median	47.67	49.87
StDev	0.36	0.42
AD Normality Test P-Value	0.16	0.33
Bartlett's Test Statistic	0.046	
P-Value	0.829	

Table 7.10: Primary rougher float feed particle size distribution 2 sample t-test

2 Sample t-Test		
Test Information		
H_0: Mean Difference = 0		
H_a: Mean Difference Not Equal To 0		
Assume Equal Variance		
Results:	**MF2 Primary float feed (-75 microns)**	**MF3 Primary float feed (-75 microns)**
Count	4	4
Mean	47.80	49.75
Standard Deviation	0.36	0.42
Mean Difference	-1.951	
Std Error Difference	0.276011	
DF	6	
t	-7.069	
P-Value (2-sided)	**0.0004**	
UC (2-sided, 95%)	-1.276	
LC (2-sided, 95%)	-2.626	

Table 7.11: Secondary mill energy intensity

14-Mar	15-Mar
MF2 Secondary mill kWhr/t	MF3 Secondary mill kWhr/t
26.85	15.73
17.15	23.28
20.40	21.38
22.74	21.44
21.49	22.54
22.01	23.81
22.63	20.16
19.21	21.94
17.24	
19.67	

Table 7.12: Secondary mill energy intensity normality test

Descriptive Statistics	MF2 Secondary mill kWhr/t	MF3 Secondary mill kWhr/t
Count	10	8
Mean	20.94	21.29
StDev	2.89	2.52
Range	9.70	8.08
Minimum	17.15	15.73
25th Percentile (Q1)	18.72	20.47
50th Percentile (Median)	20.95	21.69
75th Percentile (Q3)	22.66	23.10
Maximum	26.85	23.81
95.0% CI Mean	18.867 to 23.009	19.176 to 23.394
95.0% CI Sigma	1.9913 to 5.2851	1.668 to 5.1345
Anderson-Darling Normality Test	0.25	0.58
P-Value (A-D Test)	0.65	0.09
Skewness	0.60	-1.74
P-Value (Skewness)	0.37	
Kurtosis	0.77	3.69
P-Value (Kurtosis)	0.45	

Table 7.13: Secondary mill energy intensity variance test

Bartlett's Test For Equal Variance: MF2 Secondary mill kWhr/t - MF3 Secondary mill kWhr/t		
(Use with normal data)		
Test Information		
H_0: Variance 1 = Variance 2 = ... = Variance k		
Ha: At least one pair Variance i ≠ Variance j		
Results	MF2 Secondary mill kWhr/t	MF3 Secondary mill kWhr/t
Count	10	8
Mean	20.94	21.29
Median	20.95	21.69
StDev	2.89	2.52
AD Normality Test P-Value	0.65	0.09
Bartlett's Test Statistic	0.14	
P-Value	0.71	

Table 7.14: Secondary mill energy intensity 2 sample t-test

2 Sample t-Test		
Test Information		
H_0: Mean Difference = 0		
H_a: Mean Difference Not Equal To 0		
Assume Equal Variance		
Results:	**MF2 Secondary mill kWhr/t**	**MF3 Secondary mill kWhr/t**
Count	10	8
Mean	20.94	21.29
Standard Deviation	2.89	2.52
Mean Difference	-0.35	
Std Error Difference	1.30	
DF	16.00	
t	-0.27	
P-Value (2-sided)	0.79	
UC (2-sided, 95%)	2.41	
LC (2-sided, 95%)	-3.10	

Table 7.15: IsaMill energy intensity normality test

Descriptive Statistics	MF2 Isamill kWhr/t	MF3 Isamill kWhr/t
Count	10	8
Mean	16.31	15.98
StDev	1.11	0.61
Range	3.22	2.28
Minimum	15.02	14.84
25th Percentile (Q1)	15.02	15.98
50th Percentile (Median)	16.10	15.98
75th Percentile (Q3)	17.17	15.98
Maximum	18.24	17.12
95.0% CI Mean	15.518 to 17.103	15.472 to 16.492
95.0% CI Sigma	0.76229 to 2.0232	0.40344 to 1.2419
Anderson-Darling Normality Test	0.48	1.31
P-Value (A-D Test)	0.18	**0.00**
Skewness	0.27	0.00
P-Value (Skewness)	0.68	
Kurtosis	-0.90	3.50
P-Value (Kurtosis)	0.53	

Table 7.16: IsaMill energy intensity variance test

Results	MF2 Isamill kWhr/t	MF3 Isamill kWhr/t
Count	10	8
Mean	16.31	15.98
Median	16.10	15.98
StDev	1.11	0.61
AD Normality Test P-Value	0.18	**0.00**
Levene's Test Statistic	3.83	
DF Num	1.00	
DF Den	16.00	
P-Value	0.07	

Table 7.17: IsaMill energy intensity Mann-Whitney test

2 Sample Mann-Whitney		
Test Information		
H_0: Median Difference = 0		
H_a: Median Difference ≠ 0		
Results:	**MF2 Isamill Kwhr/t**	**MF3 Isamill kWhr/t**
Count	10	8
Median	16.10	15.98
Mann-Whitney Statistic	111.00	
P-Value (2-sided, adjusted for ties)	0.16	

Table 7.18: Final grind normality test

Descriptive Statistics	MF2 Final grind (-75 microns)	MF3 Final grind (-75 microns)
Count	6	7
Mean	88.93	88.01
StDev	3.64	2.46
Range	9.58	6.10
Minimum	83.41	84.69
25th Percentile (Q1)	85.07	85.85
50th Percentile (Median)	90.19	87.74
75th Percentile (Q3)	91.62	90.36
Maximum	93.00	90.79
95.0% CI Mean	85.113 to 92.745	85.732 to 90.279
95.0% CI Sigma	2.2697 to 8.918	1.5842 to 5.4136
Anderson-Darling Normality Test	0.36	0.37
P-Value (A-D Test)	0.31	0.32
Skewness	-0.76	-0.09

Table 7.19: Final grind variance test

Bartlett's Test For Equal Variance: MF2 Final grind (-75 microns) - MF3 Final grind (-75 microns)		
(Use with normal data)		
Test Information		
H_0: Variance 1 = Variance 2 = ... = Variance k		
Ha: At least one pair Variance i ≠ Variance j		
Results	MF2 Final grind (-75 microns)	MF3 Final grind (-75 microns)
Count	6	7
Mean	88.93	88.01
Median	90.19	87.74
StDev	3.64	2.46
AD Normality Test P-Value	0.31	0.32
Bartlett's Test Statistic	0.76	
P-Value	0.38	

Table 7.20: Final grind 2 sample t-test

2 Sample t-Test		
Test Information		
H_0: Mean Difference = 0		
H_a: Mean Difference Not Equal To 0		
Assume Equal Variance		
Results:	**MF2 Final grind (-75 microns)**	**MF3 Final grind (-75 microns)**
Count	6	7
Mean	88.93	88.01
Standard Deviation	3.64	2.46
Mean Difference	0.923538	
Std Error Difference	1.697	
DF	11	
t	0.54	
P-Value (2-sided)	0.60	
UC (2-sided, 95%)	4.66	
LC (2-sided, 95%)	-2.81	

Table 7.21: Run 1 MF2 Mass balance summary PGMs

Cell ID	Solids concentrate (kg/h)	PGM g/h	Cumulative conc mass (kg/h)	Cumulative PGM flow (g/h)	Cumulative grade (g/t)	Cumulative recovery (%)	Cumulative mass pull (%)	4T Enrichment ratio
Feed	90.083	0.323						
440-FT-01	1.641	0.099	1.641	0.099	60.437	30.666	1.822	16.835
440-FT-02	1.839	0.067	3.480	0.166	47.763	51.393	3.863	13.305
440-FT-03	0.684	0.019	4.164	0.185	44.415	57.191	4.623	12.372
440-FT-04	0.009	0.000	4.173	0.185	44.386	57.276	4.633	12.364
440-FT-05	0.009	0.000	4.182	0.185	44.330	57.326	4.642	12.348
440-FT-06	0.256	0.003	4.438	0.189	42.545	58.384	4.927	11.851
440-FT-07	0.040	0.001	4.478	0.189	42.287	58.553	4.971	11.779
440-FT-08	0.010	0.000	4.488	0.189	42.220	58.589	4.982	11.761
440-FT-09	2.189	0.026	6.676	0.216	32.320	66.723	7.411	9.003
440-FT-10	3.127	0.037	9.804	0.253	25.833	78.312	10.883	7.196
440-FT-11	1.056	0.009	10.860	0.262	24.158	81.124	12.055	6.729
440-FT-12	0.146	0.002	11.006	0.265	24.052	81.849	12.217	6.700
440-FT-13	0.029	0.000	11.034	0.265	24.011	81.927	12.249	6.688
440-FT-14	0.014	0.000	11.049	0.265	23.991	81.963	12.265	6.683
440-FT-15	0.009	0.000	11.058	0.265	23.978	81.984	12.275	6.679
440-FT-16	0.010	0.000	11.067	0.265	23.965	82.013	12.286	6.676
440-FT-17	0.706	0.000	11.773	0.265	22.537	82.043	13.069	6.278
440-FT-18	0.042	0.000	11.815	0.265	22.463	82.070	13.116	6.257

Table 7.22: Run 1 MF2 Mass balance summary copper and nickel

Cell ID	Copper flow (kg/h)	Cumulative copper flow (kg/h)	Cumulative Cu recovery (%)	Cu grade (%)	Cu Enrichment ratio	Nickel flow (kg/h)	Cumulative nickel flow (kg/h)	Cumulative Ni recovery (%)	Ni grade (%)	Ni Enrichment ratio
Feed										
440-FT-01	0.033	0.033	38.832	2.000	21.318	0.031	0.031	18.644	1.868	10.235
440-FT-02	0.013	0.046	54.732	1.329	14.169	0.026	0.057	34.480	1.629	8.926
440-FT-03	0.005	0.051	60.360	1.225	13.057	0.008	0.065	39.391	1.555	8.521
440-FT-04	0.000	0.051	60.436	1.224	13.046	0.000	0.065	39.457	1.554	8.517
440-FT-05	0.000	0.051	60.471	1.222	13.026	0.000	0.065	39.502	1.553	8.509
440-FT-06	0.001	0.052	61.528	1.172	12.489	0.002	0.067	40.731	1.509	8.268
440-FT-07	0.000	0.052	61.651	1.164	12.403	0.000	0.067	40.906	1.502	8.229
440-FT-08	0.000	0.052	61.677	1.162	12.380	0.000	0.067	40.946	1.500	8.219
440-FT-09	0.008	0.061	71.663	0.907	9.669	0.013	0.081	49.110	1.209	6.626
440-FT-10	0.007	0.067	79.681	0.687	7.322	0.018	0.099	60.276	1.011	5.539
440-FT-11	0.003	0.070	82.794	0.644	6.868	0.007	0.106	64.261	0.973	5.331
440-FT-12	0.000	0.070	83.332	0.640	6.821	0.001	0.107	65.089	0.972	5.328
440-FT-13	0.000	0.070	83.414	0.639	6.810	0.000	0.107	65.194	0.971	5.322
440-FT-14	0.000	0.071	83.442	0.638	6.803	0.000	0.107	65.244	0.971	5.320
440-FT-15	0.000	0.071	83.460	0.638	6.799	0.000	0.107	65.273	0.970	5.318
440-FT-16	0.000	0.071	83.480	0.637	6.795	0.000	0.107	65.310	0.970	5.316
440-FT-17	0.000	0.071	83.500	0.599	6.389	0.000	0.107	65.346	0.913	5.000
440-FT-18	0.000	0.071	83.536	0.598	6.369	0.000	0.108	65.396	0.910	4.986

Table 7.23: Run 1 MF3 Mass balance summary PGMs

Cell ID	Solids concentrate (kg/h)	PGM g/h	Cumulative conc mass (kg/h)	Cumulative PGM flow (g/h)	Cumulative grade (g/t)	Cumulative recovery (%)	Cumulative mass pull (%)	4T Enrichment ratio
Feed	87.60	0.38						
440-FT-01	1.547	0.123	1.547	0.123	79.660	32.720	1.766	18.525
440-FT-02	1.847	0.073	3.394	0.197	57.910	52.178	3.875	13.467
440-FT-03	0.785	0.027	4.179	0.223	53.382	59.221	4.770	12.414
440-FT-04	0.009	0.000	4.188	0.223	53.308	59.272	4.781	12.397
440-FT-05	0.009	0.000	4.198	0.223	53.227	59.314	4.792	12.378
440-FT-06	0.192	0.003	4.390	0.226	51.560	60.085	5.011	11.990
440-FT-07	0.016	0.000	4.406	0.227	51.426	60.144	5.029	11.959
440-FT-08	0.009	0.000	4.415	0.227	51.350	60.182	5.040	11.941
440-FT-09	0.152	0.005	4.567	0.232	50.711	61.482	5.214	11.793
440-FT-10	3.063	0.050	7.630	0.282	36.934	74.809	8.710	8.589
440-FT-11	2.330	0.021	9.960	0.303	30.442	80.487	11.369	7.079
440-FT-12	0.219	0.002	10.178	0.305	29.988	81.030	11.619	6.974
440-FT-13	0.031	0.000	10.210	0.305	29.921	81.095	11.655	6.958
440-FT-14	0.017	0.000	10.226	0.306	29.884	81.126	11.674	6.949
440-FT-15	0.010	0.000	10.236	0.306	29.861	81.141	11.685	6.944
440-FT-16	0.010	0.000	10.246	0.306	29.839	81.164	11.697	6.939
440-FT-17	0.305	0.004	10.552	0.310	29.348	82.208	12.045	6.825
440-FT-18	0.547	0.004	11.098	0.314	28.251	83.236	12.669	6.570

Table 7.24: Run 1 MF3 Mass balance summary copper and nickel

Cell ID	Copper flow (kg/h)	Cumulative copper flow (kg/h)	Cumulative Cu recovery (%)	Cu grade (%)	Cu Enrichment ratio	Nickel flow (kg/h)	Cumulative nickel flow (kg/h)	Cumulative Ni recovery (%)	Ni grade (%)	Ni Enrichment ratio
440-FT-01	0.032	0.032	38.818	2.062	21.978	0.031	0.031	18.644	2.007	10.556
440-FT-02	0.013	0.045	54.732	1.325	14.126	0.025	0.056	33.655	1.651	8.686
440-FT-03	0.005	0.050	60.411	1.188	12.664	0.009	0.065	39.084	1.558	8.193
440-FT-04	0.000	0.050	60.460	1.186	12.645	0.000	0.065	39.132	1.556	8.185
440-FT-05	0.000	0.050	60.497	1.184	12.625	0.000	0.065	39.177	1.554	8.176
440-FT-06	0.001	0.051	61.550	1.152	12.283	0.001	0.067	40.056	1.520	7.993
440-FT-07	0.000	0.051	61.601	1.149	12.249	0.000	0.067	40.129	1.517	7.979
440-FT-08	0.000	0.051	61.632	1.147	12.229	0.000	0.067	40.175	1.516	7.972
440-FT-09	0.001	0.052	62.806	1.130	12.047	0.002	0.069	41.292	1.506	7.920
440-FT-10	0.013	0.064	78.290	0.843	8.989	0.025	0.094	56.580	1.235	6.496
440-FT-11	0.003	0.068	82.201	0.678	7.230	0.014	0.108	64.912	1.085	5.709
440-FT-12	0.000	0.068	82.587	0.667	7.108	0.001	0.109	65.605	1.073	5.646
440-FT-13	0.000	0.068	82.632	0.665	7.090	0.000	0.109	65.684	1.072	5.636
440-FT-14	0.000	0.068	82.652	0.664	7.080	0.000	0.109	65.722	1.070	5.630
440-FT-15	0.000	0.068	82.662	0.664	7.074	0.000	0.109	65.741	1.070	5.626
440-FT-16	0.000	0.068	82.679	0.663	7.069	0.000	0.110	65.769	1.069	5.623
440-FT-17	0.001	0.069	83.597	0.651	6.940	0.001	0.111	66.616	1.051	5.530
440-FT-18	0.001	0.069	84.525	0.626	6.672	0.001	0.112	67.209	1.009	5.305

APPENDIX D

CAMPAIGN TWO DATA COLLECTION

Table 7.25: Primary mill power intensity

09-Apr	10-Apr
MF2 Primary mill kWh/t	MF3 Primary mill kWh/t
31.16	30.98
31.16	30.98
34.49	30.98
31.16	27.54
28.93	35.57
36.72	30.98
34.49	32.13
25.59	34.43
32.27	29.84

Table 7.26: Primary mill power intensity normality test

Descriptive Statistics	MF2 Primary mill kWh/t	MF3 Primary mill kWh/t
Count	9	9
Mean	31.77	31.49
StDev	3.30	2.37
Range	11.13	8.03
Minimum	25.59	27.54
25th Percentile (Q1)	30.04	30.41
50th Percentile (Median)	31.16	30.98
75th Percentile (Q3)	34.49	33.28
Maximum	36.72	35.57
95.0% CI Mean	29.239 to 34.307	29.67 to 33.319
95.0% CI Sigma	2.2267 to 6.3155	1.6032 to 4.547
Anderson-Darling Normality Test	0.28	0.48
P-Value (A-D Test)	0.55	0.17
Skewness	-0.44	0.32
P-Value (Skewness)	0.53	0.65
Kurtosis	0.49	0.52
P-Value (Kurtosis)	0.59	0.58

Table 7.27: Primary mill power intensity variance test

Bartlett's Test For Equal Variance: MF2 Primary mill kWh/t - MF3 Primary mill kWh/t		
(Use with normal data)		
Test Information		
H_0: Variance 1 = Variance 2 = ... = Variance k		
Ha: At least one pair Variance i ≠ Variance j		
Results	**MF2 Primary mill kWh/t**	**MF3 Primary mill kWh/t**
Count	9	9
Mean	31.77	31.49
Median	31.16	30.98
StDev	3.30	2.37
AD Normality Test P-Value	0.55	0.17
Bartlett's Test Statistic	0.80	
P-Value	0.37	

Table 7.28: Primary mill power intensity 2 sample t-test

2 Sample t-Test		
Test Information		
H_0: Mean Difference = 0		
H_a: Mean Difference Not Equal To 0		
Assume Equal Variance		
Results:	**MF2 Primary mill kWh/t**	**MF3 Primary mill kWh/t**
Count	9	9
Mean	31.77	31.49
Standard Deviation	3.30	2.37
Mean Difference	0.28	
Std Error Difference	1.35	
DF	16.00	
t	0.21	
P-Value (2-sided)	0.84	
UC (2-sided, 95%)	3.15	
LC (2-sided, 95%)	-2.59	

Table 7.29: Primary float feed particle size distribution normality test

Descriptive Statistics	MNC_PFF_MF2	MNC_PFF_MF3
Count	14.00	15.00
Mean	48.62	47.67
StDev	1.59	3.06
Range	5.79	10.40
Minimum	44.69	40.75
25th Percentile (Q1)	47.93	46.67
50th Percentile (Median)	48.96	47.92
75th Percentile (Q3)	49.64	50.16
Maximum	50.48	51.15
95.0% CI Mean	47.704 to 49.544	45.979 to 49.371
95.0% CI Sigma	1.155 to 2.5668	2.2423 to 4.8302
Anderson-Darling Normality Test	0.66	0.62
P-Value (A-D Test)	0.07	0.09
Skewness	-1.35	-1.06
P-Value (Skewness)	**0.03**	0.07
Kurtosis	1.96	0.47
P-Value (Kurtosis)	0.12	0.52

Table 7.30: Primary float feed particle size distribution variance test

Bartlett's Test For Equal Variance: MNC_PFF_MF2 - MNC_PFF_MF3		
(Use with normal data)		
Test Information		
H_0: Variance 1 = Variance 2 = ... = Variance k		
Ha: At least one pair Variance i ≠ Variance j		
Results	**MNC_PFF_MF2**	**MNC_PFF_MF3**
Count	14.00	15.00
Mean	48.62	47.67
Median	48.96	47.92
StDev	1.59	3.06
AD Normality Test P-Value	0.07	0.09
Bartlett's Test Statistic	5.12	
P-Value	**0.02**	

Table 7.31: Primary float feed particle size distribution 2 sample t-test

2 Sample t-Test		
Test Information		
H_0: Mean Difference = 0		
H_a: Mean Difference Not Equal To 0		
Assume Unequal Variance		
Results:	**MNC_PFF_MF2**	**MNC_PFF_MF3**
Count	14	15
Mean	48.62	47.67
Standard Deviation	1.59	3.06
Mean Difference	0.95	
Std Error Difference	0.90	
DF	21.36	
t	1.06	
P-Value (2-sided)	0.30	
UC (2-sided, 95%)	2.82	
LC (2-sided, 95%)	-0.92	

Table 7.32: Secondary mill power intensity

09-04-19	10-04-19
MF2 Secondary mill kWh/t	MF3 Secondary mill kWh/t
18.28	21.85
24.11	25.18
21.15	18.95
21.82	24.51
28.88	24.13
24.31	19.49
18.27	22.86
21.91	21.48

Table 7.33: Secondary mill power intensity normality test

Descriptive Statistics	MF2 Secondary mill kWh/t	MF3 Secondary mill kWh/t
Count	8	8
Mean	22.34	22.31
StDev	3.48	2.29
Range	10.61	6.23
Minimum	18.27	18.95
25th Percentile (Q1)	19.00	19.99
50th Percentile (Median)	21.87	22.35
75th Percentile (Q3)	24.26	24.41
Maximum	28.88	25.18
95.0% CI Mean	19.433 to 25.251	20.389 to 24.222
95.0% CI Sigma	2.3006 to 7.0818	1.5157 to 4.6656
Anderson-Darling Normality Test	0.31	0.24
P-Value (A-D Test)	0.48	0.68
Skewness	0.71	-0.32
Kurtosis	0.73	-1.26

Table 7.34: Secondary mill power intensity variance test

Bartlett's Test For Equal Variance: MF2 Secondary mill kWh/t - MF3 Secondary mill kWh/t		
(Use with normal data)		
Test Information		
H_0: Variance 1 = Variance 2 = ... = Variance k		
Ha: At least one pair Variance i ≠ Variance j		
Results	**MF2 Secondary mill kWh/t**	**MF3 Secondary mill kWh/t**
Count	8	8
Mean	22.34	22.31
Median	21.87	22.35
StDev	3.48	2.29
AD Normality Test P-Value	0.48	0.68
Bartlett's Test Statistic	1.11	
P-Value	0.29	

Table 7.35: Secondary mill power intensity 2 sample t-test

2 Sample t-Test		
Test Information		
H_0: Mean Difference = 0		
H_a: Mean Difference Not Equal To 0		
Assume Equal Variance		
Results:	**MF2 Secondary mill kWh/t**	**MF3 Secondary mill kWh/t**
Count	8	8
Mean	22.34	22.31
Standard Deviation	3.48	2.29
Mean Difference	0.04	
Std Error Difference	1.47	
DF	14.00	
t	0.02	
P-Value (2-sided)	0.98	
UC (2-sided, 95%)	3.20	
LC (2-sided, 95%)	-3.12	

Table 7.36: IsaMill power intensity normality test

Descriptive Statistics	MF2 IsaMill kWhr/t	MF3 IsaMill kWhr/t
Count	8	7
Mean	29.04	29.58
StDev	1.05	0.86
Range	2.62	2.67
Minimum	27.81	28.34
25th Percentile (Q1)	27.91	28.82
50th Percentile (Median)	29.02	29.60
75th Percentile (Q3)	30.06	30.08
Maximum	30.43	31.01
95.0% CI Mean	28.162 to 29.918	28.781 to 30.372
95.0% CI Sigma	0.69418 to 2.1369	0.55445 to 1.8947
Anderson-Darling Normality Test	0.37	0.18
P-Value (A-D Test)	0.33	0.85
Skewness	0.05	0.29

Table 7.37: IsaMill power intensity variance test

Bartlett's Test For Equal Variance: MF2 IsaMill kWhr/t - MF3 IsaMill kWhr/t		
(Use with normal data)		
Test Information		
H_0: Variance 1 = Variance 2 = ... = Variance k		
Ha: At least one pair Variance i ≠ Variance j		
Results	**MF2 IsaMill kWhr/t**	**MF3 IsaMill kWhr/t**
Count	8	7
Mean	29.04	29.58
Median	29.02	29.60
StDev	1.05	0.86
AD Normality Test P-Value	0.33	0.85
Bartlett's Test Statistic	0.233656	
P-Value	0.6288	

Table 7.38: IsaMill power intensity 2 sample t-test

2 Sample t-Test		
Test Information		
H_0: Mean Difference = 0		
H_a: Mean Difference Not Equal To 0		
Assume Equal Variance		
Results:	**MF2 IsaMill kWhr/t**	**MF3 IsaMill kWhr/t**
Count	8	7
Mean	29.04	29.58
Standard Deviation	1.05	0.86
Mean Difference	-0.54	
Std Error Difference	0.50	
DF	13.00	
t	-1.07	
P-Value (2-sided)	0.30	
UC (2-sided, 95%)	0.54	
LC (2-sided, 95%)	-1.62	

Table 7.39: Final grind normality test

Descriptive Statistics	MNC_TRT_MF2	MNC_TRT_MF3
Count	9	11
Mean	94.17	94.76
StDev	2.12	1.63
Range	5.96	5.01
Minimum	90.04	91.59
25th Percentile (Q1)	92.64	93.50
50th Percentile (Median)	95.17	95.45
75th Percentile (Q3)	95.56	95.98
Maximum	96.00	96.59
95.0% CI Mean	92.536 to 95.796	93.667 to 95.854
95.0% CI Sigma	1.4324 to 4.0626	1.1374 to 2.8568
Anderson-Darling Normality Test	0.89	0.39
P-Value (A-D Test)	**0.01**	0.31
Skewness	-1.40	-0.82
P-Value (Skewness)	0.05	0.21
Kurtosis	0.65	-0.24
P-Value (Kurtosis)	0.52	1.00

Table 7.40: Final grind variance test

Levene's Test For Equal Variance: MNC_TRT_MF2 - MNC_TRT_MF3		
(Use with non-normal data)		
Test Information		
H0: Variance 1 = Variance 2 = ... = Variance k		
Ha: At least one pair Variance i ≠ Variance j		
Results	**MNC_TRT_MF2**	**MNC_TRT_MF3**
Count	9	11
Mean	94.17	94.76
Median	95.17	95.45
StDev	2.12	1.63
AD Normality Test P-Value	**0.01**	0.31
Levene's Test Statistic	0.06	
DF Num	1.00	
DF Den	18.00	
P-Value	0.82	

Table 7.41: Final grind 2 sample t-test

2 Sample Mann-Whitney		
Test Information		
H0: Median Difference = 0		
Ha: Median Difference ≠ 0		
Results:	**MNC_TRT_MF2**	**MNC_TRT_MF3**
Count	9	11
Median	95.17	95.45
Mann-Whitney Statistic	85.00	
P-Value (2-sided, adjusted for ties)	0.49	

Table 7.42: Run 2 MF2 Mass balance PGMs

Cell ID	Solids concentrate (kg/h)	PGM g/h	Cumulative conc mass (kg/h)	Cumulative PGM flow (g/h)	Cumulative grade (g/t)	Cumulative recovery (%)	Cumulative mass pull (%)	4T Enrichment ratio
Feed	86.294	0.323						
440-FT-01	1.125	0.085	1.125	0.085	75.601	26.330	1.304	20.192
440-FT-02	2.431	0.094	3.557	0.179	50.376	55.454	4.122	13.455
440-FT-03	0.504	0.013	4.061	0.192	47.275	59.418	4.706	12.626
440-FT-04	0.008	0.000	4.069	0.192	47.223	59.475	4.716	12.613
440-FT-05	0.008	0.000	4.078	0.192	47.158	59.515	4.725	12.595
440-FT-06	0.056	0.001	4.134	0.193	46.800	59.873	4.790	12.499
440-FT-07	0.011	0.000	4.144	0.194	46.708	59.912	4.803	12.475
440-FT-08	0.009	0.000	4.153	0.194	46.639	59.947	4.813	12.457
440-FT-09	0.284	0.008	4.437	0.202	45.433	62.391	5.142	12.134
440-FT-10	2.522	0.030	6.959	0.232	33.328	71.784	8.065	8.901
440-FT-11	3.767	0.040	10.727	0.272	25.395	84.309	12.430	6.783
440-FT-12	0.415	0.003	11.141	0.276	24.736	85.296	12.911	6.607
440-FT-13	0.050	0.000	11.191	0.276	24.664	85.425	12.968	6.587
440-FT-14	0.023	0.000	11.213	0.276	24.627	85.469	12.994	6.577
440-FT-15	0.016	0.000	11.229	0.276	24.600	85.497	13.013	6.570
440-FT-16	0.014	0.000	11.244	0.276	24.578	85.530	13.029	6.564
440-FT-17	0.253	0.001	11.497	0.278	24.144	85.910	13.323	6.448
440-FT-18	0.008	0.000	11.505	0.278	24.130	85.920	13.332	6.445
440-FT-19	0.010	0.000	11.515	0.278	24.112	85.930	13.344	6.440

Table 7.43: Run 2 MF2 Mass balance base metals

Cell ID	Copper flow (kg/h)	Cumulative copper flow (kg/h)	Cumulative Cu recovery (%)	Cu grade (%)	Cu Enrichment ratio	Nickel flow (kg/h)	Cumulative nickel flow (kg/h)	Cumulative Ni recovery (%)	Ni grade (%)	Ni Enrichment ratio
440-FT-01	0.034	0.034	41.079	2.494	26.253	0.021	0.021	12.593	1.549	8.048
440-FT-02	0.022	0.056	68.117	1.582	16.650	0.028	0.049	29.250	1.376	7.150
440-FT-03	0.002	0.059	70.875	1.506	15.850	0.004	0.052	31.371	1.350	7.015
440-FT-04	0.000	0.059	70.926	1.503	15.824	0.000	0.053	31.427	1.350	7.011
440-FT-05	0.000	0.059	70.967	1.500	15.795	0.000	0.053	31.475	1.349	7.005
440-FT-06	0.000	0.059	71.025	1.496	15.752	0.000	0.053	31.569	1.348	7.001
440-FT-07	0.000	0.059	71.065	1.492	15.707	0.000	0.053	31.628	1.346	6.990
440-FT-08	0.000	0.059	71.095	1.489	15.674	0.000	0.053	31.676	1.344	6.984
440-FT-09	0.001	0.060	72.369	1.438	15.136	0.003	0.056	33.269	1.339	6.958
440-FT-10	0.005	0.065	78.261	1.013	10.667	0.019	0.074	44.495	1.167	6.065
440-FT-11	0.005	0.069	83.748	0.705	7.423	0.030	0.105	62.671	1.069	5.554
440-FT-12	0.001	0.070	84.399	0.680	7.157	0.002	0.107	63.985	1.045	5.426
440-FT-13	0.000	0.070	84.502	0.676	7.119	0.000	0.107	64.169	1.041	5.406
440-FT-14	0.000	0.070	84.530	0.675	7.103	0.000	0.107	64.226	1.039	5.397
440-FT-15	0.000	0.070	84.553	0.674	7.092	0.000	0.108	64.266	1.038	5.390
440-FT-16	0.000	0.070	84.577	0.673	7.082	0.000	0.108	64.311	1.037	5.385
440-FT-17	0.004	0.074	89.276	0.672	7.079	0.002	0.109	65.367	0.998	5.183
440-FT-18	0.000	0.074	89.293	0.672	7.074	0.000	0.109	65.382	0.997	5.180
440-FT-19	0.000	0.074	89.303	0.672	7.069	0.000	0.109	65.395	0.996	5.176

Table 7.44: Run 2 MF3 Mass balance PGMs

Cell ID	Solids concentrate (kg/h)	PGM g/h	Cumulative conc mass (kg/h)	Cumulative PGM flow (g/h)	Cumulative grade (g/t)	Cumulative recovery (%)	Cumulative mass pull (%)	4T Enrichment ratio
Feed	86.934	0.330						
440-FT-01	1.360	0.102	1.360	0.102	74.855	30.850	1.565	19.716
440-FT-02	2.196	0.089	3.557	0.191	53.726	57.892	4.091	14.151
440-FT-03	0.331	0.010	3.887	0.201	51.660	60.845	4.472	13.607
440-FT-04	0.009	0.000	3.897	0.201	51.590	60.907	4.482	13.588
440-FT-05	0.009	0.000	3.906	0.201	51.507	60.954	4.493	13.566
440-FT-06	0.014	0.000	3.920	0.201	51.398	61.040	4.509	13.538
440-FT-07	0.014	0.000	3.933	0.202	51.263	61.091	4.525	13.502
440-FT-08	0.010	0.000	3.943	0.202	51.174	61.134	4.536	13.479
440-FT-09	0.214	0.005	4.157	0.207	49.811	62.730	4.781	13.120
440-FT-10	2.221	0.029	6.378	0.236	37.037	71.569	7.337	9.755
440-FT-11	3.431	0.041	9.809	0.277	28.248	83.948	11.283	7.440
440-FT-12	0.442	0.004	10.251	0.281	27.397	85.091	11.792	7.216
440-FT-13	0.067	0.000	10.318	0.281	27.257	85.210	11.869	7.179
440-FT-14	0.027	0.000	10.345	0.281	27.199	85.252	11.900	7.164
440-FT-15	0.019	0.000	10.364	0.281	27.157	85.278	11.922	7.153
440-FT-16	0.018	0.000	10.383	0.282	27.120	85.310	11.943	7.143
440-FT-17	0.581	0.008	10.964	0.289	26.375	87.614	12.612	6.947
440-FT-18	0.010	0.000	10.974	0.289	26.357	87.631	12.623	6.942
440-FT-19	0.009	0.000	10.983	0.289	26.338	87.643	12.634	6.937

Table 7.45: Run 2 MF3 Mass balance base metals

Cell ID	Copper flow (kg/h)	Cumulative copper flow (kg/h)	Cumulative Cu recovery (%)	Cu grade (%)	Cu Enrichment ratio	Nickel flow (kg/h)	Cumulative nickel flow (kg/h)	Cumulative Ni recovery (%)	Ni grade (%)	Ni Enrichment ratio
440-FT-01	0.034	0.034	41.079	2.494	26.253	0.021	0.021	12.593	1.549	8.048
440-FT-02	0.022	0.056	68.117	1.582	16.650	0.028	0.049	29.250	1.376	7.150
440-FT-03	0.002	0.059	70.875	1.506	15.850	0.004	0.052	31.371	1.350	7.015
440-FT-04	0.000	0.059	70.926	1.503	15.824	0.000	0.053	31.427	1.350	7.011
440-FT-05	0.000	0.059	70.967	1.500	15.795	0.000	0.053	31.475	1.349	7.005
440-FT-06	0.000	0.059	71.025	1.496	15.752	0.000	0.053	31.569	1.348	7.001
440-FT-07	0.000	0.059	71.065	1.492	15.707	0.000	0.053	31.628	1.346	6.990
440-FT-08	0.000	0.059	71.095	1.489	15.674	0.000	0.053	31.676	1.344	6.984
440-FT-09	0.001	0.060	72.369	1.438	15.136	0.003	0.056	33.269	1.339	6.958
440-FT-10	0.005	0.065	78.261	1.013	10.667	0.019	0.074	44.495	1.167	6.065
440-FT-11	0.005	0.069	83.748	0.705	7.423	0.030	0.105	62.671	1.069	5.554
440-FT-12	0.001	0.070	84.399	0.680	7.157	0.002	0.107	63.985	1.045	5.426
440-FT-13	0.000	0.070	84.502	0.676	7.119	0.000	0.107	64.169	1.041	5.406
440-FT-14	0.000	0.070	84.530	0.675	7.103	0.000	0.107	64.226	1.039	5.397
440-FT-15	0.000	0.070	84.553	0.674	7.092	0.000	0.108	64.266	1.038	5.390
440-FT-16	0.000	0.070	84.577	0.673	7.082	0.000	0.108	64.311	1.037	5.385
440-FT-17	0.004	0.074	89.276	0.672	7.079	0.002	0.109	65.367	0.998	5.183
440-FT-18	0.000	0.074	89.293	0.672	7.074	0.000	0.109	65.382	0.997	5.180
440-FT-19	0.000	0.074	89.303	0.672	7.069	0.000	0.109	65.395	0.996	5.176

APPENDIX E

CAMPAIGN THREE DATA COLLECTION

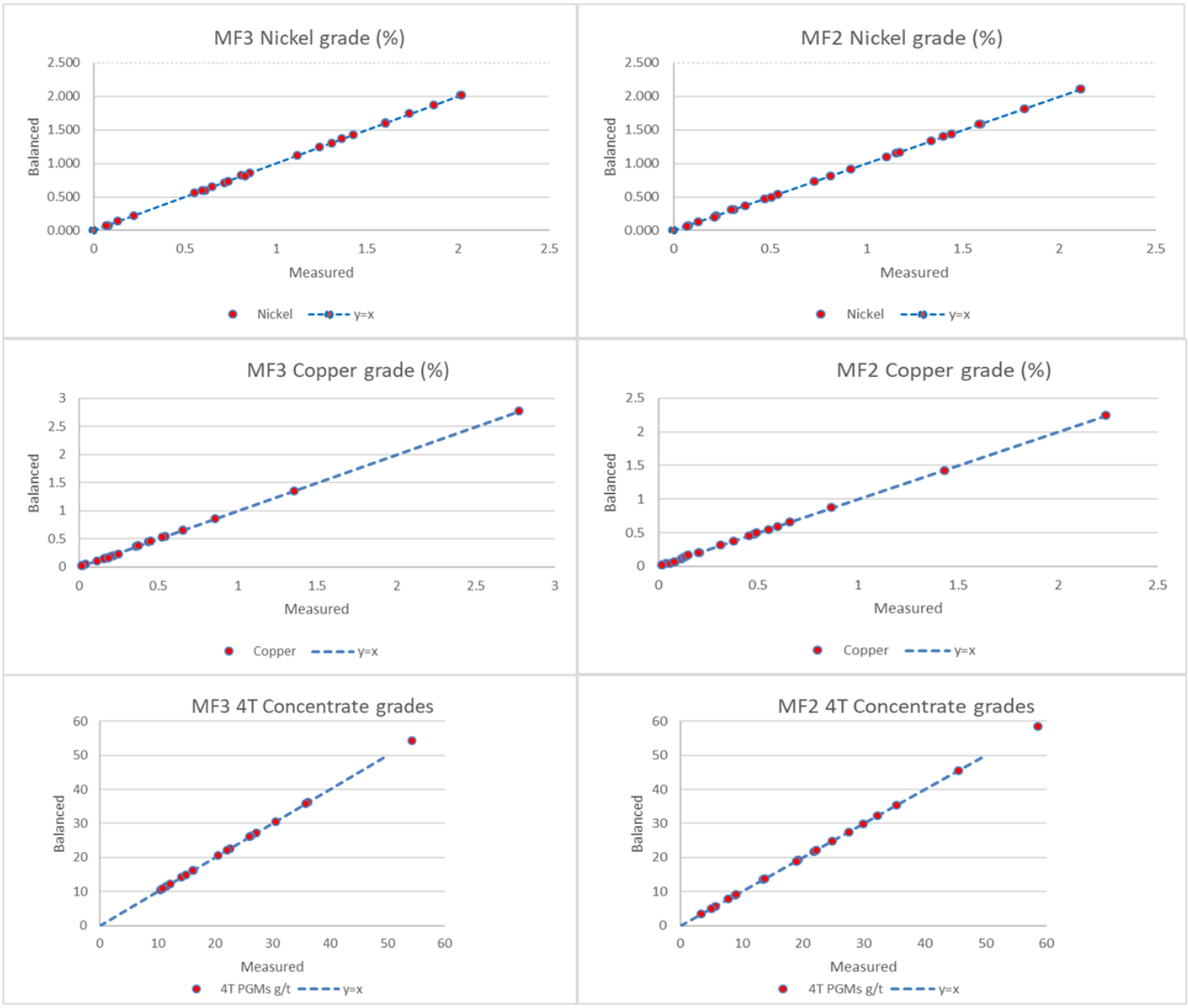

Figure 7.2: Campaign 3 data integrity

Table 7.46: Run 3 MF3 Mass balance summary PGMs

Cell ID	Solids concentrate (kg/h)	PGM g/h	Cumulative conc mass (kg/h)	Cumulative PGM flow (g/h)	Cumulative grade (g/t)	Cumulative recovery (%)	Cumulative mass pull (%)	4T Enrichment ratio
Feed	90.200	0.402						
440-FT-01	1.091	0.080	1.091	0.080	73.465	19.949	1.209	16.500
440-FT-02	1.099	0.060	2.189	0.140	63.861	34.816	2.427	14.343
440-FT-03	2.036	0.074	4.226	0.214	50.540	53.177	4.685	11.351
440-FT-04	0.012	0.000	4.238	0.214	50.484	53.268	4.698	11.339
440-FT-05	0.011	0.000	4.249	0.214	50.421	53.346	4.711	11.325
440-FT-06	0.065	0.002	4.314	0.216	50.055	53.774	4.783	11.242
440-FT-07	0.014	0.000	4.328	0.216	49.962	53.844	4.798	11.221
440-FT-08	0.011	0.000	4.339	0.216	49.880	53.887	4.810	11.203
440-FT-09	0.318	0.011	4.657	0.228	48.919	56.724	5.163	10.987
440-FT-10	1.634	0.037	6.291	0.265	42.099	65.948	6.975	9.455
440-FT-11	2.490	0.065	8.782	0.330	37.555	82.118	9.736	8.435
440-FT-12	0.508	0.008	9.290	0.338	36.384	84.161	10.299	8.172
440-FT-13	0.059	0.001	9.349	0.339	36.227	84.330	10.364	8.137
440-FT-14	0.022	0.000	9.370	0.339	36.172	84.396	10.388	8.124
440-FT-15	0.016	0.000	9.386	0.339	36.135	84.451	10.406	8.116
440-FT-16	0.015	0.000	9.401	0.339	36.095	84.491	10.422	8.107
440-FT-17	0.143	0.003	9.544	0.342	35.886	85.282	10.581	8.060
440-FT-18	0.011	0.000	9.555	0.343	35.862	85.323	10.593	8.055
440-FT-19	0.014	0.000	9.569	0.343	35.826	85.360	10.608	8.047
440-FT-20	0.000	0.000	9.569	0.343	35.826	85.360	10.608	8.047

Table 7.47: Run 3 MF3 Mass balance summary base metals

Cell ID	Copper flow (kg/h)	Cumulative copper flow (kg/h)	Cumulative Cu recovery (%)	Cu grade (%)	Cu Enrichment ratio	Nickel flow (kg/h)	Cumulative nickel flow (kg/h)	Cumulative Ni recovery (%)	Ni grade (%)	Ni Enrichment ratio
440-FT-01	0.030	0.030	29.608	2.773	24.489	0.022	0.022	11.089	2.023	9.171
440-FT-02	0.015	0.045	44.235	2.064	18.223	0.018	0.040	19.969	1.815	8.227
440-FT-03	0.018	0.063	61.513	1.487	13.131	0.035	0.075	37.786	1.780	8.066
440-FT-04	0.000	0.063	61.590	1.485	13.110	0.000	0.075	37.883	1.779	8.064
440-FT-05	0.000	0.063	61.650	1.482	13.087	0.000	0.076	37.964	1.778	8.059
440-FT-06	0.000	0.063	61.987	1.468	12.959	0.001	0.076	38.393	1.771	8.027
440-FT-07	0.000	0.063	62.047	1.464	12.931	0.000	0.077	38.470	1.769	8.017
440-FT-08	0.000	0.063	62.086	1.462	12.908	0.000	0.077	38.516	1.767	8.007
440-FT-09	0.002	0.066	64.124	1.407	12.421	0.006	0.083	41.501	1.774	8.039
440-FT-10	0.006	0.072	69.995	1.137	10.036	0.020	0.103	51.778	1.638	7.424
440-FT-11	0.009	0.081	79.136	0.921	8.128	0.034	0.137	68.986	1.563	7.086
440-FT-12	0.001	0.082	80.148	0.881	7.782	0.004	0.141	71.089	1.523	6.903
440-FT-13	0.000	0.082	80.236	0.877	7.742	0.000	0.142	71.268	1.517	6.876
440-FT-14	0.000	0.082	80.270	0.875	7.727	0.000	0.142	71.345	1.515	6.868
440-FT-15	0.000	0.082	80.299	0.874	7.717	0.000	0.142	71.409	1.514	6.863
440-FT-16	0.000	0.082	80.320	0.873	7.707	0.000	0.142	71.455	1.513	6.856
440-FT-17	0.001	0.083	80.975	0.867	7.653	0.001	0.143	71.987	1.501	6.803
440-FT-18	0.000	0.083	80.999	0.866	7.646	0.000	0.143	72.023	1.500	6.799
440-FT-19	0.000	0.083	81.020	0.865	7.637	0.000	0.143	72.061	1.499	6.793
440-FT-20	0.000	0.083	81.020	0.865	7.637	0.000	0.143	72.061	1.499	6.793

Table 7.48: Run 3 MF2 Mass balance summary PGMs

Cell ID	Solids concentrate (kg/h)	PGM g/h	Cumulative conc mass (kg/h)	Cumulative PGM flow (g/h)	Cumulative grade (g/t)	Cumulative recovery (%)	Cumulative mass pull (%)	4T Enrichment ratio
Feed	90.900	0.387						
440-FT-01	1.304	0.076	1.304	0.076	58.583	19.752	1.435	13.767
440-FT-02	1.184	0.054	2.488	0.130	52.398	33.701	2.737	12.314
440-FT-03	2.035	0.072	4.522	0.202	44.742	52.311	4.975	10.515
440-FT-04	0.013	0.000	4.536	0.203	44.698	52.415	4.990	10.504
440-FT-05	0.013	0.000	4.548	0.203	44.651	52.504	5.004	10.493
440-FT-06	0.069	0.002	4.617	0.205	44.355	52.949	5.080	10.424
440-FT-07	0.014	0.000	4.632	0.205	44.286	53.029	5.095	10.407
440-FT-08	0.010	0.000	4.642	0.205	44.233	53.078	5.106	10.395
440-FT-09	0.380	0.012	5.021	0.218	43.329	56.248	5.524	10.183
440-FT-10	1.592	0.035	6.613	0.253	38.241	65.379	7.275	8.987
440-FT-11	2.857	0.054	9.470	0.307	32.421	79.372	10.418	7.619
440-FT-12	0.597	0.008	10.067	0.315	31.301	81.463	11.075	7.356
440-FT-13	0.072	0.001	10.139	0.316	31.133	81.609	11.154	7.316
440-FT-14	0.026	0.000	10.165	0.316	31.076	81.669	11.183	7.303
440-FT-15	0.017	0.000	10.182	0.316	31.048	81.728	11.201	7.296
440-FT-16	0.022	0.000	10.204	0.316	31.000	81.781	11.226	7.285
440-FT-17	0.745	0.003	10.949	0.319	29.122	82.436	12.045	6.844
440-FT-18	0.026	0.000	10.975	0.319	29.067	82.475	12.074	6.831
440-FT-19	0.023	0.000	10.999	0.319	29.016	82.505	12.100	6.819
440-FT-20	0.000	0.000	10.999	0.319	29.016	82.505	12.100	6.819

Table 7.49: Run 3 MF2 Mass balance summary base metals

Cell ID	Copper flow (kg/h)	Cumulative copper flow (kg/h)	Cumulative Cu recovery (%)	Cu grade (%)	Cu Enrichment ratio	Nickel flow (kg/h)	Cumulative nickel flow (kg/h)	Cumulative Ni recovery (%)	Ni grade (%)	Ni Enrichment ratio
440-FT-01	0.029	0.029	28.191	2.242	19.649	0.028	0.028	13.775	2.110	9.601
440-FT-02	0.017	0.046	44.517	1.856	16.266	0.022	0.049	24.556	1.972	8.972
440-FT-03	0.018	0.064	61.622	1.414	12.386	0.032	0.081	40.730	1.799	8.187
440-FT-04	0.000	0.064	61.708	1.411	12.367	0.000	0.082	40.827	1.798	8.182
440-FT-05	0.000	0.064	61.774	1.409	12.346	0.000	0.082	40.915	1.797	8.177
440-FT-06	0.000	0.064	62.092	1.395	12.223	0.001	0.083	41.376	1.790	8.145
440-FT-07	0.000	0.064	62.160	1.392	12.199	0.000	0.083	41.458	1.788	8.136
440-FT-08	0.000	0.065	62.203	1.390	12.182	0.000	0.083	41.503	1.786	8.128
440-FT-09	0.002	0.067	64.388	1.330	11.656	0.006	0.089	44.517	1.771	8.059
440-FT-10	0.006	0.073	70.185	1.101	9.647	0.019	0.108	53.852	1.627	7.402
440-FT-11	0.009	0.082	78.974	0.865	7.581	0.031	0.139	69.600	1.468	6.681
440-FT-12	0.001	0.083	80.158	0.826	7.238	0.004	0.143	71.779	1.424	6.481
440-FT-13	0.000	0.083	80.252	0.821	7.195	0.000	0.144	71.951	1.418	6.451
440-FT-14	0.000	0.083	80.289	0.819	7.180	0.000	0.144	72.022	1.415	6.440
440-FT-15	0.000	0.083	80.321	0.818	7.171	0.000	0.144	72.090	1.414	6.436
440-FT-16	0.000	0.083	80.358	0.817	7.158	0.000	0.144	72.146	1.412	6.427
440-FT-17	0.000	0.084	80.671	0.764	6.697	0.002	0.146	72.898	1.330	6.052
440-FT-18	0.000	0.084	80.687	0.763	6.683	0.000	0.146	72.938	1.328	6.041
440-FT-19	0.000	0.084	80.703	0.761	6.670	0.000	0.146	72.974	1.325	6.031
440-FT-20	0.000	0.084	80.703	0.761	6.670	0.000	0.146	72.974	1.325	6.031

APPENDIX F

MINERALOGY

Table 7.50: Feed PGM speciation

	Sample description
AR142-11	PFF-1403
PGM Distribution	
PGM	Feed
Pt-sulphide	11.7
PtPd-sulphide	1.5
PtRh-sulphide	0.1
Pt-telluride	37.2
Pd-telluride	17.4
Pt-arsenide	4.4
Pd-arsenide	1.7
Ferroplatinum	4.4
Pt-alloys	4.1
Pd-alloys	5.1
PGE-sulpharsenides	8.4
Gold	4.0
Total	100.0
No of particles	113
PGE (3E) distribution %	100.00
PGM Liberation	
Liberation Class	Feed
Liberated PGM	46.8
Liberated PGM/BMS	0.4
PGM/BMS associated	9.1
Enclosed in silicates	33.3
Attached to silicates	0.5
Enclosed in alteration silicates	6.9
Attached to alteration silicates	3.0
Enclosed in oxides	0.0
Attached to oxides	0.0
Total	100.0
HGM	2.4
MGM	0.5
Locked	50.3

Table 7.51: Campaign 1 detailed tailings mineralogy MF3

MF3	Sample description			
AR142_1	TRT-1503*			
PGM Distribution				
PGM	Combined Tailings	Tailings-10	Tailings+10-25	Tailings+25
Pt-sulphide	4.2	5.5	3.2	4.2
PtPd-sulphide	9.3	6.1	11.9	0.8
PtRh-sulphide	4.3	4.2	4.5	0.0
Pt-telluride	16.7	24.5	10.5	30.3
Pd-telluride	20.6	23.2	18.4	31.7
Pt-arsenide	13.9	18.5	10.1	3.3
Pd-arsenide	2.1	3.0	1.3	0.2
Ferroplatinum	6.2	5.8	6.5	4.4
Pt-alloys	1.2	0.3	1.9	11.2
Pd-alloys	10.1	2.0	16.7	5.3
PGE-sulpharsenides	5.6	3.3	7.5	4.3
Gold	5.8	3.7	7.6	4.3
Total	100.0	100.0	100.0	100.0
No of particles	362	116	136	110
PGE (3E) distribution %	100.0	44.9	21.6	33.5
PGM Liberation				
Liberation Class	Combined Tailings	Tailings-10	Tailings+10-25	Tailings+25
Liberated PGM	53.4	87.7	64.8	0.0
Liberated PGM/BMS	0.9	1.1	1.6	0.0
PGM/BMS associated	1.4	0.0	0.6	3.7
Enclosed in silicates	27.9	1.1	15.4	71.8
Attached to silicates	5.2	7.9	7.8	0.0
Enclosed in alteration silicates	8.3	0.0	6.2	20.9
Attached to alteration silicates	2.8	2.2	3.5	3.3
Enclosed in oxides	0.1	0.0	0.0	0.3
Attached to oxides	0.0	0.0	0.0	0.0
Total	100.0	100.0	100.0	100.0
HGM	2.6	5.8	0.0	0.0
MGM	1.6	3.0	1.1	0.0
Locked	42.4	3.5	34.1	100.0
% Liberated PGM per Size Fraction in Tailings				
	Tailings-10	Tailings+10	Tailings+25	
Liberated PGM in tailings %	73.8	26.2	0.0	

Table 7.52: Campaign 1 detailed tailings mineralogy MF2

MF2	Sample description			
AR142_2	TRT-1403*			
PGM Distribution				
PGM	Combined Tailings	Tailings-10	Tailings+10-25	Tailings+25
Pt-sulphide	6.7	9.3	3.8	0.7
PtPd-sulphide	3.3	3.9	2.7	1.3
PtRh-sulphide	0.2	0.0	0.3	0.0
Pt-telluride	26.7	24.8	29.0	17.6
Pd-telluride	23.0	25.0	20.7	28.2
Pt-arsenide	17.9	20.6	14.8	16.0
Pd-arsenide	0.7	0.0	1.4	0.0
Ferroplatinum	14.2	8.3	21.0	14.1
Pt-alloys	0.2	0.0	0.5	3.6
Pd-alloys	2.3	0.9	3.8	4.0
PGE-sulpharsenides	0.5	0.6	0.3	7.0
Gold	4.3	6.5	1.8	7.5
Total	100.0	100.0	100.0	100.0
No of particles	364	111	126	127
PGE (3E) distribution %	100.0	53.3	25.9	20.8
PGM Liberation				
Liberation Class	Combined Tailings	Tailings-10	Tailings+10-25	Tailings+25
Liberated PGM	67.1	97.9	57.3	0.5
Liberated PGM/BMS	0.9	0.8	0.4	1.9
PGM/BMS associated	0.9	0.0	0.1	4.3
Enclosed in silicates	22.5	0.9	24.6	75.9
Attached to silicates	1.6	0.2	5.8	0.0
Enclosed in alteration silicates	4.6	0.0	5.7	15.0
Attached to alteration silicates	2.2	0.3	5.9	2.3
Enclosed in oxides	0.1	0.0	0.2	0.0
Attached to oxides	0.0	0.0	0.0	0.0
Total	99.9	100.0	100.0	100.0
HGM	0.4	0.8	0.0	0.0
MGM	1.4	0.2	5.0	0.0
Locked	31.1	1.2	37.8	99.5
% Liberated PGM per Size Fraction in Tailings				
	Tailings-10	Tailings+10	Tailings+25	
Liberated PGM in tailings %	77.8	22.1	0.2	

Table 7.53: Campaign 2 detailed tailings mineralogy MF3

MF3	Sample description			
AR142_3	TRT-1004			
PGM Distribution				
PGM	Combined Tailings	Tailings-10	Tailings+10-25	Tailings+25
Pt-sulphide	14.9	12.1	18.0	4.5
PtPd-sulphide	1.9	2.8	0.8	3.6
PtRh-sulphide	0.7	1.2	0.0	2.3
Pt-telluride	8.9	11.4	6.2	28.2
Pd-telluride	33.2	25.9	41.4	34.8
Pt-arsenide	17.0	20.0	13.6	6.1
Pd-arsenide	0.1	0.0	0.2	1.4
Ferroplatinum	4.2	2.5	6.1	4.8
Pt-alloys	1.5	1.9	0.9	0.8
Pd-alloys	3.5	5.3	1.4	2.0
PGE-sulpharsenides	4.5	8.1	0.4	5.1
Gold	9.7	8.7	10.8	6.4
Total	100.0	100.0	100.0	100.0
No of particles	341	115	112	114
PGE (3E) distribution %	100.0	53.2	31.4	15.4
PGM Liberation				
Liberation Class	Combined Tailings	Tailings-10	Tailings+10-25	Tailings+25
Liberated PGM	61.8	91.0	42.0	1.1
Liberated PGM/BMS	3.1	3.0	4.7	0.2
PGM/BMS associated	2.4	1.8	3.2	2.8
Enclosed in silicates	13.8	0.0	19.1	50.8
Attached to silicates	8.2	1.4	16.0	15.7
Enclosed in alteration silicates	7.5	0.5	9.9	26.6
Attached to alteration silicates	2.0	0.0	5.1	2.2
Enclosed in oxides	0.1	0.0	0.0	0.6
Attached to oxides	1.2	2.2	0.0	0.0
Total	100.0	100.0	100.0	100.0
HGM	1.5	1.7	1.9	0.0
MGM	0.2	0.4	0.0	0.0
Locked	36.5	6.8	56.1	98.9
% Liberated PGM per Size Fraction in Tailings				
	Tailings-10	Tailings+10	Tailings+25	
Liberated PGM in tailings %	78.4	21.3	0.3	

Table 7.54: Campaign 2 detailed tailings mineralogy MF2

MF2	Sample description			
AR142_4	TRT-0904			
PGM Distribution				
PGM	Combined Tailings	Tailings-10	Tailings+10-25	Tailings+25
Pt-sulphide	4.9	8.4	1.8	5.6
PtPd-sulphide	3.5	6.7	0.4	0.3
PtRh-sulphide	0.0	0.0	0.0	1.1
Pt-telluride	21.8	17.0	26.3	11.8
Pd-telluride	32.9	24.5	40.7	21.1
Pt-arsenide	12.4	21.6	3.9	27.0
Pd-arsenide	0.0	0.0	0.1	0.0
Ferroplatinum	4.2	4.4	4.1	5.5
Pt-alloys	2.6	3.5	1.8	0.7
Pd-alloys	6.0	2.0	9.7	3.5
PGE-sulpharsenides	3.2	3.2	3.1	6.9
Gold	8.4	8.7	8.1	16.4
Total	100.0	100.0	100.0	100.0
No of particles	335	115	111	109
PGE (3E) distribution %	100.0	48.2	34.5	17.3
PGM Liberation				
Liberation Class	Combined Tailings	Tailings-10	Tailings+10-25	Tailings+25
Liberated PGM	44.5	82.7	12.6	1.3
Liberated PGM/BMS	3.6	3.5	5.5	0.0
PGM/BMS associated	2.4	1.3	3.0	4.5
Enclosed in silicates	25.0	1.1	39.4	63.4
Attached to silicates	8.3	5.6	14.2	3.8
Enclosed in alteration silicates	11.2	0.6	18.6	25.9
Attached to alteration silicates	3.4	5.1	2.3	0.9
Enclosed in oxides	1.6	0.0	4.4	0.2
Attached to oxides	0.0	0.0	0.0	0.0
Total	100.0	100.0	100.0	100.0
HGM	2.6	3.9	2.1	0.0
MGM	4.3	8.9	0.0	0.0
Locked	48.6	4.4	85.3	98.7
% Liberated PGM per Size Fraction in Tailings				
	Tailings-10	Tailings+10	Tailings+25	
Liberated PGM in tailings %	89.7	9.7	0.5	

APPENDIX G

PLANT FLOWSHEET

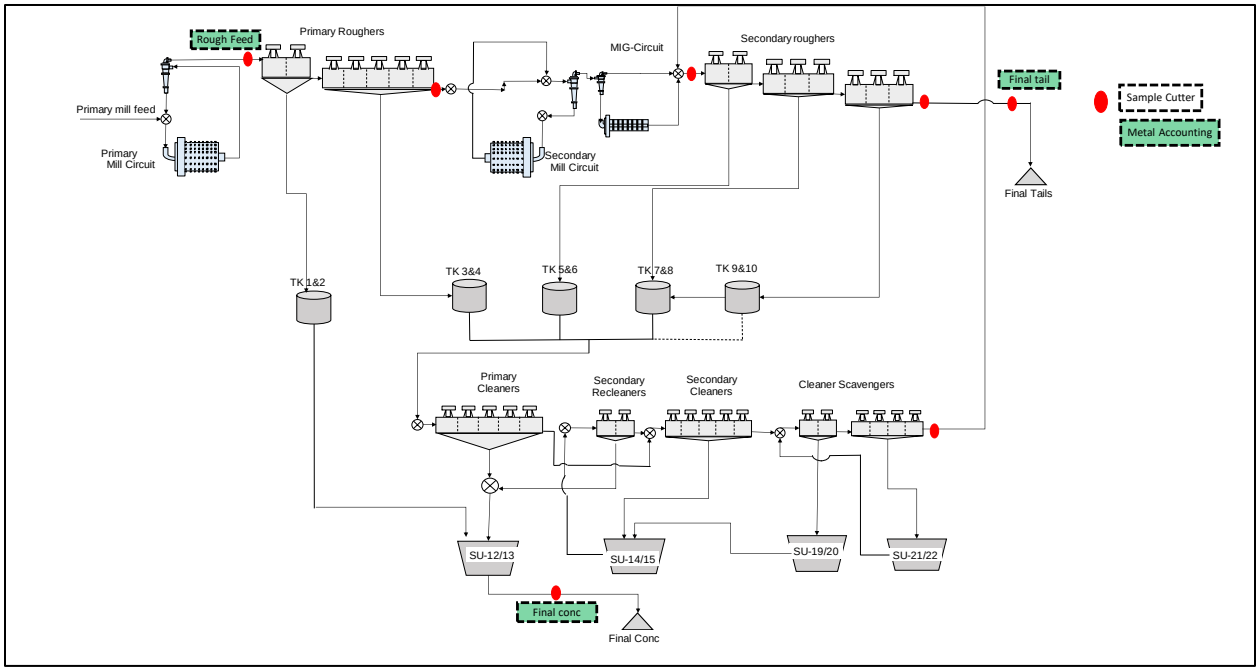

Figure 7.3: Current wet section plant setup

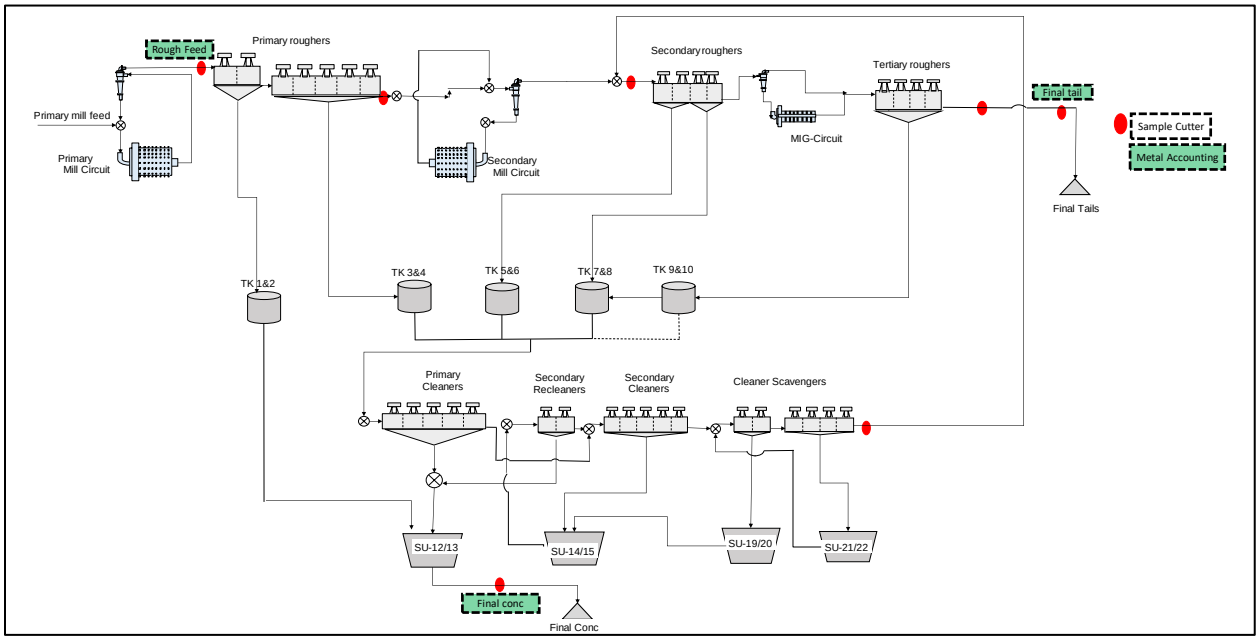

Figure 7.4: Proposed MF3 Circuit plant setup

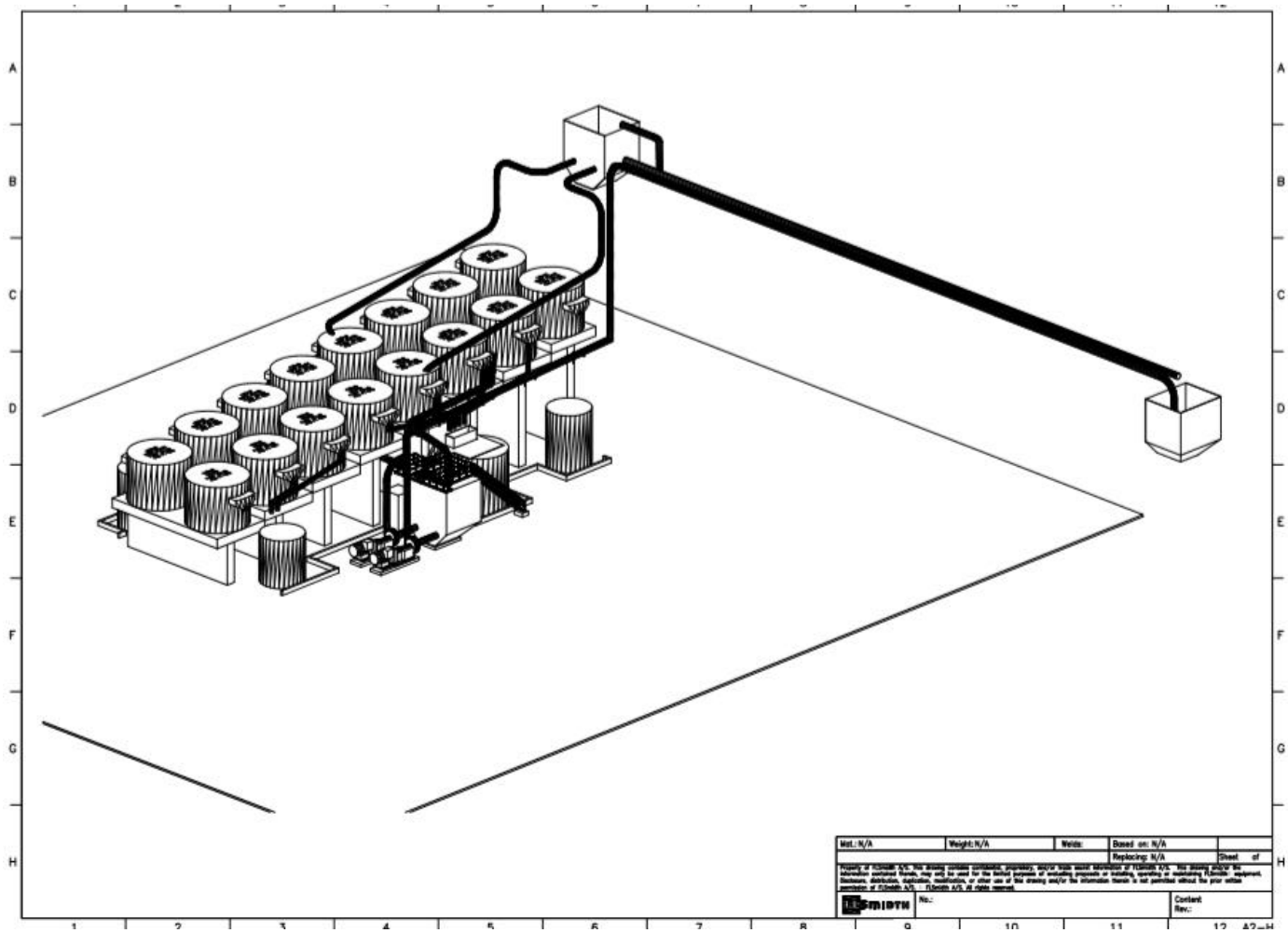

Figure 7.5: Plant retrofit conceptual design

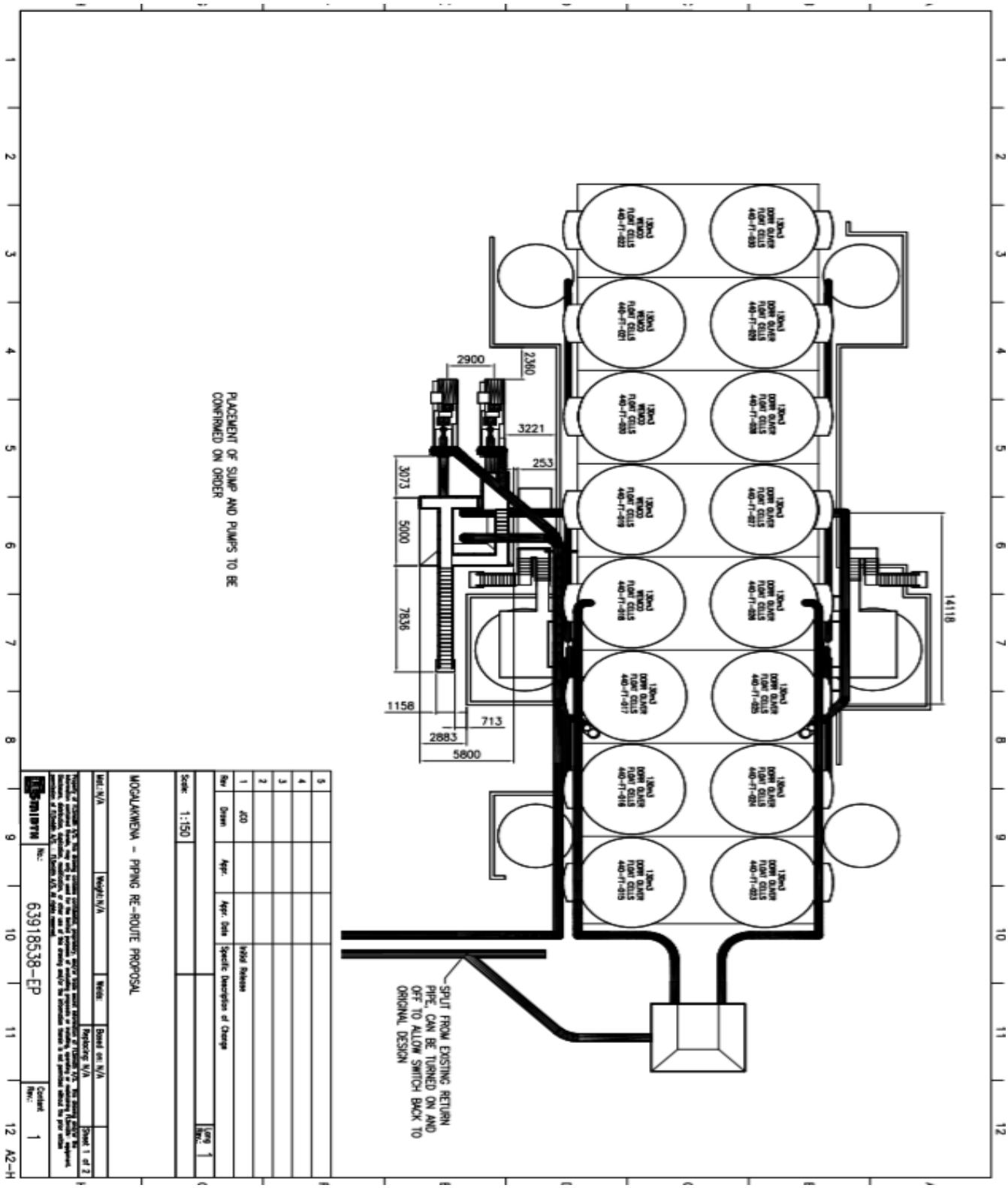

Figure 7.6: Proposed plant layout for secondary roughers and tertiary roughers

---

APPENDIX H

COST AND BENEFIT ANALYSIS

Table 7.55: Additional pump operating costs

Date	Task	Spares Used	Part Number	Quantity	Price
16-12-16	Complete Overhaul Pump	Volute Liner	H14110-A05A	1	R 139,843
		Throatbush	H14083MA05	1	R 66,686
		Impeller	GAM14147-A05A	1	R 121,703
		Frame Plate Liner Insert	H14041M-A05A	1	R 115,651
		Shaft Sleeve	GAM076-2-C23	1	R 3,276
		Shaft Oring	G109-S10	2	R 16
25-10-17	Replace Motor & Upgrade Pulleys	500 kW motor	WEG 500kW motor	1	R 437,190
22-05-18	Replace Pump	Complete Pump	16/14-G-AH-MM	1	R 912,612
18-06-18	Replace Motor	500 kW motor	WEG 500kW motor	1	R 437,190

Tons milled	12,745,925	tons
Plant productive time	11,858	hrs
Pump runtime	10,515	hrs
Proportion of tons through pump	11,302,706	tons
Operational costs	2,234,167	ZAR
Unit cost 1	0.20	ZAR/ton
Rand per kWhr	0.96	ZAR/kWhr
Pump motor rating	500	kW
Power cost	5,047,354	ZAR
Unit cost 2	0.45	ZAR/ton
Total unit cost	**0.64**	ZAR/ton

Table 7.56: Cost benefit analysis optimistic approach

Mogalakwena:MF3			2020	2021	2022	2023	**2024**	2025	**Total**
MF3			(72)	56	56	70	**77**	86	**273**
MF3			- 56	56	56	70	**77**	86	**345**
Capital			- 72						
Confidence discount applied to BP2021 -2025			100%	100%	100%	100%	**100%**	100%	
Process Excellence Achieved through value creation (Part of Recovery optimisation)			(72.10)	56	56	70	**77**	86	**273**
2020 Nominal			(72)	56	56	70	77	86	**273**
			-						
Total @ **Real 2020 (R'm)**			(72)	56	56	70	**77**	86	**273**
Discounted @11,5% real			- 72.10	49.98	44.93	50.73	49.94	49.64	11.5%
Total @ real 2020 ($'m)			(5)	4	4	5	6	6	20
Total discounted @ real 2020 ($'m)			(5)	4	3	4	4	4	12
IRR								80%	80%

Table 7.57: Pessimistic approach 150% cost of implementation

Mogalakwena:MF3	2020	2021	2022	2023	2024	2025	**Total**
MF3	(108)	56	56	70	77	86	**236**
MF3	-	56	56	70	77	86	**345**
Capital	- 108						
Confidence discount applied to BP2021 -2025	100%	100%	100%	100%	100%	100%	
Process Excellence Achieved through value creation (Part of Recovery optimisation)	(108.15)	56	56	70	77	86	**236**
2020 Nominal	(108)	56	56	70	77	86	**236**
	-						
Total @ Real 2020 (R'm)	(108)	56	56	70	77	86	**236**
Discounted @11,5% real	- 108.15	49.98	44.93	50.73	49.94	49.64	11.5%
Total @ real 2020 ($'m)	(8)	4	4	5	6	6	17
Total discounted @ real 2020 ($'m)	(8)	4	3	4	4	4	10
IRR						51%	51%
Payback							**2yr 3 mths**